Target Identification and Validation in Ibrutinib-treated Mantle Cell Lymphoma

Target-Identifizierung und Validierung im Ibrutinib-behandelten Mantelzell-Lymphom

Doctoral thesis for a doctoral degree
at the Graduate School of Life Sciences,
Julius-Maximilians-Universität Würzburg,
Section Biomedicine

submitted by

Viktoria Fuhr

from

Speyer

Würzburg 2022

To my parents

Submitted on:

Members of the Thesis Committee

Chairperson:	Prof. Dr. David Stegner
Primary Supervisor:	Prof. Dr. Andreas Rosenwald
Supervisor (Second):	Dr. Antoine-Emmanuel Saliba
Supervisor (Third):	PD Dr. Robert Hock
Supervisor (Fourth):	Dr. Hilka Rauert-Wunderlich
Supervisor (Fifth):	Prof. Dr. Stefan Gaubatz

Date of Public Defense:

Date of Receipt of Certificates:

Table of Contents

1 Summary

Ibrutinib serves as an efficient second-line therapy in relapsed/refractory mantle cell lymphoma. However, resistance to the BTK inhibitor results in a poor prognosis for patients. Since the mechanisms leading to resistance in initially responding tumor cells are poorly understood, this work aimed to decipher acquired features in ibrutinib-surviving cells of a sensitive mantle cell lymphoma cell line and evaluate these potential therapeutic targets in ibrutinib-treated mantle cell lymphoma.

Time-resolved single-cell RNA sequencing was performed to track the transcriptomic evolution of REC-1 cells across 6 and 48 hours of treatment. Single-cell analysis uncovered a subpopulation of REC-1 with potentially greater aggressiveness and survival advantage by benefiting from interaction with the tumor microenvironment. Upregulation of B-cell receptor genes, elevated surface antigen expression of CD52 and metabolic rewiring to higher dependence on oxidative phosphorylation were identified as further potential resistance features of ibrutinib-surviving cells. RNA sequencing after prolonged incubation corroborated the increase in CD52 and oxidative phosphorylation as dominant characteristics of the cells surviving the 4-day treatment, highlighting their potential as therapeutic targets in combination with ibrutinib treatment. Concomitant use of ibrutinib and the oxidative phosphorylation inhibitor IACS-010759 increased toxicity compared to ibrutinib monotherapy due to higher apoptosis and greater inhibition of proliferation. For anti-CD52 therapy, a consecutive approach with ibrutinib pretreatment followed by incubation of surviving cells with a CD52 monoclonal antibody and human serum yielded a synergistic effect, as ibrutinib-surviving mantle cell lymphoma cells were rapidly depleted by complement-dependent cytotoxicity. Regarding the effects on primary tumor cells from mantle cell lymphoma patients, ibrutinib induced upregulation of CD52 in some cases, and increased toxicity of anti-CD52 therapy was observed in ibrutinib-sensitive patient samples after pretreatment with the BTK inhibitor. The likely favorable *in vivo* efficacy of an anti-CD52 therapy might therefore be restricted to a subgroup of mantle cell lymphoma patients, also in view of the associated side effects.

Given the need for new therapeutic options in mantle cell lymphoma to overcome resistance to ibrutinib, this work highlights the potentially beneficial use of an oxidative phosphorylation inhibitor as add-on therapy. In addition, the findings suggest to further assess the value of anti-CD52 therapy as consolidation to ibrutinib in ibrutinib-sensitive patients with elevated CD52 surface levels on tumor cells to target resistant clones and minimize risk of minimal residual disease and relapse.

2 Zusammenfassung

Ibrutinib dient als wirkungsvolle Zweitlinientherapie beim rezidivierten/refraktären Mantelzell-Lymphom. Jedoch führt eine Resistenz gegen den BTK-Inhibitor zu einer schlechten Prognose für die Patienten. Da die Mechanismen, die zur Resistenz in initial ansprechenden Tumorzellen führen, nur unzureichend bekannt sind, hatte diese Arbeit zum Ziel, erworbene Eigenschaften in Ibrutinib-überlebenden Zellen einer sensitiven Mantelzell-Lymphom Zelllinie aufzudecken und darauf basierende therapeutische Ansätze im Ibrutinib-behandelten Mantelzell-Lymphom zu evaluieren.

Eine Einzelzell-RNA-Sequenzierung wurde durchgeführt, um die Entwicklung des Transkriptoms der REC-1 Zellen über eine Behandlung von 6 und 48 Stunden zu verfolgen. Die Einzelzellanalyse offenbarte eine Subpopulation der REC-1 Zelllinie, die möglicherweise eine größere Aggressivität und einen Überlebensvorteil aufwies, da sie von der Interaktion mit dem Tumormikromilieu profitieren könnte. Die Hochregulation von B-Zell Rezeptor Genen, erhöhte Oberflächenantigenexpression von CD52 und eine Umstellung des Metabolismus auf eine stärkere Abhängigkeit von der oxidativen Phosphorylierung wurden als weitere mögliche Resistenzeigenschaften der Ibrutinib-überlebenden Zellen identifiziert. Eine RNA-Sequenzierung nach längerer Inkubation bestätigte den Anstieg von CD52 und oxidativer Phosphorylierung als dominante Merkmale der Zellen, die die 4-tägige Behandlung überlebten, was ihr Potential als therapeutische Ansatzpunkte in Kombination mit einer Ibrutinib Therapie hervorhob. Die gleichzeitige Anwendung von Ibrutinib und dem Inhibitor der oxidativen Phosphorylierung, IACS-010759, erhöhte die Toxizität im Vergleich zur Ibrutinib-Monotherapie aufgrund einer gesteigerten Apoptose und einer stärkeren Hemmung der Proliferation. Bei der Anti-CD52-Therapie erzielte der konsekutive Ansatz mit Ibrutinib-Vorbehandlung und anschließender Inkubation der überlebenden Zellen mit einem monoklonalen CD52-Antikörper und humanem Serum einen synergistischen Effekt, da die unter Ibrutinib überlebenden Zellen schnell durch die komplementabhängige Zytotoxizität eliminiert wurden. Hinsichtlich der Auswirkungen auf primäre Tumorzellen von Mantelzell-Lymphom-Patienten führte Ibrutinib in manchen Fällen zu einer Hochregulierung von CD52, und in Ibrutinib-empfindlichen Patientenproben wurde nach Vorbehandlung mit dem BTK-Inhibitor eine erhöhte Toxizität der Anti-CD52-Therapie beobachtet. Die wahrscheinlich günstige *In-vivo*-Wirkung einer Anti-CD52-Therapie könnte daher auf eine Subgruppe von Mantelzell-Lymphom Patienten beschränkt sein, auch im Hinblick auf die damit verbundenen Nebenwirkungen.

Angesichts des Bedarfs an neuen therapeutischen Optionen beim Mantelzell-Lymphom zur Überwindung der Ibrutinib-Resistenz unterstreicht diese Arbeit den potentiell vorteilhaften

Einsatz eines Inhibitors der oxidativen Phosphorylierung als Zusatztherapie. Darüber hinaus legen die Ergebnisse nahe, den Nutzen einer Anti-CD52-Therapie als Konsolidierung zu Ibrutinib bei Ibrutinib-empfindlichen Patienten mit erhöhter CD52 Oberflächenexpression auf Tumorzellen näher zu untersuchen, um resistente Klone zu beseitigen und das Risiko einer minimalen Resterkrankung und eines Rückfalls zu minimieren.

3 List of Figures

4 List of Tables

5 Abbreviation Index

% (w/v)	Percent weight per volume
% (v/v)	Percent volume per volume
× g	Relative centrifugal force
°C	Degree Celsius
A	Ampere
ADCC	Antibody-dependent cellular cytotoxicity
ADCP	Antibody-dependent cellular phagocytosis
AKT	RAC-alpha serine/threonine-protein kinase
alloSCT	Allogeneic stem cell transplantation
APS	Ammonium persulfate
ATF3	Cyclic AMP-dependent transcription factor ATF-3
ATM	*ATM serine/threonine kinase*
autoSCT	Autologous stem cell transplantation
BAC	Bendamustine, cytarabine
BANK1	*B cell scaffold protein with ankyrin repeats 1*
BATF	Basic leucine zipper transcriptional factor ATF-like
BCL10	B-cell lymphoma/leukemia 10
BCL2	Apoptosis regulator Bcl-2
BCL2A1	*BCL2 related protein A1*
BCL6	B-cell lymphoma 6 protein
BCR	B-cell receptor
BEAM	Carmustine, etoposide, cytarabine, melphalan
BHLHE40/41	Class E basic helix-loop-helix protein 40/41
BIRC3	*Baculoviral IAP repeat containing 3*
BMI1	*BMI1 proto-oncogene, polycomb ring finger*
BNIP3	*BCL2 interacting protein 3*
BP	Biological processes
BR	Bendamustine, rituximab
BSA	Bovine serum albumin
BTK BTK	*Bruton tyrosine kinase* Tyrosine-protein kinase BTK
CARD11 CARD11	*Caspase recruitment domain family member 11* Caspase recruitment domain-containing protein 11
CAR T cell	Chimeric antigen receptor T cell

Cbl	Chlorambucil
CCND1/*D2*/*D3*/*E1*/*E2* CCND1	*Cyclin D1*/*D2*/*D3*/*E1*/*E2* G1/S-specific cyclin-D1
CD10	Neprilysin
CD19	B-lymphocyte antigen CD19
CD20	B-lymphocyte antigen CD20
CD23	Low affinity immunoglobulin epsilon Fc receptor
CD37	Leukocyte antigen CD37
CD40 CD40	*CD40 molecule* Tumor necrosis factor receptor superfamily member 5
CD40L	CD40 ligand
CD5	T-cell surface glycoprotein CD5
CD52 CD52	*CD52 molecule* CAMPATH-1 antigen
CD79A, CD79B *CD79A*, *CD79B*	B-cell antigen receptor complex-associated protein alpha/beta chain *CD79a molecule, CD79b molecule*
CD83	*CD83 molecule*
CDC	Complement-dependent cytotoxicity
CDK4	*Cyclin dependent kinase 4*
CDKN2A	*Cyclin dependent kinase inhibitor 2A*
CEBPB	CCAAT/enhancer-binding protein beta
CHOP	Cyclophosphamide, doxorubicin, vincristine, prednisone
CIRBP	*Cold inducible RNA binding protein*
CLL	Chronic lymphocytic leukemia
CML	Chronic myeloid leukemia
CO_2	Carbon dioxide
CT	Computed tomography
Ctr	Control
CVP	Cyclophosphamide, vincristine, prednisone
CXCL10	*C-X-C motif chemokine ligand 10*
DAG	Diacylglycerol
d	Day(s)
DDIT3 DDIT3	*DNA damage inducible transcript 3* DNA damage-inducible transcript 3 protein
DDIT4	*DNA damage inducible transcript 4*
DEG	Differentially expressed genes
DHAP	Dexamethasone, high-dose cytarabine, cisplatin

DLBCL	Diffuse large B-cell lymphoma
DMSO	Dimethyl sulfoxide
DPBS	Dulbecco's Phosphate Buffered Saline
DTT	Dithiothreitol
DUSP2	*Dual specificity phosphatase 2*
ECAR	Extracellular acidification rate
EDTA	Ethylenediaminetetraacetic acid
EGFR	Epidermal growth factor receptor
ETC	Electron transport chain
ERK	Mitogen-activated protein kinase
et al.	et alia
ETS1	Protein C-ets-1
FACS	Fluorescence-activated cell sorting
FBS	Fetal bovine serum
FDA	United States Food and Drug Administration
FDG	Fluorodeoxyglucose
FISH	Fluorescence in situ hybridization
FL	Follicular lymphoma
GEM	Gel Beads-in-emulsion
GRN	Gene regulatory network
GSEA	Gene set enrichment analysis
h	Hour(s)
HCl	Hydrochloric acid
HCVAD	Cyclophosphamide, vincristine, doxorubicin, dexamethasone
HIF-1α	Hypoxia-inducible factor 1-alpha
HILPDA	*Hypoxia inducible lipid droplet associated*
HIS	Heat-inactivated human serum
HIV	Human immunodeficiency virus
HMGB3	High mobility group protein B3
HMGN3	*High mobility group nucleosomal binding domain 3*
H_2O_2	Hydrogen peroxide
IC_{50}	Half maximal inhibitory concentration
IGHV	Immunoglobulin heavy chain variable region
IgM, IgD, IgG	Immunoglobulin M, D, G
IKK	Inhibitor of nuclear factor kappa-B kinase

IL-4	Interleukin-4
IP3	Inositol 1,4,5-trisphosphate
IRF4	Interferon regulatory factor 4
ITAM	Immunoreceptor tyrosine-based activation motif
ITK	Tyrosine-protein kinase ITK/TSK
IκB	Inhibitor of nuclear factor kappa-B
JUNB	Transcription factor JunB
K_2HPO_4	Dipotassium hydrogen phosphate
KEGG	Kyoto Encyclopedia of Genes and Genomes
Ki-67	Proliferation marker protein Ki-67
KRAS	*KRAS proto-oncogene, GTPase*
LDH	L-lactate dehydrogenase
LDHA	*Lactate dehydrogenase A*
LDHA	L-lactate dehydrogenase A chain
LGALS1	*Galectin 1*
Log2FC	Log2FoldChange
LTB	Lymphotoxin-beta
LYN	Tyrosine-protein kinase Lyn
M	Molar concentration [mol/l]
mAb	Monoclonal antibody
MAC	Membrane-attack complex
MALT1	Mucosa-associated lymphoid tissue lymphoma translocation protein 1
MAPK	Mitogen-activated protein kinase
MARCKSL1	MARCKS-related protein
MCL	Mantle cell lymphoma
MFI	Mean fluorescence intensity
mIg	Membrane immunoglobulin
min	Minute(s)
MIPI-c	Combined MCL International Prognostic Index
MRD	Minimal residual disease
mTOR	Serine/threonine-protein kinase mTOR
mTORC1	Mammalian target of rapamycin complex 1
MTT	3-[4,5-Dimethylthiazol-2-yl]-2,5-diphenyltetrazolium bromide
Multiple sclerosis	MS
MXI1	Max-interacting protein 1

MYC	*MYC proto-oncogene, BHLH Transcription factor*
$Na_2HPO_4 \times 2H_2O$	Disodium hydrogen phosphate dihydrat
NaCl	Sodium chloride
NaN_3	Sodium azide
Na-O-V	Sodium orthovanadate
NF-κB	Nuclear factor kappa B
NFKB1	Nuclear factor NF-κB p105 subunit
NFKB2	Nuclear factor NF-κB p100 subunit
NFKBIA	*NFKB inhibitor alpha*
NFKBID	*NFKB inhibitor delta*
NHL	Non-Hodgkin Lymphoma
NHS	Normal human serum
NK cell	Natural killer cell
NOTCH1/2	*Notch receptor 1/2*
ns	Not significant
NSD2	*Nuclear receptor binding SET domain protein 2*
OCR	Oxygen consumption rate
OXPHOS	Oxidative phosphorylation
padj	Adjusted *P*-value
PARP	Poly (ADP-ribose) polymerase
PBMC	Peripheral blood mononuclear cells
PBS	Phosphate-buffered saline
PCA	Principal component analysis
PCR	Polymerase chain reaction
PET	Positron emission tomography
PGK1	*Phosphoglycerate kinase 1*
PI	Propidium iodide
PI3K	Phosphatidylinositol 4,5-bisphosphate 3-kinase
PIP2	Phosphatidylinositol 4,5-bisphosphate
PIP3	Phosphatidylinositol 3,4,5-trisphosphate
PKCβ	Protein kinase C beta type
PLCγ	1-Phosphatidylinositol 4,5-bisphosphate phosphodiesterase gamma-1
PMSF	Phenylmethyl sulphonyl fluoride
POU2AF1/2	POU domain class 2-associating factor 1/2
PTEN	Phosphatase and tensin homolog

QC	Quality control
qRT-PCR	Quantitative reverse transcription PCR
R	Rituximab
RB1	*RB transcriptional corepressor 1*
REL REL	*REL proto-oncogene*, *NF-κB subunit* Proto-oncogene c-Rel
RELB	Transcription factor RelB
RIN	RNA integrity number
RNA-seq	RNA sequencing
RR	Relapsed/refractory
RT	Room temperature
SCENIC	Single-cell regulatory network inference and clustering
scRNA-seq	Single-cell RNA sequencing
SDS	Sodium dodecyl sulfate
SDS-PAGE	Sodium dodecyl sulfate polyacrylamide gel electrophoresis
SEM	Standard error of the mean
SLC16A3	*Solute carrier family 16 member 3*
SOX11 SOX11	*SRY-box transcription factor 11* Transcription factor SOX-11
SP1	Transcription factor Sp1
SPI1 SPI1	*Spi-1 proto-oncogene* Transcription factor PU.1
SPIB SPIB	*Spi-B transcription factor* Transcription factor Spi-B
SPP1	*Secreted phosphoprotein 1*
TBS	Tris-buffered saline
TBS-T	Tris-buffered saline with Tween® 20
TEMED	Tetramethylethylenediamine
TF	Transcription factor
THAM	Total body irradiation, high-dose cytarabine, melphalan
TME	Tumor microenvironment
TNF	Tumor necrosis factor
TP53	*Tumor protein p53*
TRAF2/3	*TNF receptor associated factor 2/3*
TRIB3	*Tribbles pseudokinase 3*
UMAP	Uniform manifold approximation and projection
UMI	Unique molecular identifier

US	United States
Versus	vs
VPREB3	*V-set pre-B cell surrogate light chain 3*
VR-CAP	Rituximab, cyclophosphamide, doxorubicin, bortezomib, prednisone
w & w	Watch and wait
WB	Western blot
WHO	World Health Organization
XBP1	X-box-binding protein 1
XLA	Immunodeficiency X-linked agammaglobulinemia

6 Introduction

6.1 Hallmarks of cancer

Deviations from the regulated cell life cycle can cause abnormal growth and spread of cells and eventually lead to the emergence of cancer. Next to diseases of the circulatory and respiratory system, malignant neoplasms are the leading causes of death in the world, emphasizing the need for a deeper understanding of this heterogeneous disease to improve patient care [1].

Despite the differences between cancers, some specific characteristics of cancer cells that distinguish them from healthy cells have been defined as the Hallmarks of Cancer (Figure 1; [2, 3]).

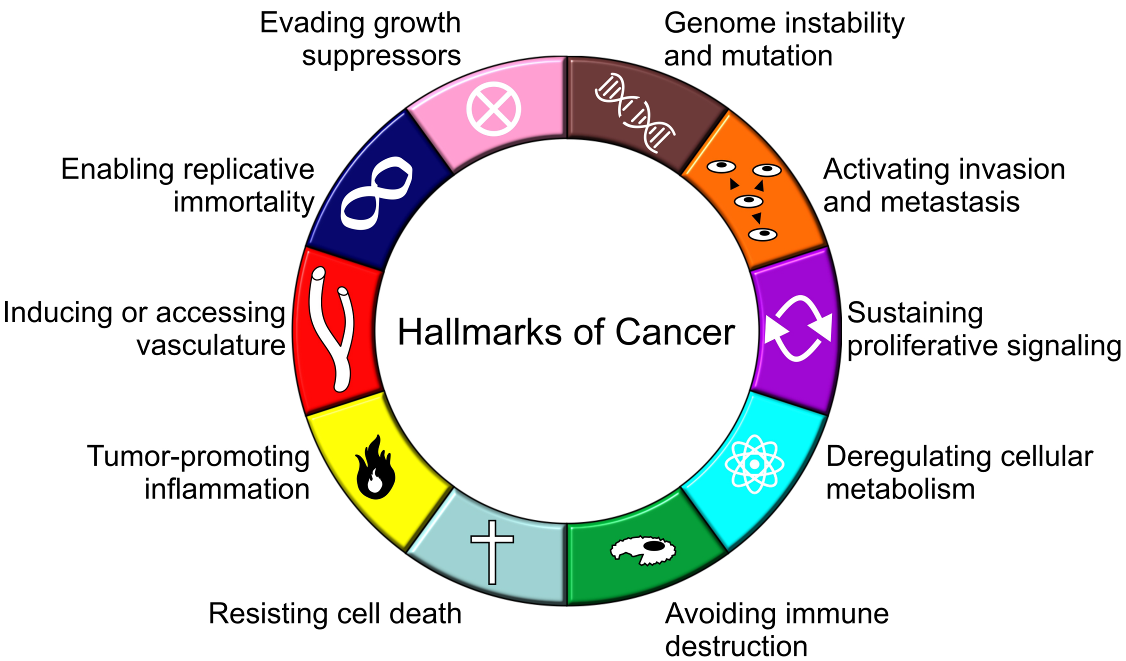

Figure 1: The Hallmarks of Cancer. The Hallmarks of Cancer include the two enabling characteristics of genome instability and mutation, as well as tumor-promoting inflammation, and the eight functional features of sustaining proliferative signaling, deregulating cellular metabolism, avoiding immune destruction, resisting cell death, inducing or accessing vasculature, enabling replicative immortality, evading growth suppressors, as well as activating invasion and metastasis. Modified from Hanahan 2022 [3].

Cancer cells are characterized by enhanced proliferation profiting from the interaction with surrounding stromal cells [4]. Cellular aging is evaded by unlimited replicative potential attained by the cancer cells' intrinsic mechanisms to maintain their telomeres [5]. Immortality is achieved by bypassing tumor suppressive systems like defects in tumor suppressor genes [6]. When the interplay of pro- and antiapoptotic players is not properly regulated, the cells can circumvent controlled cell death [7]. The acquisition of aberrant features is based on the genomic instability and the widely occurring mutations [8]. While cancer cells can escape the immune system, which is normally meant to remove aberrant cells, they also take advantage of the presence of immune cells and the inflammatory conditions that provide, for instance, signaling molecules for angiogenesis [9]. Angiogenesis is crucial for cancer cells, since it ensures sufficient access to nutrients [10]. By altering cellular functions, cancer cells can invade to other tissues and metastasize [11]. Besides, oncogenesis is associated with adaptations and alterations in cellular metabolism [12]. Although these properties confer aggressive features to tumor cells, they also provide targets for cancer therapy.

6.2 Mature B-cell neoplasms

The International Classification of Diseases for Oncology, Third Edition (ICD-O-3), classifies cancer according to its localization in the body (topography), tissue or cells of origin and their behavior (morphology) [13]. Neoplasms are categorized as carcinomas, sarcomas, myelomas, leukemias, or lymphomas, which refer to tumors of the lymphatic system.

Historically, mature lymphoid malignancies have been subdivided into Hodgkin-lymphoma, with the characteristic presentation of Reed-Sternberg cells, and the more common Non-Hodgkin lymphomas (NHL), which account for 90% of all lymphomas [14]. According to the World Health Organization (WHO) classification from 2016, NHL are nowadays classified as mature T-cell, natural killer (NK)-cell, and mature B-cell neoplasms, the latter representing more than 80% of NHL [15-17]. NHL rank among the most common neoplasms and occupied the 13th place in the ranking of new cancer cases in 2020 (Globocan 2020, [18]). The group of these diverse entities is dominated by follicular lymphoma (FL), which usually has an indolent course, and diffuse large B-cell lymphoma (DLBCL), which is characterized by a more aggressive behavior [19]. The initial event driving oncogenesis in B cells is often a translocation involving the immunoglobulin heavy chain variable region (IGHV) locus on chromosome 14q32. During B-cell development, when recombination of V(D)J segments occurs, translocations can lead to the juxtaposition of proto-oncogenes to enhancer regions of the IGHV region. Constitutive expression of these oncogenic drivers, such as *cyclin D1* (*CCND1*) in mantle cell lymphoma (MCL), causes the transformation into aberrant B cells [20]. However, this event is quite rare considering that MCL is diagnosed in only 3-10% of NHL [21, 22].

6.3 Mantle cell lymphoma

Mantle cell lymphoma is a mature B-cell neoplasm with characteristic presentation of aberrant small B cells in the mantle zone of lymphoid follicles [15]. Besides the primary localization in the lymph nodes, MCL often involves the bone marrow, spleen, gastrointestinal tract, liver, and peripheral blood [23]. Although it is classified as an aggressive B-cell lymphoma, patients may also follow an indolent course without requiring immediate treatment [24]. MCL is still considered incurable, and the median overall survival is only 3-5 years [23]. However, young patients in particular have benefited from the use of cytarabine and rituximab-based treatments and autologous stem cell transplantation (autoSCT), improving the progression-free and overall survival rates [25]. The disease mostly occurs at older ages, above 60 years, with men more commonly affected than women, at a ratio of 3:1 [24, 26].

6.3.1 Molecular background

Mantle cell lymphoma cells are thought to originate from pre-B cells in the bone marrow, although in some cases the initiating oncogenic alteration may also occur at a later stage of mature B-cell development [27, 28]. Following rearrangement of the heavy and light chain regions, chromosomal breaks are required for the formation of a functional B-cell receptor (BCR; [29]). In MCL, *CCND1*, at chromosome 11q13, comes under the control of the immunoglobulin heavy chain enhancer at chromosome 14q32 leading to overexpression of the proto-oncogene and to cell cycle deregulation [30]. The translocation t(11;14)(q13;q32) with *CCND1* overexpression represents the genetic hallmark of MCL [27]. In a few cases with histology and phenotype of MCL, negativity for G1/S-specific cyclin-D1 (CCND1) is observed, whereas transcription factor SOX-11 (SOX11) is expressed and can serve as marker [31]. Instead of *CCND1*, *cyclin D2* (*CCND2*) rearrangements and, less frequently, *cyclin D3* (*CCND3*) are detected in these cases, with a small subgroup showing only *cyclin E1*/*cyclin E2* (*CCNE1*/*CCNE2*) dysregulation [32].

MCL cases are categorized according to the WHO classification 2016. Two different molecular pathways of tumor cell expansion are mainly distinguished resulting in the classical and leukemic non-nodal subtype [15, 33]. In more than 90% of MCL cases, SOX11 is overexpressed, and the patients are assigned to the classical (conventional) form with nodal involvement [31, 34]. The naïve-like B cells do not transit the germinal center (pre-germinal center cells), are characterized by genomic instability, and show minimal or no mutations in the IGHV [35, 36]. The leukemic non-nodal variant, with involvement of bone marrow and spleen next to peripheral blood, often follows a more indolent course [37]. The memory-like B cells enter the germinal center (post-germinal center cells), acquire IGHV somatic hypermutations, and present a more stable genome with minimal or lacking SOX11 expression [38]. Secondary genetic alterations are more common in classical than in non-nodal MCL and may result in a more aggressive tumor of pleomorphic and blastoid variant (10% to >20% of cases) [39, 40]. Apart from the classical and non-nodal subtype, *in situ* mantle cell neoplasia is distinguished as a rare and early manifestation of MCL in the inner mantle zones, characterized by CCND1 positivity, low proliferation, and an indolent course [41].

Aggressive features of MCL derive from genomic alterations such as somatic mutations which occur more often in MCL than in chronic lymphocytic leukemia (CLL), but less often than in DLBCL or other lymphoid malignancies [42, 43]. Next to the typical t(11;14) translocation, rearrangements of *MYC proto-oncogene, BHLH Transcription factor* (*MYC*) have been observed, however these are rather rare [44]. Other genetic alterations that are associated with cell cycle deregulation in MCL include loss of *cyclin dependent kinase inhibitor 2A* (*CDKN2A*; [45]) and *RB transcriptional corepressor 1* (*RB1*; [46]) or amplification of *BMI1 proto-oncogene, polycomb ring finger* (*BMI1*; [47]), and *cyclin dependent kinase 4* (*CDK4*; [48]). The most common mutations affect *ATM serine/threonine kinase* (*ATM*; 42-55%) and *tumor protein p53* (*TP53*; mutations 11%, deletions 16%) causing aberrant DNA damage repair and dysregulated apoptosis [49-51]. Mutations of *notch receptor 1/2* (*NOTCH1/2*) contribute to dysregulated cell death, as well as cell proliferation, and were linked to poor overall survival in MCL [52, 43]. Additionally, somatic mutations in the alternative nuclear factor kappa B (NF-κB) pathway were described for its negative regulators *baculoviral IAP repeat containing 3* (*BIRC3*, 6%) and *TNF receptor associated factor 2* (*TRAF2*, 10%) leading to reduced dependency on classical NF-κB signaling [53].

6.3.2 Diagnosis and clinical background

Initial presentation of MCL patients mostly occurs at progressed disease (Ann Arbor Stage III, IV) with lymphadenopathy and systemic B symptoms (fever, night sweats, unintentional weight loss; [54]). Diagnosis is based on lymph node biopsies or blood aspirates and bone marrow biopsies [55]. Following histopathology, the MCL cells can be assigned to classical variant with small to medium sized B cells containing irregular nuclei or the more aggressive blastoid or pleomorphic variant [26]. The blastoid variant is characterized by medium sized cells resembling lymphoblasts with fine chromatin and roundish nuclei, whereas pleomorphic cells are larger, contain irregular nuclei and resemble DLBCL [56]. In immunohistochemistry, MCL cells usually present with positivity for the T-cell surface glycoprotein CD5 (CD5), the B-lymphocyte antigens CD19 and CD20 (CD19 and CD20), surface immunoglobulin M and D (IgM and IgD), the CD20 epitope FMC-7, strong nuclear positivity for CCND1, SOX11, and are negative for low affinity immunoglobulin epsilon Fc receptor (CD23), neprilysin (CD10), and B-cell lymphoma 6 protein (BCL6; [57]). Uncommonly, MCL patients can also present with $CD10^{+}$, $CD5^{-}$, $CCND1^{-}$, $SOX11^{-}$, and $CD23^{+}$. Fluorescence in situ hybridization (FISH) analysis is performed for the detection of the translocation t(11;14) and may include *TP53* status. Further methods include computed tomography (CT) of neck, chest, abdomen, and pelvis, gastrointestinal endoscopy to detect or assess gastrointestinal involvement, full blood count including L-lactate dehydrogenase (LDH), uric acid levels, and testing for infections with immunodeficiency virus (HIV), hepatitis B and C [57, 58]. As the central nervous system is only rarely affected, lumbar punctures are performed only in the case of neurological symptoms or for high-risk patients. The Ann Arbor classification serves for initial staging and for evaluating disease progression with respect to number and localization of affected lymph node regions, extranodal or extralymphatic involvement (early stage I, II; advanced stage III, IV), and includes an additional indicator for the presence or absence of systemic B symptoms [59]. The combined MCL International Prognostic Index (MIPI-c) assigns patients to four prognostic groups (high, high-intermediate, low-intermediate, low) based on their age, Eastern Cooperative Oncology performance status, LDH levels, leucocyte count, and proliferation marker protein Ki-67 (Ki-67) index. Ki-67 status helps to assess the aggressiveness of tumor cells, with Ki-67 expression above 30% indicating high proliferative activity associated with worse overall survival [39].

6.3.3 B-cell receptor signaling

The expression and proper function of the BCR is imperative for B-cell development [60]. Research in the field of primary immunodeficiency X-linked agammaglobulinemia (XLA) by the pediatrician Dr. Ogden Bruton led to the discovery that a mutated tyrosine kinase gene, named *Bruton tyrosine kinase* (*BTK*) after its inventor, resulted in dysfunctional B-cell development with a deficiency of mature peripheral B and plasma cells in circulation [61]. As de Weers et al. showed, that stimulation of the BCR leads to tyrosine phosphorylation of the tyrosine-protein kinase BTK (BTK), the kinase endowed a central role in functional BCR signaling [62].

The BCR consists of a membrane immunoglobulin (mIg) and a disulfide-bonded B-cell antigen receptor complex-associated protein alpha and beta chain (CD79A-CD97B) heterodimer, whose cytoplasmic domains contain the immunoreceptor tyrosine-based activation motifs (ITAMs) [63]. Upon binding of antigens and cross-linking of BCR, downstream signaling involves 1-phosphatidylinositol 4,5-bisphosphate phosphodiesterase gamma-1 (PLCγ), mitogen-activated protein kinase (ERK, MAPK), NF-κB signaling molecules and RAC-alpha serine/threonine-protein kinase (AKT). These non-receptor protein tyrosine kinases mediate the key signaling in B cells. In detail, ITAMs are phosphorylated after cross-linking of the BCR by a Src-family protein tyrosine kinase, e.g. tyrosine-protein kinase Lyn (LYN), resulting in the activation of tyrosine-protein kinase SYK (SYK) at created docking sites [64]. Following phosphorylation of the cytoplasmic domain of the BCR co-receptor CD19 by LYN, phosphatidylinositol 4,5-bisphosphate 3-kinase (PI3K) is activated and then produces phosphatidylinositol 3,4,5-trisphosphate (PIP3) [65]. One function of PIP3 is the recruitment of AKT to the cell membrane, where it is phosphorylated twice to become fully activated [66]. AKT exerts anti-apoptotic functions and mediates pro-survival signals through activation of serine/threonine-protein kinase mTOR (mTOR; [67, 68]). Secondly, PIP3 recruits BTK to the cell membrane, where SYK or LYN phosphorylates the BTK causing subsequent autophosphorylation and leading to its full activation [69, 70]. The BTK is then able to phosphorylate PLCγ2, which, in turn, cleaves phosphatidylinositol 4,5-bisphosphate (PIP2) into inositol 1,4,5-trisphosphate (IP3) and diacylglycerol (DAG), which acts as a second messenger activating protein kinase C beta type (PKCβ) [71]. PKCβ can then activate MAPK family members, such as ERK1/ERK2 by phosphorylation via RAS signaling or directly activate the classical NF-κB pathway through the CBM complex consisting of caspase recruitment domain-containing protein 11 (CARD11), B-cell lymphoma/leukemia 10 (BCL10), and mucosa-associated lymphoid tissue lymphoma translocation protein 1 (MALT1) [72]. The CBM complex induces activation of the multi-subunit inhibitor of nuclear factor kappa-B kinase (IKK) complex which phosphorylates the inhibitor of nuclear factor kappa-B (IκB) releasing the bound NF-κB into the nucleus. Saba et al. proved the importance of BCR and canonical NF-κB signaling for tumor proliferation especially in MCL of the lymph nodes [73].

6.3.4 Frontline treatment

Even though MCL may progress aggressively, patients with asymptomatic presentation, low tumor burden, and stable disease can be monitored with a “watch and wait”-strategy for a long period of time [74]. However, most patients require immediate treatment tailored to their physical condition and age (Figure 2). The toxicity of the chosen therapy and the patient’s comorbidities dictate the therapeutic regimen to ensure the best possible quality of life, as chemotherapies, particularly in elderly patients, can be associated with severe side effects such as hematologic malignancies, myelotoxicity, and neurotoxicity, limiting their applicability [75].

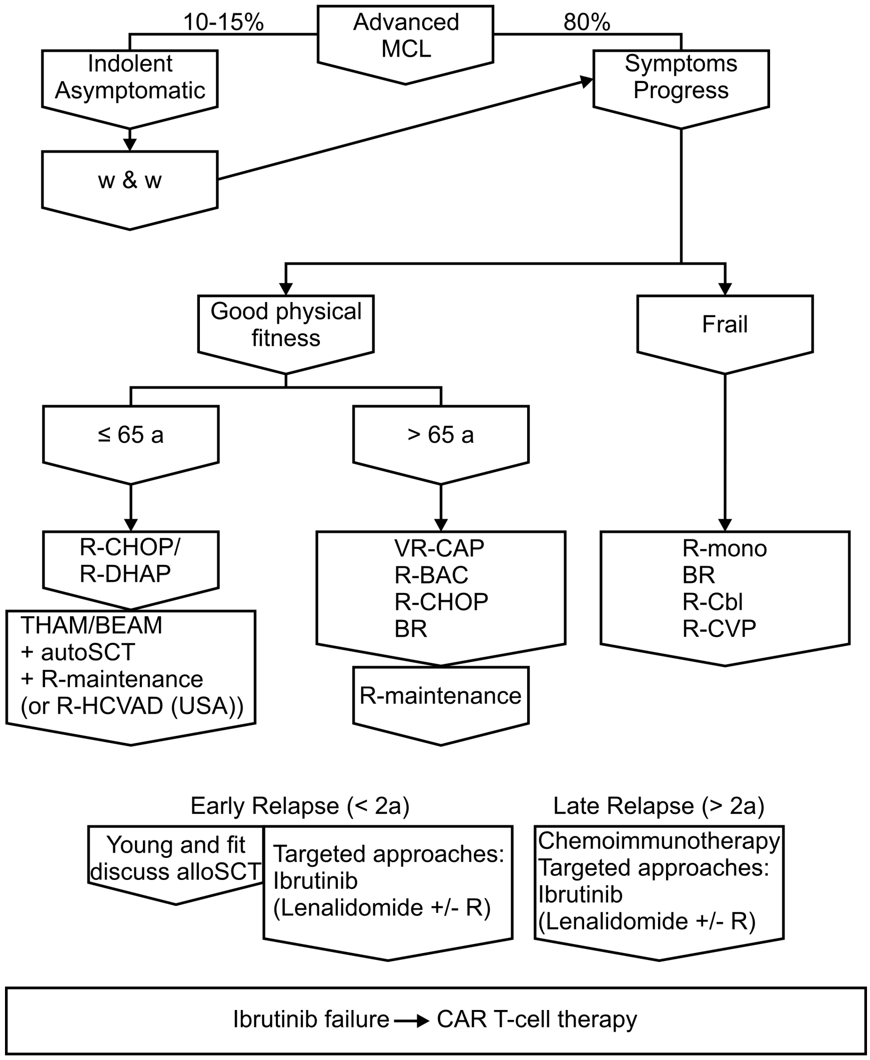

Figure 2: Treatment of advanced mantle cell lymphoma (Ann Arbor Stage III, IV). Abbreviations: w & w – watch and wait; R – rituximab; CHOP – cyclophosphamide, doxorubicin, vincristine, prednisone; DHAP – dexamethasone, high-dose cytarabine, cisplatin; THAM – total body irradiation, high-dose cytarabine, melphalan; BEAM – carmustine, etoposide, cytarabine, melphalan; HCVAD – cyclophosphamide, vincristine, doxorubicin, dexamethasone; VR-CAP – rituximab, cyclophosphamide, doxorubicin, bortezomib, prednisone; BAC – bendamustine, cytarabine; BR – bendamustine, rituximab; Cbl – chlorambucil; CVP – cyclophosphamide, vincristine, prednisone; autoSCT – autologous stem cell transplantation; alloSCT – allogeneic stem cell transplantation. Modified from onkopedia guidelines on mantle cell lymphoma (May 2021; [58]) and Silkenstedt et al. [23].

Autologous stem cell transplantation following chemoimmunotherapy in combination with rituximab and high-dose consolidation regimen represents the most promising option for young (≤ 65 years) and fit patients [26]. Owing to the superiority of cytarabine-based regimens before transplantation, induction therapy includes R-DHAP (rituximab plus dexamethasone, high-dose cytarabine, and cisplatin [or oxaliplatin, carboplatin]) as a standard of care [76, 26]. A regimen with alternating cycles of R-DHAP and R-CHOP (rituximab with cyclophosphamide, doxorubicin, vincristine, and prednisone) was shown to prolong remission compared to R-CHOP alone and reduces the usage of toxic alkylating (cyclophosphamide) and anthracycline (doxorubicin) agents [77]. Total-body irradiation with high-dose cytarabine and melphalan (THAM), accompanied by a higher risk for long-term toxicity, and/or R-BEAM (rituximab, carmustine, etoposide, cytarabine, and melphalan) serve as transplantation conditioning regimens [78]. Rituximab maintenance following autoSCT improved overall survival of young patients significantly [79]. An intensive chemoimmunotherapy containing hyperfractionated cyclophosphamide, vincristine, doxorubicin, and dexamethasone plus rituximab (R-HCVAD) with alternating methotrexate/cytarabine represents a common strategy in the United States (US) which yielded high complete response rates but was accompanied by toxic side effects [57, 23].

As the disease most commonly affects people of advanced age (> 65 years), dose-intensified approaches may be inappropriate. Conventional chemoimmunotherapies including R-CHOP or bendamustine in combination with rituximab (BR) plus rituximab maintenance are selected for older patients who are not eligible for autoSCT [80]. A regimen including bortezomib, rituximab, cyclophosphamide, doxorubicin, and prednisone (VR-CAP) may serve as another option, as it improved the overall survival of patients dramatically compared to R-CHOP [81]. Despite of its efficacy, the treatment may only be administered to high-risk patients due to the reported hematological toxicity. The same is true for treatment with rituximab, bendamustine, and cytarabine (R-BAC) [82].

In elderly patients with multiple comorbidities, less aggressive, low-dose chemoimmunotherapies such as rituximab monotherapy or rituximab in combination with bendamustine (BR), chlorambucil (R-Cbl) or cyclophosphamide, vincristine, and prednisolone (R-CVP) are chosen [23].

6.3.5 Treatment at first relapse

Even though the initial response rate in MCL is high, patients relapse, and the remission duration shortens with each line of treatment [83]. An allogeneic stem cell transplantation (alloSCT) as consolidation after response to second-line treatment allows for long-term disease-free survival [84]. Due to the high risk for severe side effects and transplant-related mortality, the approach may be considered for young and fit patients with aggressive variants and without active disease [23]. Nevertheless, most patients are not available for alloSCT and receive a non-cross resistant chemotherapy with rituximab, that is high-dose cytarabine or bendamustine-based regimens such as R-BAC, when CHOP served as frontline treatment [26].

Over the past decade, targeted approaches extended the range of therapy options in relapsed/refractory (RR) MCL. Since conventional chemotherapies are associated with severe toxicities, targeted treatment approaches are preferred as they ideally harm the tumor cells with fewer side effects on normal tissues and organs [85].

The use of immunomodulatory agent lenalidomide, with direct cytotoxicity on tumor cells and positive stimulating effects on immune cells in microenvironment, resulted in longer progression-free survival in RR MCL compared with other single-agent therapies and is approved as treatment in relapse setting [86]. Despite the associated adverse events of neutropenia and thrombocytopenia, the combination with rituximab in first-line therapy proved clinical efficacy with respect to high response rates and survival [87].

The proteasome inhibitor bortezomib represents the first targeted approach which was approved as single-agent therapy for treatment of RR MCL in the US [88]. Due to the improved outcome with VR-CAP treatment, bortezomib was also approved for frontline therapy of MCL in the US and Europe [81]. In other settings, e.g. in combination with high-dose cytarabine in RR MCL [89] or with CHOP after first relapse [90], bortezomib showed activity in heavily pretreated patients and improved response and survival compared to CHOP only, respectively.

The mTOR inhibitor temsirolimus improved survival and response in RR MCL compared to other single agents leading to its approval by the European Medicine Agency in 2009 [91]. In combination with bendamustine and rituximab, temsirolimus yielded promising results considering the response in relapsed MCL [92].

Targeting the apoptosis regulator Bcl-2 (BCL2) with venetoclax is a promising strategy, as the inhibitor achieved a response rate of 75% in MCL, which was the highest among the included NHL subtypes [93].

Due to the compelling results of single-agent ibrutinib in RR MCL in 2013, the BTK inhibitor revolutionized the field and much research and clinical trials focused on its efficacy over the past decade [94]. Besides its good tolerability, its superior efficacy compared with other therapies was particularly evident when used in early relapse (< 2 a) from first-line and is therefore the recommended second-line therapy [95, 96]. Since the combination of venetoclax and ibrutinib showed high efficacy in RR MCL, a phase III study started to assess whether the combination is superior to single ibrutinib therapy (SYMPATICO, NCT03112174; [97]).

6.3.6 Ibrutinib

A historic breakthrough in targeted treatment was the efficient inhibition of a dysregulated protein kinase in chronic myeloid leukemia (CML) by imatinib leading to its approval by the United States Food and Drug Administration (FDA) in 2001 [98]. Along this line, small molecules were developed which were able to block the BTK following the identification of its structure in the context of research on XLA in 1993 [99]. The first promising candidate, PCI-32765, later named ibrutinib, demonstrated clinical activity in dogs with spontaneous

B-cell NHL and was enrolled in clinical trials [100]. The inhibitor covalently and irreversibly binds to the cysteine 481 in the active site of BTK with an half maximal inhibitory concentration (IC_{50}) of 0.5 nM [101]. The inhibition of BTK was associated with reduced cell growth and survival of tumor cells [102]. Ibrutinib weakened the phosphorylation of downstream kinases AKT and ERK1/2 which could be linked to the triggered cell death [103]. In clinical setting, ibrutinib causes decreased adhesion and chemotactic activity in MCL cells and provokes the redistribution of tumor cells into the blood [104].

Advani et al. published the first results of ibrutinib treatment in RR B-cell malignancies, whereby the responses in MCL patients were outstanding [105]. Due to the superior effects compared to standard chemotherapy in RR MCL, ibrutinib gained approval by the FDA in 2013 as well as in Europe in 2014 and is sold under the trade name Imbruvica® [94]. By now, the FDA has approved ibrutinib for CLL, Waldenström's macroglobulinemia, RR marginal zone lymphoma, and previously treated chronic graft-versus-host disease.

Ibrutinib is a well-tolerated drug, which can be easily taken orally by patients at home [106]. Preliminary results suggested that a combination of ibrutinib with rituximab as first-line therapy may be beneficial in MCL, as its efficacy might be higher in treatment-naïve state and it would provide a chemotherapy-free option for old patients with frail condition [107].

6.3.6.1 Ibrutinib resistance

Apart from primary resistance, which occurs in 10.2% to 35% of cases, 17.5 – 54% of MCL patients acquire a secondary resistance to the BTK inhibitor [108]. The reasons for resistance are multifaceted and only some have been studied so far.

In primary resistance, dysregulation of distal BCR signaling such as persistent PI3K-AKT activation is assumed to play a role [109]. Additionally, MCL cells become insensitive to BTK inhibition when dependency on BCR-driven activation of the classical NF-κB pathway is lost by activating mutations in the alternative NF-κB pathway [53]. These characteristics were found in the MCL lines Z-138 and MAVER-1, which carry deletions in the negative regulators of the alternative NF-κB pathway TRAF2 and TRAF3, respectively [53]. Aberrant activation of the alternative pathway can also be triggered by Epstein-Barr virus infection as in the MCL cell lines Granta-519, JVM-2, and JVM-13 [110].

Previously reported mechanisms of secondary resistance include a C481S mutation at the ibrutinib binding site of the BTK, which results in reduced binding of the inhibitor and is associated with higher BTK and PI3K-AKT activity [109]. However, the *BTK* mutation is a rather rare event occurring in 16-17% of cases, whereas mutations in *TP53*, *ATM*, and *nuclear receptor binding SET domain protein 2* (*NSD2*) are more common at disease progression after ibrutinib therapy [111, 112]. In 5.5% of patients in an MCL cohort, a

mutation in *caspase recruitment domain family member 11* (*CARD11*) was detected which may support the chronic activation of BCR in MCL cells downstream of BTK [113].
Next to inherent characteristics of tumor cells, adjacent cells can shield them from chemotherapeutic agents by forming protective niches. In MCL, the tumor microenvironment (TME) may trigger initiation of cell cycle progression and confer drug resistance [114]. Additionally, Zhao et al. identified PI3K-AKT-mTOR and β1-integrin signaling as pivotal drivers of TME-mediated ibrutinib resistance [115].

6.3.6.2 Second generation BTK inhibitors

In addition to BTK, ibrutinib can inhibit the epidermal growth factor receptor (EGFR), the tyrosine-protein kinase ITK/TSK (ITK), and other kinases of the TEC family [116]. As these kinases are also expressed by T cells, NK cells, platelets, and macrophages, ibrutinib impairs their proper cell function [117-120]. Off-target activity of the covalent inhibitor may contribute to some clinically observed adverse events including bleeding, diarrhea, rash, infection, and atrial fibrillation [121, 118, 122]. Therefore, second generation BTK inhibitors have been developed. Similar to ibrutinib, acalabrutinib and zanubrutinib bind covalently to Cys481 and irreversibly block BTK, with acalabrutinib having the lowest off-target rate and highest selectivity among the three, and reduced cardiotoxicity compared to ibrutinib [116, 123]. Non-covalent inhibitors are studied since, as opposed to their irreversible counterparts, they may also be effective in C418 mutated tumors due to a different mechanism of BTK inhibition. Pirtobrutinib has been tested in advanced B-cell malignancies including MCL and showed efficacy and good tolerability [124]. As the inhibitor reversibly binds to the ATP-binding pocket of BTK, but at a different site than the C418 residue, it is also beneficial for patients with prior covalent BTK inhibitor therapy [125].

6.3.7 Treatment of ibrutinib-resistant patients

Ibrutinib-resistant MCL cells are characterized by high proliferation, poor response to following treatments, and patients have a short survival [126]. The progression of the disease with blastoid transformation is often associated with *TP53* mutations [112].
At the second relapse, chemoimmunotherapy or targeted approaches may be appropriate, preferably within clinical trials. While one study showed that salvage chemoimmunotherapy has very poor outcome with only 32% response rate in post-ibrutinib patients [127], the R-BAC regimen revealed a high response rate of 83% in patients pretreated with a BTK inhibitor (ibrutinib, acalabrutinib, tirabrutinib, M7583) and allowed successful bridging to alloSCT [128]. Venetoclax monotherapy with 53% response rate might provide another option with low toxicity [129]. Treatment with lenalidomide or lenalidomide combinations

only yielded 29% response and a median duration of response of only 5 months [130]. The use of second generation BTK inhibitors may serve as a future alternative. Cohen et al. reported 52% overall response rate for pirtobrutinib in MCL patients pretreated with covalent BTK inhibitors in a phase I/II clinical trial [125]. Except for the promising results with R-BAC, the overall and complete response to therapies after ibrutinib failure is poor, with short survival rates of barely more than one year.

The latest and most impressive innovation for treatment of RR MCL is Chimeric antigen receptor T (CAR T)-cell therapy [131]. The ZUMA-2 study (NCT02601313) evaluated brexucabtagene autoleucel (KTE-X19) autologous anti-CD19 CAR T-cell therapy (Tecartus®) in RR MCL following one to five therapies including a BTK inhibitor [132]. The high objective response rate of around 90% with durable response in this heavily pretreated group led to its approval for RR MCL in the US (2020) and in Europe (2021). Due to the promising 3-year follow-up, extended follow-up is awaited to assess long-term remission with CAR-T KTE-X19 and its potential curative role [133]. Even though the safety profile of CAR T-cell therapy is considered as tolerable, treatment can cause severe life-threatening adverse events like cytokine release syndrome or immune effector cell-associated neurotoxicity syndrome [134]. Consequently, not all patients, usually of advanced age and with multiple comorbidities, are eligible.

6.4 Single-cell RNA sequencing in cancer

Next-generation sequencing has enabled high-throughput analysis of the genome, transcriptome, and epigenome, paving the way for genome-driven oncology [135]. Apart from the understanding of genetic alterations as the root for cancer, genome activity determines the behavior of diverse entities and subtypes. Therefore, exploring the transcriptomic landscape of cancer cells is crucial for functional genomic analysis identifying pathway dependencies or other vulnerabilities [136]. Intratumoral heterogeneity requires resolution at the single-cell level to detect biologically relevant differences within seemingly homogenous cancer cells [137]. Especially cell-to-cell differences in response to drug treatment dictate the success and duration of therapy, given the risk of resistant clones [138].

Analysis of individual cells has first been realized by microscopy and flow cytometry, and has progressed to single-cell microarrays and multiplexed quantitative reverse transcription polymerase chain reaction (qRT-PCR) with microfluidic systems to study differential gene expression [139]. However, these methods are limited by sensitivity and scope of information. Single-cell RNA sequencing (scRNA-seq) combines advanced techniques in cell isolation and ultra-high-throughput analysis enabling sequencing of thousands of cells and genes at reduced costs [140]. Compared to bulk RNA sequencing (RNA-seq), scRNA-seq can identify rare cell populations and elucidate variable temporal dynamics across evolutionary processes or exposure to extrinsic stimuli at unprecedented resolution [141].

6.4.1 Droplet-based single-cell RNA sequencing

To overcome limitations concerning throughput of plate-based methods for the isolation of single cells by fluorescence-activated cell sorting (FACS), microfluidic approaches were refined using droplet-based techniques [142]. 10x Genomics offers a commercially available platform for capturing high numbers of cells by applying the GemCode™ technology [143]. In the 10x Genomics Chromium Controller with a multi-channel microfluidic chip, a single cell in solution with reagents for reverse transcription is encapsulated together with one unique barcoded gel bead by an oil phase forming the single-cell Gel Beads-in-emulsion (GEM). This reaction chamber allows for separated cell lysis, reverse transcription of transcripts into cDNA, and unique barcoding of the cDNA of every cell. Thereby, each transcript can be assigned to its cell of origin after pooled PCR amplification, library preparation and sequencing. The chemistry used by 10x covers only the 3' ends of the transcripts, not the full-length sequence as is the case with Smart-seq2 [144]. Besides, the protocol uses polydT primers for reverse transcription to specifically capture polyadenylated mRNA. Cell capture efficiency is approximately 50% and about 15% of mRNA transcripts per cell are detected using v2 chemistry of 10x. However, since multiple cells from the same subpopulation are sequenced, coverage of nearly the entire transcriptome is ensured [142].

7 Aim of this Thesis

Despite the improved prognosis with second-line ibrutinib therapy in MCL, patients ultimately relapse. In view of the diminishing response to any subsequent treatment with increased aggressiveness and proliferation of resistant cells, the ibrutinib regimen must be improved. As resistance to the BTK inhibitor is poorly understood, the transcriptomic alterations of sensitive MCL cells were tracked across treatment by time-resolved scRNA-seq using a cell line model to elucidate escape mechanisms that are potential targets for ibrutinib add-on or follow-up therapies. The identified adaptations to treatment were evaluated in cell lines and primary cells for their potential as therapeutic approaches in MCL to enhance the efficacy of ibrutinib therapy and circumvent acquired resistance.

8 Materials

8.1 Reagents and cell culture media

Name	Manufacturer
3-[4,5-dimethylthiazol-2-yl]-2,5-diphenyltetrazolium bromide (MTT)	Sigma-Aldrich, St.Louis, MO, USA
Ammonium persulfate (APS)	Sigma-Aldrich
Aprotinin	AppliChem, Darmstadt
β-Mercaptoethanol	AppliChem
Bovine serum albumin (BSA)	Sigma-Aldrich
Bradford Reagent	Sigma-Aldrich
Bromophenolblue	AppliChem, Darmstadt
Dipotassium hydrogen phosphate (K_2HPO_4)	AppliChem
Disodium hydrogen phosphate dihydrat ($Na_2HPO_4 \times 2H_2O$)	Sigma-Aldrich
Dithiothreitol (DTT)	Sigma-Aldrich
DMEM medium, Gibco™	Thermo Fisher Scientific, Waltham, MA, USA
Dymethyl sulfoxide (DMSO)	AppliChem
Dulbecco’s Phosphate Buffered Saline (1x, DPBS)	Sigma-Aldrich
Ethanol absolute for molecular biology	AppliChem
Ethylenediaminetetraacetic acid (EDTA)	AppliChem
Fetal bovine serum (FBS), Gibco™	Thermo Fisher Scientific
Ficoll® Paque Plus	Cytiva, Marlborough, MA, USA
GelRed™ 10000X	Genaxxon bioscience, Ulm
Glycerol	Carl Roth
Glycine	AppliChem
Hydrogen peroxide (H_2O_2) 30%	Merck, Darmstadt
Horse serum, Gibco™	Thermo Fisher Scientific
Human IL-4, premium grade	Miltenyi biotec, Bergisch Gladbach
Hydrochloric acid (HCl)	AppliChem
IACS-010759	Selleck Chemicals, Absource Diagnostics, Munich
Ibrutinib	Selleck Chemicals
Igepal® CA-630	Sigma-Aldrich
IMDM medium, Gibco™	Thermo Fisher Scientific

Name	**Manufacturer**
Isopropanol	AppliChem
L-Glutamine 200 mM	PAN-Biotech, Aidenbach
MEGACD40L® Protein	Enzo Life Sciences, Lörrach
MEM NEAA, Non-Essential Amino Acid Solution (100x)	PAN-Biotech
Methanol	AppliChem
Milk Powder	Heirler Cenovis, Radolfzell
OptiPrep™ - Iodixanol	Serumwerk Bernburg, Bernburg
PageRuler™ Plus Prestained Protein Ladder	Thermo Fisher Scientific
Pefablock	Sigma-Aldrich
Penicillin-Streptomycin	PAN-Biotech
Phenylmethyl sulphonyl fluoride (PMSF)	Carl Roth
Poly-D-lysine hydrobromide	Sigma-Aldrich
Ponceau S solution	Sigma-Aldrich
Potassium chloride (KCl)	Sigma-Aldrich
Propidium iodide	Sigma-Aldrich
Radiance Plus	Azure Biosystems, Dublin, CA, USA
RNase A	Qiagen, Hilden
Rotiphorese®Gel 30 (37.5:1)	Carl Roth, Karlsruhe
RPMI 1640 medium, Gibco™	Thermo Fisher Scientific
Seahorse XF 200 mM glutamine solution	Agilent Technologies, Santa Clara, CA, USA
Seahorse XF 1.0 M glucose solution	Agilent Technologies
Seahorse XF Calibrant	Agilent Technologies
Seahorse XF RPMI medium pH 7.4	Agilent Technologies
Sodium azide (NaN_3)	Sigma-Aldrich
Sodium chloride (NaCl)	AppliChem
Sodium dodecyl sulfat (SDS)	AppliChem
Sodium orthovanadate (Na-O-V)	AppliChem
StemMACS™ HSC Expansion Media XF, human	Miltenyi biotec
SuperSignal™ West Pico Plus Chemiluminescent Substrate	Thermo Fisher Scientific
Tetramethylethylenediamine (TEMED)	AppliChem
Tris ultrapure	AppliChem
Triton® X-100	AppliChem

Name	Manufacturer
Trypan blue	Sigma-Aldrich
Tween® 20	AppliChem
Water (sterile)	Sigma-Aldrich

8.2 Antibodies

8.2.1 Western blot

Name	Catalog Number	Manufacturer
β-Actin	4970	Cell Signaling Technologies, Danvers, MA, USA
AKT	4691	Cell Signaling Technologies
p-AKT	4058	Cell Signaling Technologies
Anti-rabbit IgG, HRP-linked Antibody	7074	Cell Signaling Technologies
BTK	3533	Cell Signaling Technologies
p-BTK	5082	Cell Signaling Technologies
Caspase-9	9502	Cell Signaling Technologies
ERK1/2	9102	Cell Signaling Technologies
p-ERK1/2	9101	Cell Signaling Technologies
LDHA	3582	Cell Signaling Technologies
PARP	9532	Cell Signaling Technologies

8.2.2 Flow cytometry

Name	Catalog Number	Manufacturer
C3b/iC3b-FITC	846108	BioLegend, San Diego, CA, USA
CD19-FITC	FAB4867F	R&D Systems, Minneapolis, MN, USA
CD37-PE	103-123-329	Miltenyi Biotech, Bergisch Gladbach
CD40-PE	130-111-063	Miltenyi Biotech
CD52-APC	130-099-632	Miltenyi Biotech
CD52-PE	130-123-972	Miltenyi Biotech
CD79B-PE	130-099-106	Miltenyi Biotech
Mouse IgG1κ-FITC	IC002F	R&D Systems
REA Control Antibody (S), PE	130-113-438	Miltenyi Biotech

Name	Catalog Number	Manufacturer
REA Control Antibody (S), APC	130-113-434	Miltenyi Biotech

8.2.3 Cytotoxicity

Name	Catalog Number	Manufacturer
CD52 Monoclonal Antibody (YTH34.5)	MA5-16999	Invitrogen, Thermo Fisher Scientific, Waltham, MA, USA
Rat IgG2bκ Isotype Control (eB149/10H5), Functional Grade, eBioscience™	16-4031-81	Invitrogen, Thermo Fisher Scientific

8.3 Consumption items

Name	Manufacturer
Amersham™ Hyperfilm™ ECL	Cytiva, Marlborough, MA, USA
Amersham™ Protran™ nitrocellulose membrane	Cytiva
Blotting paper (0.35 mm, medium absorbent)	Hartenstein, Würzburg
Tubes, cell culture flasks and well plates	Greiner Bio-One, Kremsmünster, Austria
Millipak® 0.22 µm filter	Merck, Darmstadt
Pipette tips	Biozym Scientific, Hessisch Oldendorf; Nerbe Plus, Winsen
S1 Flowcell	Illumina, San Diego, CA, USA
Safety-Multifly®-Needle	Sarstedt, Nümbrecht
Seahorse XFe96 Cell Culture Microplate and XF sensor cartridges	Agilent Technologies, Santa Clara, CA, USA
Serological pipettes, tubes for flow cytometry, reaction tubes, tissue culture dishes	Sarstedt
S-Monovette® Serum, 7.5 ml	Sarstedt
S-Monovette® K3 EDTA	Sarstedt

8.4 Laboratory equipment

Name	Manufacturer
2100 Bioanalyzer Instrument	Agilent Technologies, Santa Clara, CA, USA
BD FACS Aria III	BD Biosciences, Franklin Lakes, NJ, USA
BD FACS Canto II	BD Biosciences

Name	Manufacturer
Chromium Controller	10x Genomics, Pleasanton, CA, USA
Countess® II FL Automated Cell Counter	Thermo Fisher Scientific, Waltham, MA, USA
Countess™ Reusable Slide	Thermo Fisher Scientific
Discovery Comfort multichannel pipettes	HTL Lab Solution, Warszawa, Poland
Eppendorf 5415R Refrigerated Centrifuge	Eppendorf, Hamburg
Eppendorf 5425 Centrifuge	Eppendorf
EVOS^{TM} M7000 Microscope	Thermo Fisher Scientific
FLUOstar® Omega Microplate Reader	BMG Labtech, Ortenberg
Fusion SL, western blot imager	Vilber Lourmat, Eberhardzell
Hybex® Microsample Incubator	SciGene, Sunnyvale, CA, USA
Heracell^{TM} 150 CO_2 Incubator	Thermo Fisher Scientific
Heraeus^{TM} Labofuge^{TM} 400R	Thermo Fisher Scientific
Heraeus^{TM} Megafuge^{TM} 1.0	Thermo Fisher Scientific
Microscope Labovert	Ernst Leitz, Wetzlar
Micropipettes	Eppendorf; Gilson, Middleton, WI, USA
Milli-Q® EQ 7000 Ultrapure water purification system	Merck, Darmstadt
Mini-PROTEAN® Tetra Cell	Bio-Rad, Hercules, CA, USA
Mini-PROTEAN® Tetra Cell Casting Stand and Clamps	Bio-Rad
Mr. Frosty™ Freezing Container	Thermo Fisher Scientific
NanoDrop 1000 Spectrophotometer	Thermo Fisher Scientific
NextSeq® 500 System	Illumina, San Diego, CA, USA
NovaSeqTM 6000 System	Illumina
Perfect Blue^{TM} Tank-Electroblotter	VWR, Leuven, Belgium
Pipette controller accu-jet® pro	Brand, Wertheim
PowerPac^{TM} 200 Power Supply	Bio-Rad
Qubit^{TM} 3.0 Fluometer	Thermo Fisher Scientific
Seahorse XFe96 Metabolic Flux Analyzer	Agilent Technologies
Unimax 1010 Shaker	Heidolph Instruments, Schwabach
Vortex-Genie 2	Scientific Industries, Bohemia, NY, USA
WTW inoLab® pH 720	Xylem Analytics, Weilheim

8.5 Solutions and buffers

Solutions and buffers were prepared with ultrapure water. Percentages indicate weight of solid solutes per volume of solution (w/v, [g/100 ml]) and volume of liquid solutes per volume of solution (v/v, [ml/100ml]).

Name	**Composition**
Buffer for flow cytometry (FACS-buffer)	1x PBS 0.5% BSA 2 mM EDTA
Blotting buffer	1x WB buffer 0.03% SDS 20% Methanol
Loading buffer (4x)	200 mM Tris, pH 6.8 40% Glycerol 8% SDS 4% β-Mercaptoethanol 0.01% Bromophenolblue 50 mM EDTA
Lysis buffer	20 mM HEPES, pH 7.9 350 mM NaCl 1 mM $MgCl_2$ 0.5 mM EDTA, pH 8.0 0.1 mM EGTA, pH 8.0 1 mM Na-O-V 1% Igepal® 0.5% DTT 0.1 mg/ml Pefablock 1 µg/ml Aprotinin 0.6 µg/ml PMSF
MTT solution	5 mg/ml MTT in DPBS
Phosphate-buffered saline (PBS; 10x)	27 mM KCl 20 mM K_2HPO_4 1.37 mM NaCl 100 mM $Na_2HPO_4 \times 2H_2O$
Running buffer	1x WB buffer 0.1% SDS
Separating gel buffer	1.5 M Tris, pH 8.8 0.4% SDS
Separating gel (10% acrylamide)	4.6 ml Ultrapure water 2.75 ml separating gel buffer 3.7 ml Rotiphorese®Gel 30 187 µl APS (10%) 15.4 µl TEMED
Solubilization buffer for MTT assay	0.01 M HCl 10% SDS

Name	Composition
Stacking gel buffer	1 M Tris, pH 6.8 0.4% SDS
Stacking gel (6% acrylamide)	3.8 ml Ultrapure water 1.75 ml stacking gel buffer 1.4 ml Rotiphorese®Gel 30 84 µl APS (10%) 7 µl TEMED
Tris-buffered saline (TBS, 10x)	200 mM Tris, pH 7.6 1.37 mM NaCl
Tris-buffered saline with Tween® 20 (TBS-T)	1x TBS 0.1% Tween® 20
Trypan blue solution	0.5% Trypan blue 0.9% NaCl
Western blot (WB) buffer (10x)	250 mM Tris 1.92 M Glycine

8.6 Kits

Name	Manufacturer
Agilent DNA 1000 Kit	Agilent Technologies, Santa Clara, CA, USA
Agilent High Sensitivity DNA Kit	Agilent Technologies
Agilent RNA 6000 Nano Kit	Agilent Technologies
AllPrep DNA/RNA Mini Kit	Qiagen, Hilden
Chromium Single Cell 3' Library & Gel Bead Kit v2	10x Genomics, Pleasanton, CA, USA
PhiX Control	Illumina, San Diego, CA, USA
RNase-Free DNase Set	Qiagen
TruSeq Stranded mRNA Library Preparation Kit	Illumina
Venor® GeM OneStep kit	Minerva Biolabs, Berlin

8.7 Software

Name	Version/Year	Manufacturer/Developer Reference
Bcl2fastq2	2.20.0.422	Illumina, San Diego, CA, USA
Cell Ranger	3.0.1	10x Genomics, Pleasanton, CA, USA
Corel PHOTO-PAINT	2019	Alludo, Ottawa, ON, Canada
Cutadapt	2.5	Martin et al. [145]
FACS Diva Software	6.1.3	BD Bioscience, CA, USA

Name	Version/Year	Manufacturer/Developer Reference
Flowing Software	2.5.1	Perttu Terho, Turku Center for Biotechnology, University of Turku, Finland, in collaboration with Turku Bioimaging
ImageJ	1.53e	Schneider et al. [146]
Microsoft Excel	2016	Microsoft Corporation, Redmond, WA, USA
OriginPro®	2021b	OriginLab Corporation, Northampton, MA, USA
R	3.6.0	R Development Core Team [147]
RStudio	1.1.456	RStudio Team [148]
R packages		
ClusterProfiler	3.14.3	Yu et al. [149]
DESeq2	1.24.0	Love et al. [150]
featureCounts	1.6.4	Liao et al. [151]
SCENIC	1.1.2.2	Aibar et al. [152]
Seurat	3.0.2	Butler et al. [153]
STAR	2.7.2b	Dobin et al. [154]

9 Methods

9.1 Serum

9.1.1 Preparation of human serum

Human blood was provided by the Interdisciplinary Bank of Biomaterials and Data and was used in compliance with the ethical guidelines of the Medical Faculty. Blood was collected in tubes containing clot activators (S-Monovette® Serum). The tubes were flipped several times and left in the upright position for 30 min to ensure complete coagulation of the blood before they were centrifuged at 2 000 × g for 10 min at room temperature (RT). The serum was aspirated and stored in 2 ml freezing tubes at -20 °C.

9.1.2 Heat-inactivation of serum

Fetal bovine serum (FBS), horse serum, and human serum were heat-inactivated for 30 min at 56 °C using a water bath.

9.2 Culturing of cell lines and primary cells

9.2.1 Cell lines

The MCL cell lines REC-1 (ACC 584), MAVER-1 (ACC 717), JEKO-1 (ACC 553), MINO (ACC 687), GRANTA-519 (ACC 342), JVM-2 (ACC 12), and JVM-13 (ACC 19) were obtained from the Deutsche Sammlung von Mikroorganismen und Zellkulturen (DSMZ, Braunschweig) and the Z-138 was supplied from the American Type Culture Collection (ATCC, Manassas, VA, USA) via the Lymphoma Research Foundation. UPN-1 and HBL-2 were provided by Dolors Colomer (Institut d'Investigacions Biomèdiques August Pi i Sunyer [IDIBAPS], Barcelona, Spain) and Florian Bassermann (Department of Medicine III, Technical University of Munich, Munich) respectively. A working stock and master stock system was applied for the storage and cultivation of all cell lines. The REC-1, JVM-2, JVM-13, UPN-1, and HBL-2 grew in RPMI 1640 medium supplemented with 2 mM glutamine and 10% of heat-inactivated FBS. MAVER-1, JEKO-1, and MINO were cultured in RPMI 1640 medium with 2 mM glutamine and 20% of heat-inactivated FBS. Z-138 and GRANTA were maintained in IMDM containing 10% heat-inactivated horse serum and DMEM with 10% heat-inactivated FBS, respectively. All cell lines were cultured in cell culture incubators at 37 °C, 5% CO_2, and humidified atmosphere. Medium was changed every 2 to 3 d. The supernatant of all cell lines regularly underwent a standardized endpoint PCR with gel electrophoresis (Venor® GemOneStep kit) to rule out mycoplasma contamination in cell culture.

9.2.2 Primary cells

9.2.2.1 Primary cell isolation

Primary cells were leftover material from diagnostic procedures used in anonymized fashion and in compliance with the ethical guidelines of the Medical Faculty. Whole blood samples were collected in S-Monovette® K3 EDTA. Cells from lymph nodes were isolated using cell sieves. Blood or resuspended cells from lymph nodes were diluted with the same volume of Dulbecco's Phosphate Buffered Saline (DPBS) and up to 35 ml were carefully layered onto 15 ml of Ficoll® Paque Plus media in 50 ml centrifuge tubes. The tubes were centrifuged at 390 × g for 30 min at RT with the brake off. The cell layer at the Ficoll-plasma interface was aspirated and collected in a new centrifuge tube. The cells were suspended with the same volume of DPBS before centrifugation at 340 × g for 10 min at RT. The supernatant was removed, the cells were resuspended in DPBS, and the cell count was determined following trypan blue staining. The cells were centrifuged at 340 × g for 10 min at RT, the cell pellet was resuspended in freezing medium (RPMI 1640, 10% DMSO, 10% heat-inactivated human serum [HIS]), and the resuspended cells were then immediately distributed into 2 ml freezing tubes and stored in precooled freezing containers at -80 °C overnight. Primary cells were transferred to liquid nitrogen for long-term storage.

9.2.2.2 Thawing of cells

Freezing tubes containing frozen cells were thawed at 37 °C. The cell suspension was pipetted from the tube, when only a small ice crystal remained, and was poured into 10 ml of 37 °C prewarmed wash medium (10% FBS in RPMI 1640 with 2 mM L-Glutamine). The cell suspension was centrifuged and cells were washed once again with 5 ml of warm wash medium.

9.2.2.3 Cultivation with cytokines

Peripheral blood mononuclear cells (PBMCs) were either resuspended in standard cultivation medium (RPMI 1640 with 2 mM L-Glutamine, 10% HIS, 1% non-essential amino-acids, 1% penicillin-streptomycin [P/S]) or MACS medium (StemMACS™ HSC Expansion Media XF, 10% HIS, 1% P/S). For microscopy and analysis by flow cytometry, 2×10^6 cells per 2 ml were plated in a 12-well suspension plate. In a 96-well microplate, 1.2 × 10^5 cells per well were seeded in triplicate for the 3-(4,5-dimethylthiazol-2-yl)-2,5-diphenyltetrazolium bromide (MTT) assay. Interleukin-4 (IL-4; 50 IU/ml) and/or CD40L (100 ng/ml) were added to the cells cultured with MACS medium. After 24 h, cells received 400 nM ibrutinib or DMSO for further 3 d incubation. Following the total 4 d incubation, MTT was stopped and microscopy pictures were taken by EVOS™ M7000 microscope using diffuser and phase-contrast. After microscopy, cells were washed with FACS-buffer and stained with CD19-FITC (1 µg/ml) or isotype for 30 min at 4°C. CD52-APC (1.65 µg/ml) or isotype was added for the last 10 min of staining, before the samples were washed with FACS-buffer and stained with propidium iodide (PI, 10 µg/ml) to analyze cells by flow cytometry. For analysis of MTT assay data, the background absorption of cells treated with 1:1000 hydrogen peroxide (H_2O_2) in RPMI or MACS medium was subtracted from absorption of samples.

9.3 Molecular biological methods

9.3.1 Trypan blue staining

Cells resuspended in growth medium were mixed with the same volume of trypan blue solution. Concentration of living cells was determined by Countess® II FL Automated Cell Counter using Countess™ Reusable Slides.

9.3.2 3-(4,5-Dimethylthiazol-2-yl)-2,5-diphenyltetrazolium bromide (MTT) assay

Cells were plated and stimulated in triplicate in 96-well microplates with a final volume of 100-125 µl/well. After the indicated time period, 10 µl of the MTT solution was added to each well. The plate was returned to the incubator for 2 ½ h before 90 µl of solubilization buffer was added to lyse the cells and release the purple formazan crystals during overnight incubation in the incubator. The absorbance was measured by a microplate reader at 560 nm. Cell proliferation was calculated in Excel as the percentage of healthy control cells (100%, either untreated or treated with highest concentration of vehicle) and dead cells (0%, treated with a final concentration of 1:1000 H_2O_2 to account for background staining).

When treated with ibrutinib for 4 d, the number of seeded cells per well was 1.5 × 10^4 for MAVER-1, 1.2 × 10^4 for Z-138 and REC-1, 2.2 × 10^4 for JVM-2, 3 × 10^4 for JVM-13, 1.6 × 10^4 for GRANTA-519, 1.8 × 10^4 for UPN-1, 1.2 × 10^4 for HBL-2, and 1.6 × 10^4 for MINO and JEKO-1 (for Figure 3A). For 3 d treatment with IACS-010759, cells were plated at 2 × 10^4 for MAVER-1, 1.6-2 × 10^4 for Z-138, 1.6 × 10^4 for REC-1, 2-2.4 × 10^4 for JVM-2, 2.4 × 10^4

for JVM-13, 2 × 10^4 for GRANTA-519, 2.4 × 10^4 for UPN-1, 1.6 × 10^4 for HBL-2, and 2.4 × 10^4 for MINO and JEKO-1 per well (for Figure 14 left). The 4-day titration of IACS-010759 was performed using 1.1 × 10^4 REC-1 or MAVER-1 cells per well (for Figure 14 right). For all other MTT assays, cell numbers are indicated in the corresponding method section.

9.3.3 Protein lysates

Cells were seeded as follows, 8.1 × 10^5 cells per 6 ml for 48 h treatment with ibrutinib (for Figure 3B), 5 × 10^5 cells per 4 ml for 4 d treatment with ibrutinib (for Figure 10C), and for all other protein lysates, number of seeded cells are mentioned in the corresponding method section. After treatment as indicated, the cell suspension was centrifuged, the cells were washed with DPBS, and kept on ice for the following procedure. After aspiration of the DPBS, the cells were resuspended in lysis buffer and incubated on ice for 20 min. The cellular remnants were pelleted during centrifugation at 161 × g for 15 min at 4 °C and the lysate was taken off and stored in a fresh 1.5 ml tube at -80 °C. After determining protein content via the Bradford assay, the lysates were boiled with 4× Loading Buffer at 96 °C for 5 min, placed on ice for 3 min, and were kept at -20 °C until use.

9.3.4 Bradford assay

An aliquot of the lysate was diluted 1:10 or 1:20 with water to determine the protein content in triplicate. 290 µl of Bradford reagent were pipetted into each well of a 96-well microplate with flat bottom. 10 µl of water (blank), diluted lysates, and bovine serum albumin (BSA) standard solutions (0.1, 0.25, 0.35, 0.5, 0.7, and 1 mg/ml) were added per well and were incubated for 4 min at RT in the dark. The absorption was measured at 595 nm with a microplate reader and concentration was calculated in Excel using the BSA standard curve.

9.3.5 Western blot

The proteins were separated by size applying sodium dodecyl sulfate polyacrylamide gel electrophoresis (SDS-PAGE). The SDS gels with 6% stacking and 10% separating gel were prepared with the Mini-PROTEAN® Tetra Cell Casting Stand & Clamps. After completed polymerization, glass plates with gels were inserted into the Mini-PROTEAN® Tetra Cell filled with running buffer. The thawed and vortexed protein lysates were pipetted into the pockets next to 3 µl of the PageRuler™ Plus Prestained Protein Ladder. The gels ran at 90 V for 15 min, then the voltage was set to 120 V for 75 min. Separated proteins were transferred from the gel to a nitrocellulose membrane applying a wet blotting system. Therefore, each component was equilibrated in blotting buffer. A nitrocellulose was layered on the gel and 3 blotting papers enclosed the composite at each side. After insertion into the blotting chamber, proteins were transferred at 0.4 A for 90 min. The membranes were shortly stained with Ponceau S solution to visualize the protein bands and ensure proper transfer. The Ponceau S solution was washed off with deionized water, and the membranes were washed 3 times with tris-buffered saline with Tween® 20 (TBS-T) for 5 min in small boxes before blocking with 5% milk in TBS-T for 1 h at RT. Primary antibodies diluted in 5% BSA in TBS-T solution (0.03% NaN_3) were added and the membrane was incubated at 4 °C overnight on a platform shaker. The next day, the membranes were washed 3 times with TBS-T for 5 min and incubated for 2 h while shaking with the freshly prepared secondary antibody diluted in 5% milk in TBS-T. After washing the membranes 3 times with TBS-T for 5 min, they were incubated with a 1:1 mixture of SuperSignal™ West Pico chemiluminescent substrate solutions. For weak signals, Radiance Plus solution from azure biosystems was used. Protein bands were detected on Amersham™ Hyperfilm™ ECL or by a western blot imager. Relative protein expression after normalization to β-actin was determined measuring area of protein bands by ImageJ [146].

9.3.6 Cell cycle analysis

5×10^5 cells per sample were seeded in 1.5 ml medium and 400 nM ibrutinib was added for 48 h (DMSO as control). After incubation, cells were harvested and washed with phosphate-buffered saline (PBS). The cells were resuspended in 1 ml PBS to add them dropwise to a 15 ml centrifugation tube with 2.5 ml ice-cold absolute ethanol while gently vortexing. The tubes were left at -20 °C overnight. The next day, the tubes were centrifuged at 390 × g for 5 min at RT, the supernatant was removed, and the fixed cells were washed with PBS. The cells were then stained with a solution containing PI (0.05 mg/ml), Triton X (0.1 %), and RNAse A (7000 units/ml) in PBS for 40 min at 37 °C. After staining, 2 ml PBS were added to each tube and after centrifugation and removal of the staining solution, cells were resuspended in PBS before entering flow cytometry analysis (FACS Canto II). The PI signal was measured at linear scale. Gates were set with Flowing Software to determine the percentage of cells with low PI signal (G1 phase), intermediate PI signal (S phase) or high PI signal (G2M phase).

9.3.7 Extracellular flux analysis

Cells for 3-day ibrutinib treatment were seeded at 2×10^6 cells per 6 ml (for Figure 10D, 10E). For measurement of extracellular flux after treatment with ibrutinib and IACS-010759, cell numbers are described in the corresponding method section.

The day before the extracellular flux assay, 200 µl of Seahorse XF Calibrant were pipetted into each well of the utility plate. The sensor cartridge was lowered onto the utility plate and the assembly was placed in a plastic bag to prevent evaporation during overnight storage in a non-CO_2 incubator at 37 °C.
At the day of the assay, the Seahorse XFe96 cell culture microplate was coated with 20 µl of 100 µg/ml poly-D-lysine per well. The plate was covered for 20 min. The poly-D-lysine was removed, and the wells were washed with 200 µl sterile water twice, before the plate was left to dry for at least 30 min (air dry).
The assay medium (Seahorse XF RPMI medium with 10 mM D-Glucose and 2 mM L-Glutamine) was warmed to 37 °C. 50 µl of the assay medium were filled in the background wells (A1, A12, H1, and H12) and all empty wells. The cells were harvested after incubation as indicated and were centrifuged. After removing the supernatant, the cells were resuspended in prewarmed assay medium and were counted following trypan blue staining. The cells were diluted with assay medium to plate out 50 µl per well with 1.1×10^5 cells into the coated XFe96 cell culture microplate (6 replicates for every sample). After centrifugation at 500 × g for 5 min, the plate was transferred to a non-CO_2 incubator at 37 °C for 30 min. Before incubation of the plate for another 25 min in the non-CO_2 incubator at 37 °C, 130 µl assay medium were carefully pipetted to each well. Meanwhile, the sensor cartridge was loaded into the Seahorse XFe96 Metabolic Flux Analyzer for calibration. The cell culture plate was directly transferred from the incubator to the Seahorse XFe96 Metabolic Flux Analyzer and oxygen consumption rate (OCR) and extracellular acidification rate (ECAR) were measured. Data was acquired 3-5 times with 30 s mixing pauses.

9.3.8 Flow cytometry of cell surface antigens

Cells were treated as indicated, with 1×10^6 per 5 ml (for Figure 9B) and $4\text{-}5 \times 10^5$ per 2 ml (for Figure 17A) seeded cells per sample. After washing with FACS-buffer, antibody and isotype controls were added to 100 µl of cells resuspended in FACS-buffer. Cells were stained with CD52-PE (3 µg/ml), CD37-PE (2 µg/ml), CD40-PE (2 µg/ml), and CD79B (2.75 µg/ml) for 10 min at 4 °C. The cells were washed and resuspended in FACS-buffer before measurement by flow cytometry (FACS Canto II) and subsequent analysis by Flowing Software. Isotype controls were checked to exclude unspecific antibody binding.

9.3.9 Microscopy

An EVOS^{TM} M7000 Imaging System was used for taking pictures of cells. For anti-CD52 assay, images were converted to grayscale (8-bit) by Corel PHOTO-PAINT (for Figure 17F).

9.4 RNA sequencing

9.4.1 Single-cell RNA sequencing

9.4.1.1 Setup of single-cell RNA sequencing experiment

In a 6-well plate, 3×10^6 REC-1 cells in 5 ml medium were plated per sample and were cultivated for 48 h. Ibrutinib (400 nM) was added to the first sample at seeding (48 h treatment), the second sample was treated for the last 6 h (6 h treatment) with the inhibitor, and the third sample received no treatment and served as control (Ctr). After culturing, the cells were washed with DPBS.

The following steps and analysis of the data were carried out in close collaboration with the Core Unit Systems Medicine of the University of Würzburg and the Helmholtz-Institute for RNA-based Infection Research in Würzburg (HIRI). The viability stain PI (2 µg/ml) was added to the cells shortly before entering the FACS machine (BD FACS Aria III) for excluding cell debris (SSC-A versus [vs] FSC-A) and doublets (SSC-W vs SSC-A), and sorting of 3×10^4 PI negative, viable cells (SSC-A vs PE-A). The cells were stained with trypan blue and were counted before single cells were separated in the 10x Genomics Chromium Controller and libraries were set up using the Single cell 3' Kit v2 Chemistry. The procedure adhered to the 10x Genomics protocol. The Qubit™ 3.0 Fluometer quantified the libraries, and the 2100 Bioanalyzer with the High Sensitivity DNA kit determined the quality of the libraries. A S1 flowcell was loaded to sequence the reads (100 bp in paired-end format) on a NovaSeq™ 6000.

The experiment was repeated within three months to create two biological replicates. The REC-1 cells of both replicates originated from separately thawed and cultured cells.

9.4.1.2 Data analysis

10x Genomics provided the Cell Ranger software which was used to demultiplex and process the single-cell data. The Cell Ranger analysis included generation of FASTQ files and alignment of reads to the reference genome GRCh38. The different data sets were aggregated applying the *cellranger aggr* function including depth normalization of the data. The created feature-barcode matrices were then loaded into R ([147]; RStudio [148]) to perform downstream analysis with the R package Seurat [153]. As a first step, the data was checked for low-quality cells. Cells with low or high amount of unique molecular identifiers (UMI, reflecting mRNA content), low or high number of genes, and high mitochondrial gene content were excluded. The corrected data was log normalized, 2000 variable features were selected, and the data was scaled. Principal component analysis (PCA) was performed to assess the heterogeneity of the data set. After ranking of principal components by the *ElbowPlot* function, the first 40 principal components were included for the graph-based clustering approach. The resolution parameter was set from 0.1 to 1, producing low to high number of cell clusters, to find biologically meaningful clustering of cells. The visualization in low-dimensional space was realized by applying uniform manifold approximation and projection (UMAP) representing a non-linear reduction technique. Differentially expressed features specifying the cell clusters were determined by the *FindAllMarkers* function which used the Wilcoxon Rank Sum test as default.

9.4.1.3 Data integration and cell cycle regression

After quality-control, the data of the two replicates of Ctr were integrated following the default protocol in Seurat which applied the Canonical Correlation Analysis [155]. Besides the reduction of batch effects on heterogeneity of the data, the effect of cell cycle was reduced by Seurat's cell-cycle scoring and regression tool. The cells were assigned to the cell cycle phase S or G2M owing to the expression of specific canonical markers or were classified as non-cycling/G1 in case they did not express any of these marker genes. Seurat produced a corrected expression matrix following data scaling to mitigate the impact of cell cycle on the heterogeneity of the data.

9.4.1.4 ClusterProfiler analysis

Functional enrichment analysis was performed with the R package ClusterProfiler using Kyoto Encyclopedia of Genes and Genomes (KEGG) and gene ontology of biological processes (BP; [149]). The analysis included differentially expressed genes (DEGs) with log fold change > 0.1 and adjusted *P*-value (padj) < 0.001. The results were visualized in dot plots.

9.4.1.5 SCENIC analysis

The heterogeneity of gene regulatory networks (GRNs) in the data set of Ctr + 6 h + 48 h was employed by the R package SCENIC [152]. The raw count matrix of the combined data was prepared with Seurat to exclude low-quality cells and subpopulation E accounting for only 1% of the cells. The analysis was performed adhering to the default workflow. After searching for coexpression of transcription factors and target genes, the RcisTarget tool validated direct-binding targets using the hg19 motif ranking database. Transcription factor modules comprising less than 10 mapped genes were excluded, but "low confidence" annotations (with the suffix "_extended") were kept for further analysis. The final visualization of regulatory networks was realized by a heatmap which was resolved according to the clustering by Seurat.

9.4.2 Bulk RNA sequencing

9.4.2.1 Setup of bulk RNA sequencing experiment

Cells were seeded at 5×10^5 cells per 6 ml and 400 nM ibrutinib was added at the indicated time points (4 d, 3 d, and 2 d treatment). One sample stayed untreated. After 4 d incubation, viable cell fraction was isolated (see 9.5.1) and washed with DPBS. RNA was isolated with the AllPrep DNA/RNA Mini Kit according to manufacturer's instructions including DNase digestion using DNase I (1500 Kunitz units, RNase-Free DNase Set). The concentration of eluted RNA was measured by NanoDrop 1000 spectrophotometer.
The following steps were performed in collaboration with the Core Unit Systems Medicine in Würzburg. An RNA 6000 Nano Kit was used to determine quality of isolated RNA by a 2100 Bioanalyzer system. The RNA integrity number (RIN) for all samples was ≥ 8. The TruSeq Stranded mRNA Library Preparation Kit was used to generate DNA libraries suitable for sequencing from 500 ng of total RNA with oligo-dT capture beads for poly-A-mRNA enrichment as per the manufacturer's instructions (1/2 volume). After 15 cycles of PCR amplification, the size distribution of the barcoded DNA libraries was estimated ~330 bp by electrophoresis on Agilent DNA 1000 Bioanalyzer microfluidic chips.
On the NextSeq® 500 platform, pooled libraries spiked with 1% PhiX control library were sequenced at 25 million reads/sample in single-end mode with 75 nt read length utilizing High output sequencing kits.

9.4.2.2 Data analysis

Analysis of bulk RNA-seq data was performed in collaboration with the Core Unit Systems Medicine in Würzburg. The software bcl2fastq2 was used to prepare demultiplexed FASTQ files. Illumina reads were quality- and adapter-trimmed using Cutadapt [145] with a cutoff Phred score of 20 in NextSeq mode to ensure high sequence quality. Reads without remaining bases were sorted out (command line parameters: --nextseq-trim=20 -m 1 -a AGATCGGAAGAGCACACGTCTGAACTCCAGTCAC). STAR was applied using the default parameters to map processed reads to the human reference genome (Ensembl GRCh38; [154]). The program featureCounts from the Subread package served as tool to produce read counts on exon level summarized for each gene [151]. Multi-mapping and multi-overlapping reads were counted strand-specific and reversely stranded with a fractional count for each alignment and overlapping feature (command line parameters: -s

2 -t exon -M -O --fraction). DESeq2 determined DEGs based on the count output and normalized read counts [150]. In addition, fold-change shrinkage was applied by setting the parameter "betaPrior=TRUE". The Benjamini-Hochberg correction was used to adjust *P*-values, and genes with padj < 0.05 |log2FoldChange| ≥ 1 were considered as differentially expressed. The ClusterProfiler tool [149] was used to perform gene set enrichment analysis (GSEA) based on KEGG pathways for DEGs ranked by their DESeq2 log2FoldChange (log2FC).

9.5 Anti-CD52 and IACS-010759 treatment

9.5.1 Viable cell isolation

After incubation of cells as indicated, they were harvested, centrifuged in 15 ml tubes, the supernatant was removed, and the cell pellet was resuspended in 3.25 ml Optimix solution consisting of OptiPrep™ media mixed with growth medium to yield 14% iodixanol. 200 µl of DPBS were layered on top and the tubes were centrifuged at 2 122 × g for 7 min. The DPBS phase containing the viable cell fraction was aspirated and diluted and washed with medium.

9.5.2 Concomitant and consecutive treatment with ibrutinib and a CD52 monoclonal antibody or IACS-010759

In concomitant setup, cells were treated with 400 nM ibrutinib (or DMSO) and 10 µg/ml CD52 monoclonal antibody (mAb; or isotype) or 25 nM IACS-010759 (or DMSO) for the indicated time periods in a cell culture incubator. For consecutive regimen, cells were pretreated with 400 nM ibrutinib (or DMSO) for 3 d, viable cells were selected (see 9.5.1), and cells were again seeded and incubated with 10 µg/ml CD52 mAb (varying concentrations of 1-30 µg/ml for CD52 mAb titration, or isotype) or 25 nM IACS-010759 (or DMSO) for the indicated time periods in a cell culture incubator.
The use of CD52 mAb required preincubation of cells with CD52 mAb (or isotype) in serum-free medium for 30 min on ice with subsequent addition of 10% normal human serum (NHS). NHS served as a source of complement, and HIS was used as negative control with inactivated complement proteins. As human serum was not sterile, 1% P/S was added to growth medium for anti-CD52 assays. For analysis of cell viability after titration of CD52 mAb, cells were washed and resuspended in FACS-buffer for staining with PI (10 µg/ml) and analysis by flow cytometry (FACS Canto II).

For the consecutive treatment approach using IACS-010759, 5 × 10^6 cells were seeded in 15 ml growth medium for pretreatment with ibrutinib, and 5-6 × 10^4 cells per well for MTT assay (for Figure 15A), 2 × 10^6 cells per 7.5 ml for protein lysates (for Figure 15B), and 3 × 10^6 cells per 7.5 ml for extracellular flux analysis (for Figure 15C, 15D) for subsequent treatment with ibrutinib and IACS-010759. When cells were concomitantly treated with ibrutinib and IACS-010759, 1.1 × 10^4 cells per well were seeded for MTT assay (for Figure 16A), 1.6 × 10^6 cells per 6 ml for protein lysates (for Figure 16B), and 2 × 10^6 cells per 7 ml for extracellular flux analysis (for Figure 16C, 16D).

Regarding anti-CD52 treatment, 3 × 10^6 cells were plated per 15 ml for pretreatment with ibrutinib, followed by seeding of 7 × 10^4 pretreated cells per well for CD52 mAb titration (for Figure 17B) and MTT assay (for Figure 17C), 1.2 × 10^5 cells per well for C3b deposition (for Figure 17E), and 1.4 × 10^5 cells per 200 µl in a 48-well plate for microscopy (for Figure 17F). For the concomitant use of ibrutinib and CD52 mAb, 2 × 10^4 cells per well were seeded for MTT assay (for Figure 17D).

9.5.3 CD52 levels and anti-CD52 treatment in primary mantle cell lymphoma cells

After thawing of primary cells (see 9.2.2), an aliquot of resuspended primary cells was put on ice for determining the viability and CD52 level of the $CD19^+$ cells by flow cytometry. The rest of the cells was centrifuged, the pellet was resuspended in cultivation medium, and the cells were counted after trypan blue staining. 3 × 10^6 cells were seeded in 2 ml cultivation medium per well of a 12-well suspension plate. Primary cells were either treated with 400 nm ibrutinib, DMSO or were untreated and cells were cultivated for 2-3 d depending on their fitness. After cultivation, the cells were harvested, centrifuged, washed with cold DPBS, and finally resuspended in cold cultivation medium without serum. The cells remained on ice during cell counting. 1.2-1.5 × 10^5 cells were plated per well in a 96-well microplate with flat bottom. An ibrutinib or DMSO dilution in 1% P/S in RPMI 1640 according to the received pretreatment and 10 µg/ml anti-CD52 antibody (isotype and medium [untreated] as control) were added. Following incubation for 30 min on ice, NHS (10%) was pipetted to every sample. The plate was transferred to a cell culture incubator for 10 min. To stop complement activation, plate was put on ice, centrifuged at 4°C, medium was removed, and the cells were washed with cold FACS-buffer. The cells were resuspended in 200 µl FACS-buffer, 100 µl were transferred to two FACS tubes for staining with CD19-FITC (1 µg/ml) or isotype and PI. The aliquot of cells on ice was also washed with FACS-buffer and stained with CD19-FITC (1 µg/ml) or isotype for 30 min at 4°C. CD52-APC (1.65 µg/ml) or isotype was added for the last 10 min, before the samples were washed with FACS-buffer. PI (10 µg/ml) was added to all samples shortly before analysis (FACS Canto II).

9.5.4 C3b deposition

Following consecutive incubation of cells with ibrutinib and CD52 mAb (see 9.5.2) complement activation was stopped after 15 min of serum addition by putting the plate on ice, centrifugation at 283 × g for 5 min at 4 °C, and replacing the medium with cold FACS-buffer. Cells were stained with C3b-FITC (3 µg/ml) or isotype for 15 min on ice in the dark, washed with FACS-buffer, and stained with PI (10 µg/ml). Deposition of C3b on the surface was detected and measured by flow cytometry (FACS Canto II).

9.6 Statistical analysis

The standard error of the mean (SEM) was calculated and was displayed as error bar in the graphs. Following F-test, a two-sided t-test (for equal variances) or a Welch's t-test (for unequal variances) was applied to compare the means of two groups. If more than 2 groups were compared, the one-way ANOVA analysis was used with Tukey posthoc pairwise comparison to test for significant differences between groups. In case the groups were related, a paired t-test was performed after normal distribution of data was ensured by Shapiro-Wilk test. Statistical significance was indicated by asterisks (* $P \leq 0.05$, ** $P \leq 0.01$, *** $P \leq 0.001$, ns for not significant $P > 0.5$). The calculation was performed in Excel and Origin.

9.7 Data availability

The scRNA-seq and bulk RNA-seq data sets are available in the Gene Expression Omnibus repository GSE162234 and GSE214725, respectively.

10 Results

10.1 The mantle cell lymphoma cell line REC-1 is most sensitive to ibrutinib

The MCL cell lines MAVER-1, Z-138, JVM-2, JVM-13, GRANTA-519, UPN-1, HBL-2, MINO, JEKO-1, and REC-1 were treated with ibrutinib concentrations from 1 nm to 3000 nM for 4 d (Figure 3A, top).

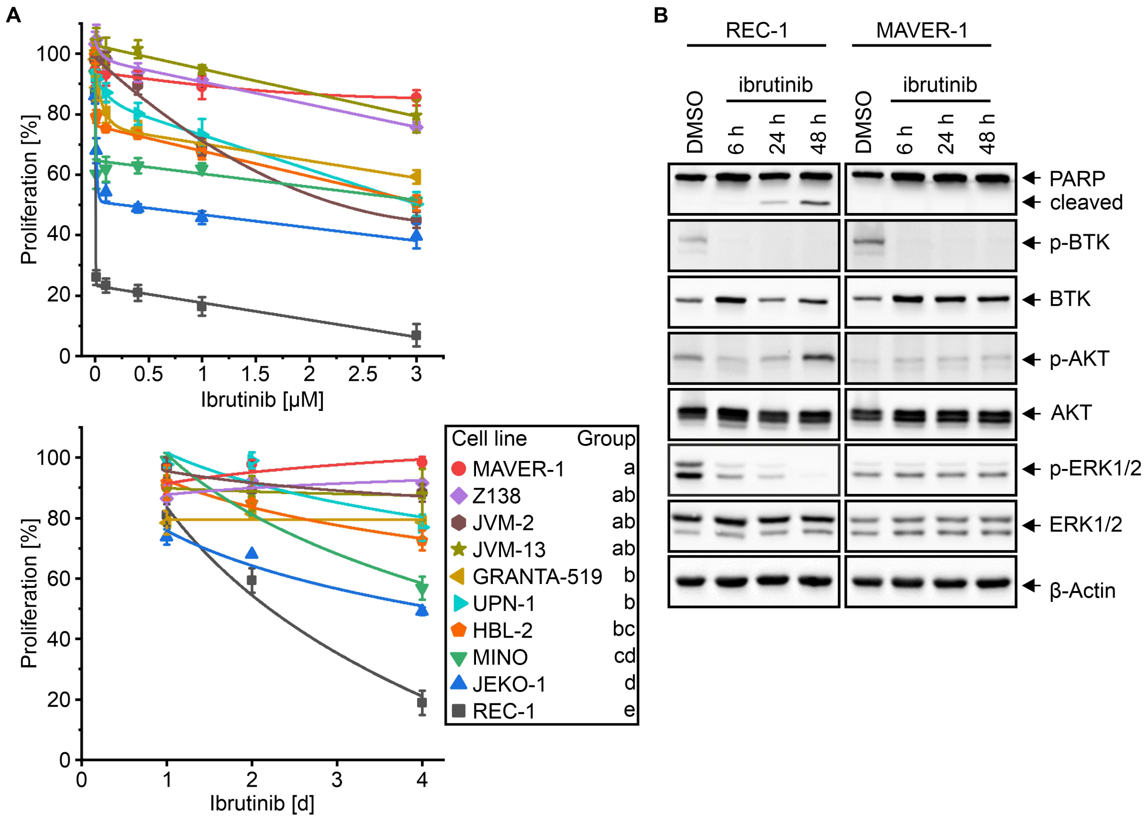

Figure 3: Impact of ibrutinib on proliferation and B-cell receptor signaling of mantle cell lymphoma cell lines. A) Proliferation of 10 mantle cell lymphoma (MCL) cell lines under different ibrutinib concentrations after 4 d treatment (top) and at 400 nM ibrutinib after different incubation times (below), as determined by 3-(4,5-dimethylthiazol-2-yl)-2,5-diphenyltetrazolium bromide (MTT) assay; data presented as mean ± SEM; MCL cell lines were grouped (a-e) according to their proliferation after 4 d treatment with 400 nM ibrutinib as assessed by one-way ANOVA followed by Tukey posthoc pairwise comparison ($P \leq 0.05$; N = 3). B) Western Blot showing protein expression of PARP, p-BTK, BTK, p-AKT, AKT, p-ERK1/2, ERK1/2, and β-Actin (loading control) after 6 h, 24 h, and 48 h treatment of REC-1 and MAVER-1 with 400 nM ibrutinib; representative blots are shown (data was captured by a western blot imager).

The proliferation decreased exponentially in the range of 1-100 nM ibrutinib followed by a linear decrease at higher concentrations. REC-1 showed the sharpest drop at even low concentrations, in contrast to MAVER-1, Z-138, and JVM-13, which were barely affected. The influence of 400 nM ibrutinib on cell proliferation was assessed over 4-day treatment

(Figure 3A, below). Besides REC-1, with proliferation decreasing by 80% after 4 d, the proliferation of JEKO-1 and MINO was reduced to 50-60%, whereas HBL-2, UPN-1, GRANTA-519, JVM-13, JVM-2, Z-138, and MAVER-1 showed only a small decrease to still over 70%. According to 4 d treatment with 400 nM ibrutinib, REC-1 was the most sensitive and most distinct from all other cell lines (group e). The proliferation of JEKO-1 and MINO was also significantly reduced (group d), whereas the other cell lines were not or only slightly affected by ibrutinib (group a and b).

Ibrutinib treatment inhibited phosphorylation of BTK in REC-1 and MAVER-1 (Figure 3B). BTK inhibition was followed by early deactivation of BCR signaling in REC-1, as phosphorylation of AKT and ERK1/2 was reduced after 6 h of treatment. However, REC-1 reactivated AKT, as indicated by increasing phosphorylation after 48 h. After 24 h to 48 h of treatment, considerable poly (ADP-ribose) polymerase (PARP) cleavage linked ibrutinib treatment with apoptosis in REC-1, whereas no PARP inactivation or reduced phosphorylation of p-AKT and p-ERK1/2 was observed in MAVER-1. According to their opposite response to ibrutinib, REC-1 was designated as an ibrutinib-sensitive cell line and MAVER-1 as an ibrutinib-resistant cell line.

10.2 Single-cell RNA sequencing of the ibrutinib-sensitive mantle cell lymphoma cell line REC-1

The ibrutinib-sensitive cell line REC-1 was selected for the time-resolved scRNA-seq approach across ibrutinib treatment (Figure 4).

The cells were cultivated for 48 h. One sample stayed untreated and served as control (Ctr), the second was treated for 6 h (6 h), and the third sample for 48 h (48 h) with 400 nM ibrutinib. Fluorescence activated cell sorting ensured that the surviving cell population was included for scRNA-seq using the 10x Genomics platform. The transcripts were uniquely barcoded to unveil gene expression on single-cell level after high-throughput sequencing.

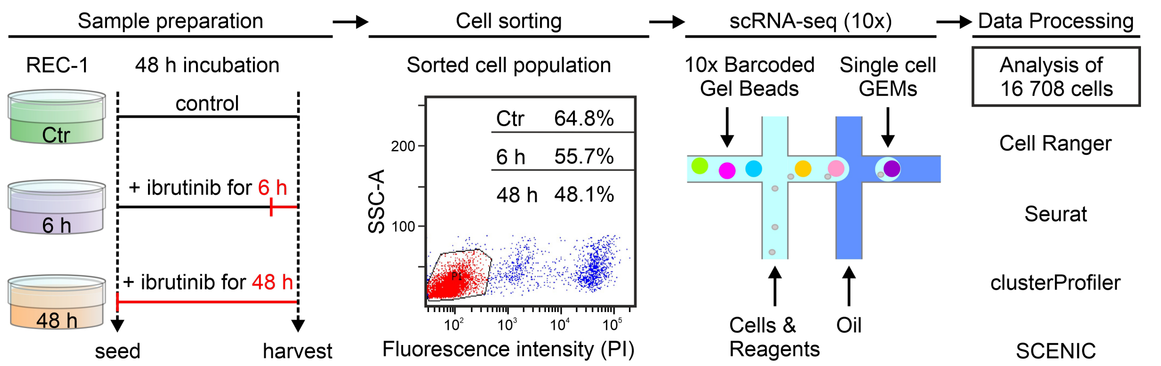

Figure 4: Design of the single-cell RNA sequencing experiment. REC-1 cells were treated with 400 nM ibrutinib for 6 h or 48 h, untreated cells were used as control (Ctr). Proportion of viable, propidium iodide (PI) negative cells (gate P1, highlighted in the scatterplot of 48 h) is indicated for each treatment, as determined by flow cytometry. Viable cells entered the 10x Genomics Chromium Controller, where single cells were partitioned in Gel Beads-in-emulsion (GEMs) in microfluidic chips for subsequent reverse transcription of their mRNA resulting in unique barcoding of the cDNA. Following library preparation and sequencing, data was processed with Cell Ranger and R tools (Seurat, clusterProfiler, SCENIC). Modified from Fuhr et al. [156]; reproduced with permission from Springer Nature [157].

The data of two independent biological replicates of each condition underwent individual quality control with respect to unique molecular identifier (UMI) counts, number of unique genes, and mitochondrial gene content (Table 1).

Table 1: Thresholds for quality control of single-cell data.

Samples (both replicates)	Quality Control			Analysis	
	UMIs	Genes	Mito. genes [%]	No. of genes	No. of cells
Ctr	6 500 – 35 000	2 000 – 5 300	< 8	15 654	5 177
6 h	6 250 – 62 500	2 000 – 6 500	< 8	16 435	5 737
48 h	6 000 – 45 000	1 500 – 5 500	< 9	15 635	5 676
Combined data (Ctr + 6 h + 48 h)	5 000 – 35 000	1 500 – 5 200	< 9	17 352	16 708

Ctr = control (untreated); UMI = unique molecular identifier; Mito. = Mitochondrial; No. = Number.

The downstream analysis focused on untreated REC-1 (Ctr) and the combined analysis of Ctr + 6 h + 48 h.

10.2.1 Replicates show biological reproducibility

The two replicates of Ctr were aggregated by applying the Cell Ranger analysis pipeline and resulted in 5 177 cells following quality control by Seurat (Figure 5).

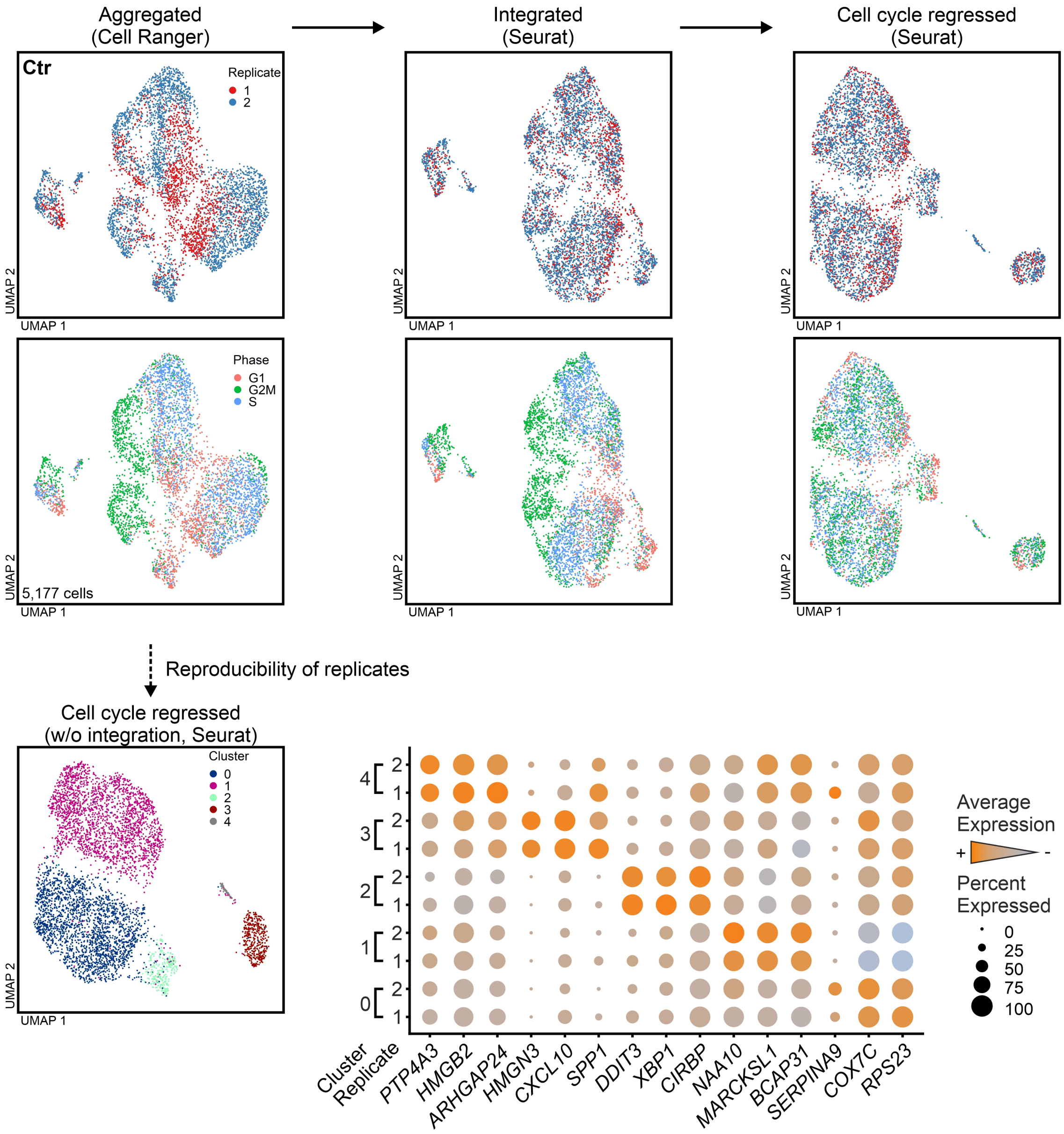

Figure 5: Processing and reproducibility of the single-cell data. Uniform manifold approximation and projection (UMAP) plots of untreated cells (Ctr) at resolution 0.3 (upper part) with aggregation of data (left), followed by integration (center), and cell cycle regression (right). Cells are colored according to their replicate of origin (top) and cell cycle phase (below). Reproducibility of replicates was ensured using cell cycle regressed Ctr data without (w/o) integration (lower part). The corresponding dotplot shows average expression of selected top 10 cluster markers and the proportion of expressing cells, illustrated by color and dot size, respectively. Modified from Fuhr et al. [156].

As the cells of the replicates separated from each other in the UMAP plot, the data was integrated to correct for technical variation. In the integrated version, the cells within a cluster distributed according to their cell cycle phase. The impact of cell cycle was minimized to investigate underlying sources of heterogeneity. Integration in combination with cell cycle regression by Seurat resulted in even spreading of cells with respect to their origin data set and cell cycle phase.

The reproducibility of the two replicates was examined in the aggregated, cell cycle regressed Ctr data set (Figure 5, below). The cells separated into two major and three smaller clusters in the UMAP plot. A similar expression pattern of cluster marker genes of both replicates across the 5 clusters corroborated biological reproducibility.

10.2.2 REC-1 cells are heterogeneous on the single-cell level

The integrated, cell cycle regressed Ctr data set comprised 5 177 cells separated into 7 clusters (Figure 6A).

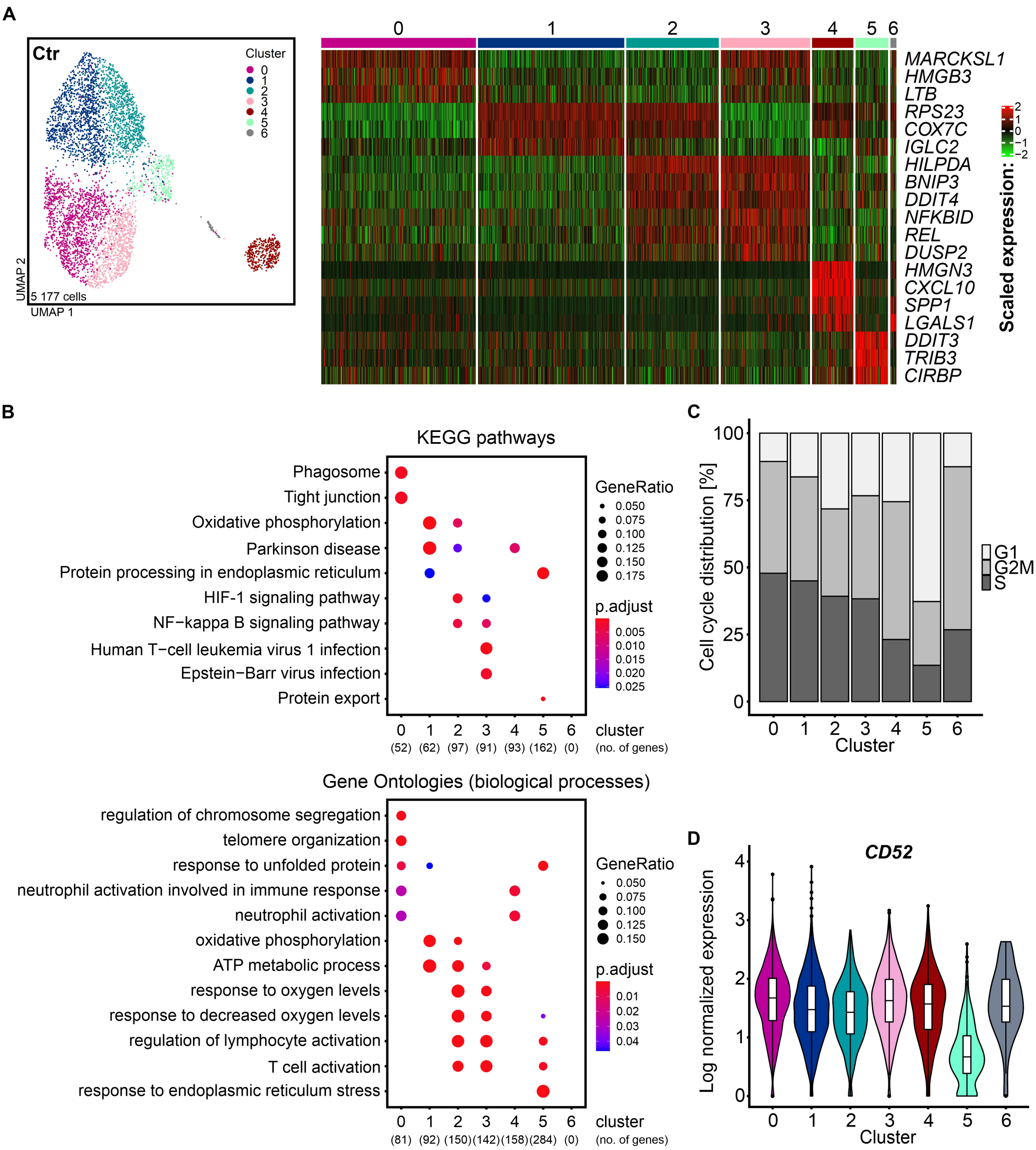

Figure 6: Heterogeneity of REC-1. A) Uniform manifold approximation and projection (UMAP) representation of integrated and cell cycle regressed data of untreated cells (Ctr) at resolution 0.4

and scaled expression of selected top 10 markers for the 7 clusters in the corresponding heatmap. B) Enrichment analysis of Kyoto Encyclopedia of Genes and Genomes (KEGG) pathways (top) and gene ontologies with respect to biological processes (BP) (bottom); differentially expressed genes (DEGs) of Ctr with log fold change > 0.1 and adjusted *P*-value < 0.001 were included for analysis (no. = number of genes). C) Distribution of cell cycle phases in clusters of Ctr. D) Log normalized expression levels of *CD52* are illustrated by a violin plot. Modified from Fuhr et al. [156]; reproduced with permission from Springer Nature [157].

The clusters 0 and 3, accounting for 43% of cells, shared the increased expression of genes encoding for the actin binding MARCKS-related protein (MARCKSL1), the chromatin binding high mobility group protein B3 (HMGB3), and the cytokine lymphotoxin-beta (LTB). Predominant expression of mitochondrial and ribosomal genes was common to clusters 1 and 2, comprising 42% of Ctr cells. Besides the similarities between cluster 1 and 2, cluster 2 shared higher activity of NF-κB (*NFKB inhibitor delta* [*NFKBID*]; *REL proto-oncogene*, *NF-κB subunit* [*REL*]; *dual specificity phosphatase 2* [*DUSP2*]) with cluster 3 and both clusters showed a hypoxic cell state with respect to the markers *hypoxia inducible lipid droplet associated* (*HILPDA*), *BCL2 interacting protein 3* (*BNIP3*), and *DNA damage inducible transcript 4* (*DDIT4*). The KEGG pathway analysis revealed a dominance of an oxidative phosphorylation (OXPHOS)-based metabolism in cluster 1 and increased NF-kB signaling together with hypoxia-inducible factor 1 (HIF-1) signaling pattern in the cluster 3 (Figure 6B). KEGG analysis reflected the detected biological processes showing ATP metabolic processes in cluster 1 and response to decreased oxygen levels in cluster 3. The cluster 2 combined all of these features according to the functional enrichment analysis (Figure 6B). Two smaller clusters, with 7% of Ctr cells in cluster 4 and 6% in cluster 5, differed from the other clusters. Focusing on the distribution of cell cycle phases revealed that cluster 5 contained the most resting cells (G1 cells, Figure 6C). Besides, cluster 5 showed increased expression of *DNA damage inducible transcript 3* (*DDIT3*), *tribbles pseudokinase 3* (*TRIB3*), and *cold inducible RNA binding protein* (*CIRBP*), indicating a response to endoplasmic reticulum stress and to unfolded protein (Figure 6A and 4B). Additionally, cluster 5 had lowest *CD52 molecule* (*CD52*) levels (Figure 6D).

The markers *high mobility group nucleosomal binding domain 3* (*HMGN3*), *C-X-C motif chemokine ligand 10* (*CXCL10*), *secreted phosphoprotein 1* (*SPP1*), encoding for an extracellular matrix protein (osteopontin), and *galectin 1* (*LGALS1*), encoding for a proangiogenic protein (galectin-1), dominated cluster 4 (Figure 6A and Figure 7A).

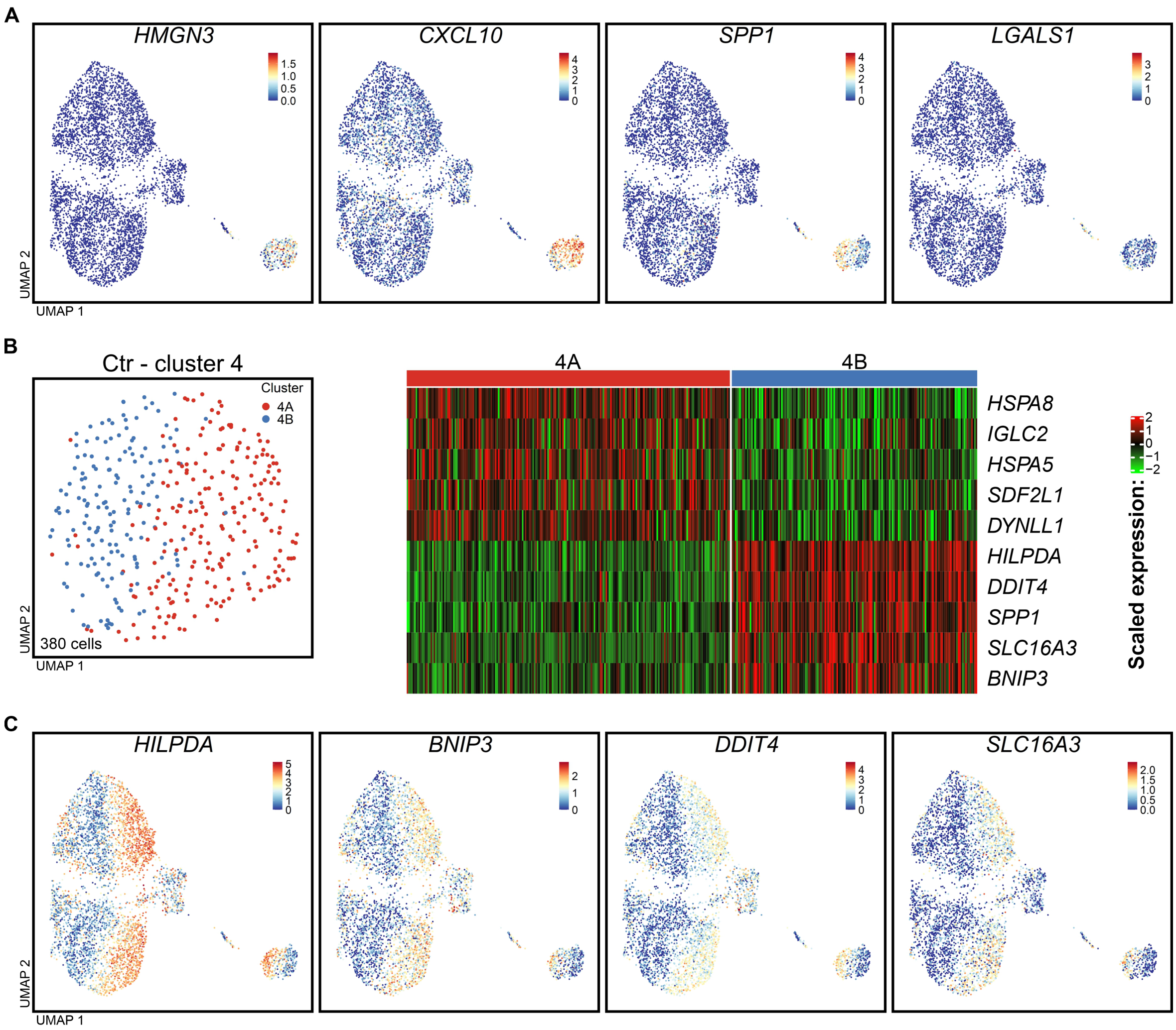

Figure 7: Features of cluster 4 and expression of glycolysis/hypoxia associated genes. A) Log normalized expression of marker genes in cluster 4 displayed in a uniform manifold approximation and projection (UMAP) plot. B) UMAP plot of cluster 4 with 2 subgroups (cluster 4A and 4B) after separate reclustering at resolution 0.6, and scaled expression of selected top 10 markers depicted in the heatmap. C) UMAP plots showing log normalized expression of glycolysis/hypoxia associated genes. Modified from Fuhr et al. [156].

A renewed analysis of cluster 4 uncovered a subset of cells that had higher expression of *HILPDA*, *DDIT4*, *solute carrier family 16 member 3* (*SLC16A3*), and *BNIP3* (cluster 4B in Figure 7B) pointing to a glycolytic/hypoxic cell state as in the clusters 2 and 3. The expression of *SPP1* was restricted to this subset. The visualization of the expression of *HILPDA*, *BNIP3*, *DDIT4*, and *SLC16A3* underlined the separation of Ctr cells into two metabolic states with either high or low activity of these genes (Figure 7C). As cluster 6 consisted of only 1% of all cells, it was not included for further analysis.

The untreated REC-1 cells showed heterogeneity on the single-cell level, which was caused by distinct metabolic states, differing activity of NF-kB signaling, varying stress levels, and special features of cell subsets.

10.2.3 REC-1 cells alter surface antigen levels and B-cell receptor genes across ibrutinib treament

The evolution of REC-1 cells during ibrutinib exposure was assessed by aggregating the data of both replicates from the treatments Ctr (5 177 cells), 6 h (5 737 cells), and 48 h (5 676 cells; Figure 8A).

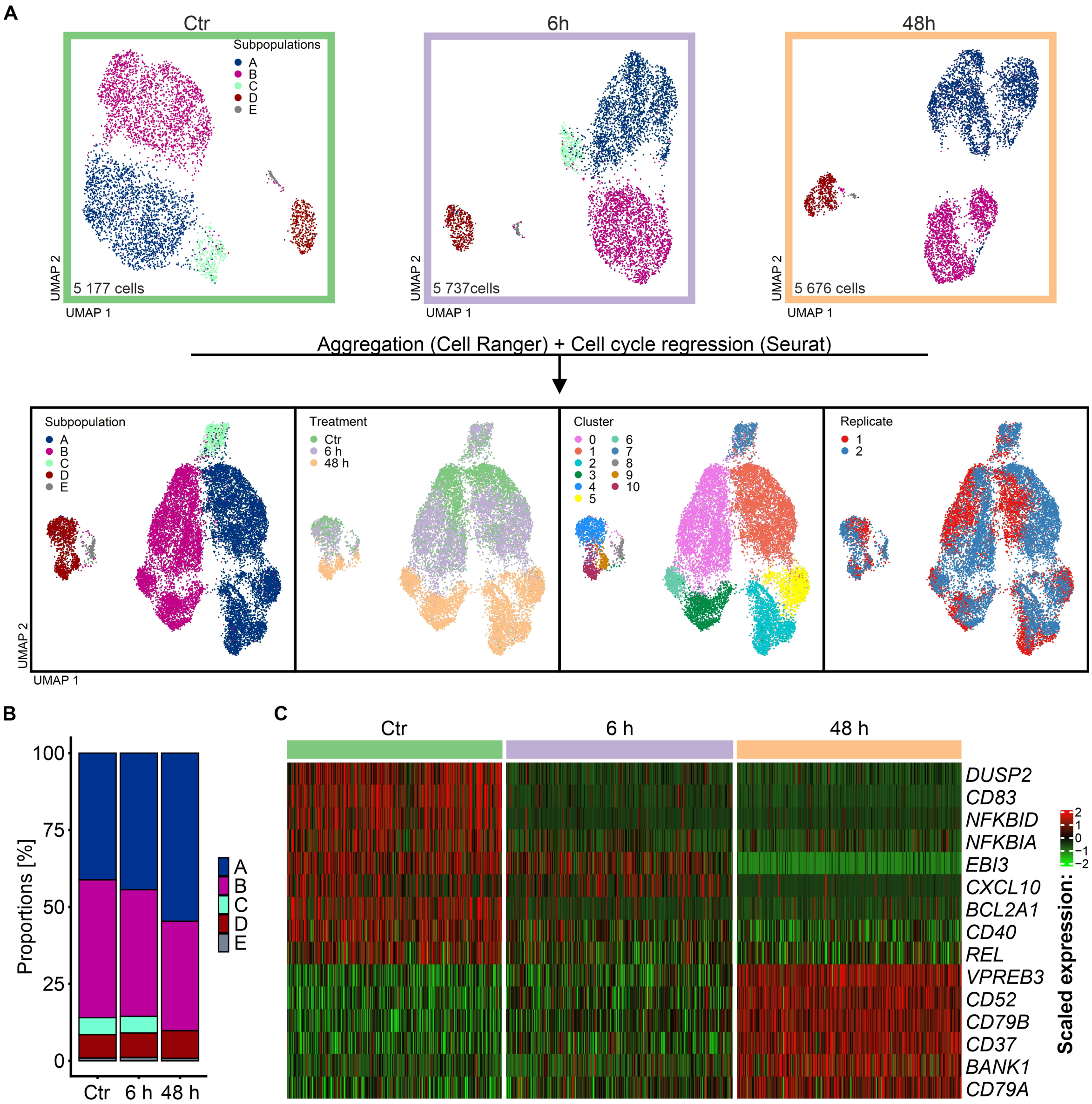

Figure 8: Transcriptional evolution of REC-1 across ibrutinib treatment. A) Uniform manifold approximation and projection (UMAP) plots of cell cycle regressed data of untreated (Ctr), 6 h and 48 h ibrutinib-treated cells with highlighted subpopulations (top); Ctr, 6 h, and 48 h were aggregated and cell cycle regressed and the combined data is visualized by UMAP plots resolved by subpopulations, treatment, clustering at resolution 0.4 (subclustering of subpopulation D at resolution 0.3), and replicates (bottom). B) Distribution of subpopulation proportions across treatment. C)

Heatmap with scaled expression of selected top marker genes of Ctr, 6 h, and 48 h. Modified from Fuhr et al. [156]; reproduced with permission from Springer Nature [157].

After cell cycle regression, five subpopulations comprising 16 708 cells in 11 clusters were defined and tracked over time. Cluster 8 accounted for less than 1% of cells and was not further analyzed. The visualization by UMAP revealed, that the Ctr and 6 h cells were more similar and therefore still clustered together (cluster 0, 1, 4, and 7). Increased incubation with ibrutinib led to more evident transcriptomic alterations and separation of 48 h cells (cluster 2, 3, 5, 6, 9, and 10). All but subpopulation C survived 48 h treatment. The proportion of subpopulation A and D increased slightly, whereas B decreased, but none of the subpopulations dominated after 48 h (Figure 8B). Comparing the gene expression of the three treatments revealed a common response to ibrutinib despite the presence of distinct subpopulations (Figure 8C). In the 6 h sample, a fast downregulation of NF-kB regulating genes (*NFKBID* and *NFKB inhibitor alpha* [*NFKBIA*]), NF-kB target genes (*DUSP2*, *CD83 molecule* [*CD83*], *BCL2 related protein A1* [*BCL2A1*], and *CXCL10*), and *REL* were detected. The upregulation of BCR associated genes (*CD79a molecule* [*CD79A*], *CD79b molecule* [*CD79B*], and *V-set pre-B cell surrogate light chain 3* [*VPREB3*]), BCR signaling genes (*B cell scaffold protein with ankyrin repeats 1* [*BANK1*]*)* followed at 48 h. While the expression of the NF-kB target gene *CD40 molecule* (*CD40*) was reduced, the increased expression of genes encoding for the surface leukocyte antigen CD37 (CD37) and CAMPATH-1 antigen (CD52) was triggered upon ibrutinib treatment.

10.2.4 REC-1 cells increase CD52 levels and enter a quiescent state

In accordance with the scRNA-seq data, a higher level of the tetraspanin CD37 and the glycoprotein CD52 were detected on the cell surface of REC-1 cells following 3 d ibrutinib treatment by flow cytometry analysis (Figure 9A and 9B). The expression of tumor necrosis factor receptor superfamily member 5 (CD40) was reduced, whereas increased CD79B could not be demonstrated at the protein level in REC-1. The ibrutinib-resistant MAVER-1 did not alter the expression of CD52, CD37, and CD40. However, a small but significant increase in CD79B level was observed.

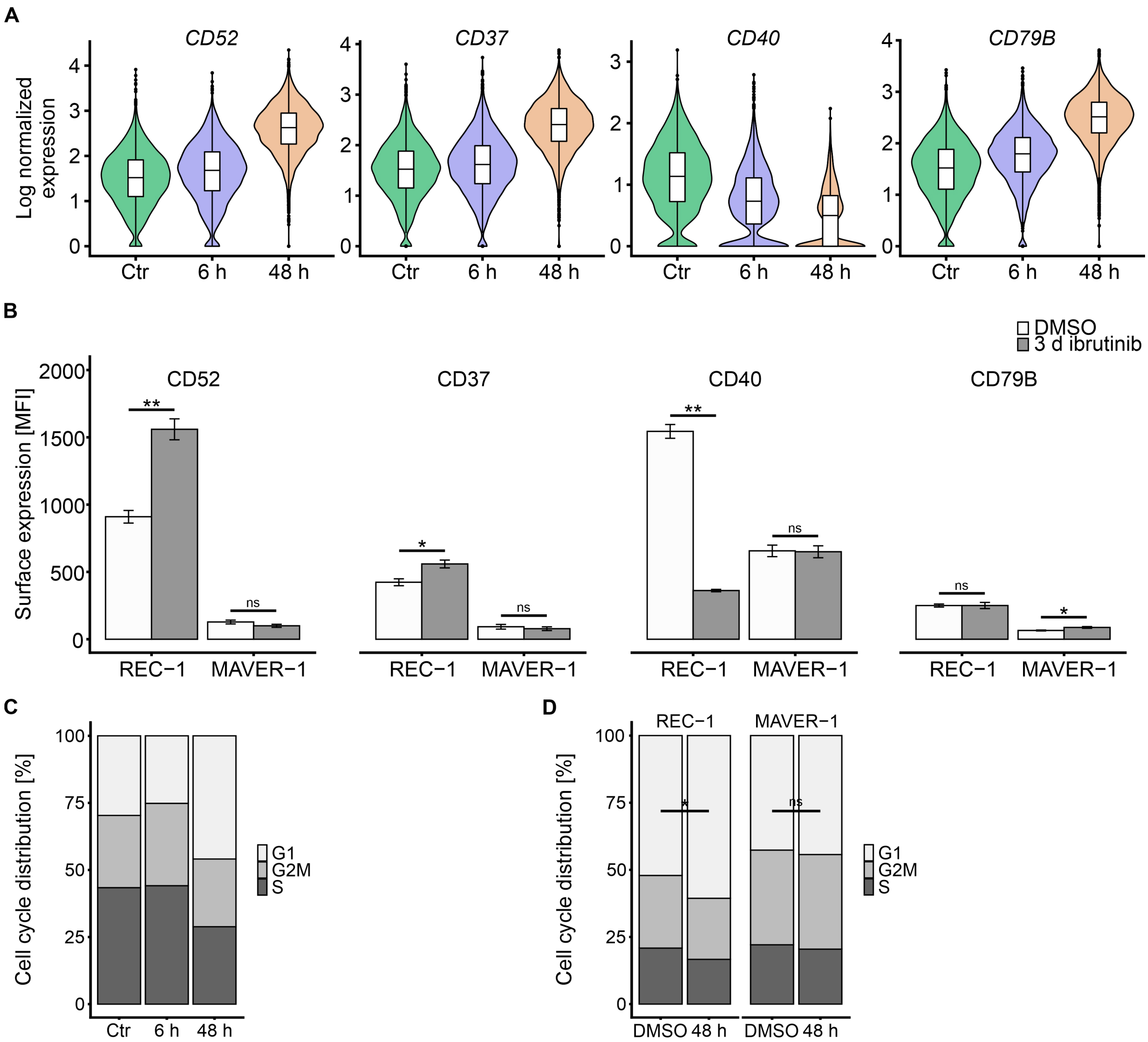

Figure 9: Validation of altered surface antigen expression levels and cell cycle shift following ibrutinib treatment. A) Violin plots illustrating the log normalized gene expression of the surface antigens (scRNA-seq). B) Mean fluorescence intensities (MFI, geometric mean) of the surface antigens as determined by flow cytometry after 400 nM ibrutinib for 3 d, DMSO as control (N = 3). C) Distribution of cell cycle phases across Ctr, 6 h, and 48 h (scRNA-seq). D) Flow cytometry analysis of cell cycle phases in REC-1 and MAVER-1 after 48 h with 400 nM ibrutinib (48 h), DMSO as control (N = 3). B) and D) Data shown as mean (± SEM for [B]). Significant alterations were assessed by two-sided t-test (* $P \leq 0.05$, ** $P \leq 0.01$, and ns = not significant). Modified from Fuhr et al. [156]; reproduced with permission from Springer Nature [157].

Focusing on the distribution of cells cycling in G2M phase, S phase or non-cycling cells (referred to as G1) unveiled a shift towards a higher percentage of cells which entered a quiescent state and were assigned to G1 after 48 h of treatment in single-cell analysis (Figure 9C). A higher proportion of G1 cells after 48 h of ibrutinib treatment was also observed by analyzing the DNA content after PI staining of ibrutinib-treated REC-1 (Figure 9D). The cell cycle of the ibrutinib-resistant cell line MAVER-1 was not affected.

10.2.5 Ibrutinib alters metabolic activity of REC-1

Besides the common response to treatment, the subpopulations A, B, and D, comprising 7 809, 6 770, and 1 364 cells, respectively, were studied separately to track individual responses over treatment (Figure 10A).

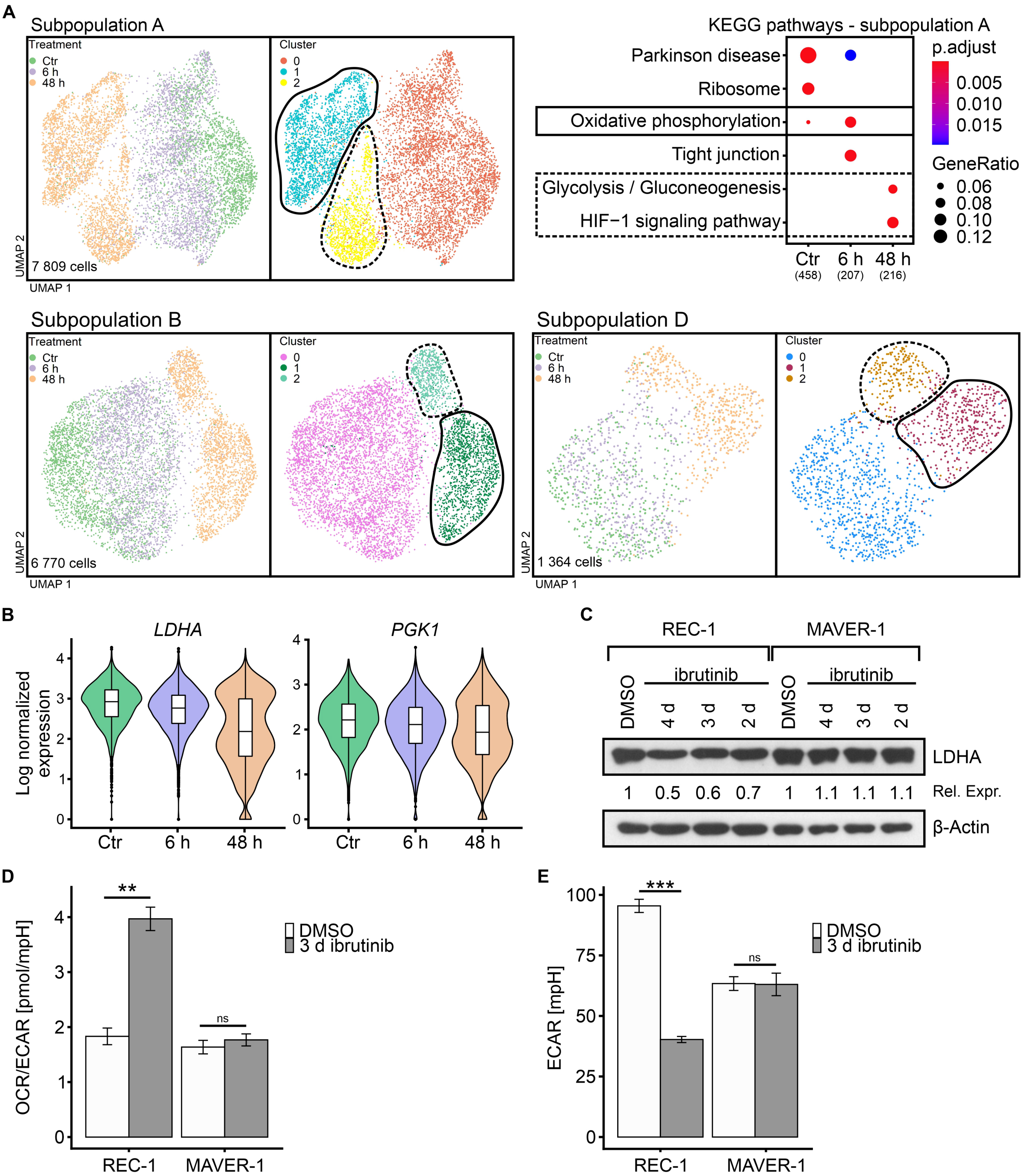

Figure 10: Analysis of subpopulations and metabolic evolution during ibrutinib treatment. A) Uniform manifold approximation and projection (UMAP) plots of the subpopulations A, B, and D including untreated (Ctr), 6 h and 48 h ibrutinib-treated cells; clustering at resolution 0.2 for A and B, 0.3 for D; solid and dashed lines highlight clusters according to assigned Kyoto Encyclopedia of Genes and Genomes (KEGG) pathway analysis for oxidative phosphorylation and glycolysis/HIF-1 signaling, respectively; KEGG analysis is shown for subpopulation A representatively, with genes of log fold change > 0.1 and adjusted *P*-value < 0.001 (no. = number of genes). B) Violin plots with log

normalized expression of *LDHA* and *PGK1* (scRNA-seq). C) LDHA expression in REC-1 and MAVER-1 across 4 d treatment with 400 nM ibrutinib; relative LDHA expression of ibrutinib- vs DMSO-treated samples were calculated following normalization of intensities to the loading control β-Actin; western blot representative for N = 3. D) Ratio of oxygen consumption rate (OCR) to extracellular acidification rate (ECAR) in REC-1 and MAVER-1 as determined by extracellular flux analysis after 3 d treatment with 400 nM ibrutinib, DMSO as control (N = 3). E) ECAR values of (D). D) and E) Data shown as mean ± SEM. Significant alterations were assessed by two-sided t-test (** $P \leq 0.01$, *** $P \leq 0.001$, and ns = not significant). Modified from Fuhr et al. [156]; reproduced with permission from Springer Nature [157].

Reclustering produced 3 clusters in each subpopulation, separating the Ctr and 6 h from the 48 h cells. The 48 h cells grouped again in two subsets. One subset was assigned to OXPHOS by the KEGG pathway analysis (cluster 1 in subpopulations A, B, and D), while the other cells were linked to glycolysis/gluconeogenesis and the HIF-1 signaling pathway (cluster 2 in subpopulations A, B, and D). The metabolic partitioning was reflected by the appearance of two subsets in 48 h with either high or low expression of *lactate dehydrogenase A* (*LDHA*) and *phosphoglycerate kinase 1* (*PGK1*), encoding for proteins involved in glycolysis (Figure 10B). However, the overall expression level of both genes decreased across treatment. At the protein level, a decrease in L-lactate dehydrogenase A chain (LDHA) was evident, whereas the ibrutinib-resistant MAVER-1 consistently expressed LDHA (Figure 10C).

An extracellular flux analysis was performed to study the OCR and ECAR representing indicators for mitochondrial respiration or OXPHOS and glycolysis, respectively. In contrast to ibrutinib-resistant cells, a shift towards higher OCR/ECAR ratio was detected after 3 d ibrutinib treatment in REC-1, indicating higher dependence on mitochondrial respiration and OXPHOS (Figure 10D). This alteration was caused by decreased ECAR in REC-1, pointing to weakened glycolysis triggered by ibrutinib in sensitive cells (Figure 10E).

10.2.6 Ibrutinib influences gene regulatory networks in REC-1

The single-cell regulatory network inference and clustering (SCENIC) method enabled the analysis of gene regulatory networks (GRN) and their adaptations across ibrutinib treatment. SCENIC identified the activity of transcription factors (TFs) together with their cofactors and target genes building the GRNs. As the predominant alterations in the transcriptome were observed between Ctr/6h cells towards 48h cells, differences in GRN activities between these two time periods were assessed and resolved according to the Seurat clustering approach (Figure 11A, see Figure 8A for clustering).

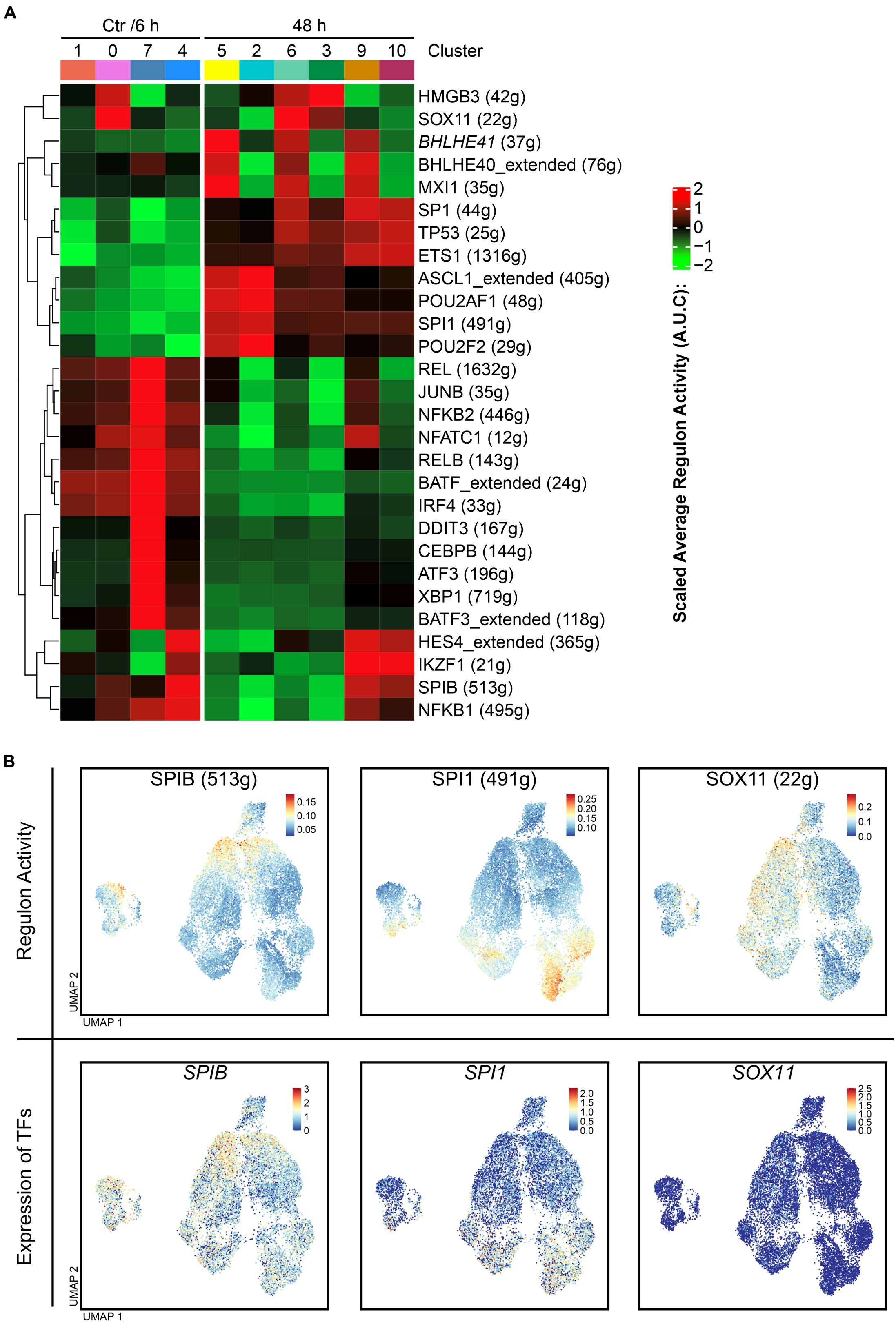

Figure 11: Gene regulatory network analysis. A) Scaled average regulon activity across ibrutinib treatment in the eleven clusters of the combined analysis (see clustering in Figure 8A); number of genes (g) of regulons are indicated in parenthesis next to the transcription factors. B) Uniform manifold approximation and projection (UMAP) plots of combined data presenting regulon activity (top) and log normalized gene expression of the corresponding transcription factors (below). Modified from Fuhr et al. [156].

Some GRNs were characteristic of all Ctr/6h cells and were suppressed following ibrutinib treatment. The activity of TFs associated with NF-kB signaling (proto-oncogene c-Rel [REL], nuclear factor NF-κB p100 subunit [NFKB2], transcription factor RelB [RELB], transcription factor JunB [JUNB]) was higher in untreated cells or at early treatment. Only subpopulation D (cluster 9 and 10) was still regulated by nuclear factor NF-κB p105 subunit (NFKB1) in 48 h. In turn, other transcription factors essential for proper B-cell function were more dominant in 48 h. Especially the takeover of transcription factor PU.1 (SPI1; together with POU domain class 2-associating factor 1 and 2 [POU2AF1 and POU2F2]) in place of transcription factor Spi-B (SPIB; together with basic leucine zipper transcriptional factor ATF-like [BATF] and interferon regulatory factor 4 [IRF4]), having redundant functions, highlighted the alterations in B-cell regulatory processes during ibrutinib treatment. The GRN analysis correlated with the gene expression of *Spi-B transcription factor* (*SPIB*) and *Spi-1 proto-oncogene* (*SPI1*), which were expressed at higher levels in the untreated and 48 h treated cells, respectively (Figure 11B). The GRNs of TP53, transcription factor Sp1 (SP1), involved in regulation of oncogenes and tumor suppressors, and protein C-ets-1 (ETS1), associated with oncogenic properties, defined the 48 h cells (Figure 11A).

Next to the general alterations, some GRNs were specific for single clusters or subpopulations. The activity of the TFs HMGB3 and SOX11 were elevated in the subpopulation B throughout treatment (cluster 0, 3, and 6; Figure 11A). However, the gene expression of *SRY-box transcription factor 11* (*SOX11*) was not enhanced compared to the other subpopulations (Figure 11B). The subpopulation D was dominated by the GRN of *hes family bHLH transcription factor 4* (*HES4*) representing a known NOTCH1 target gene, and maintained activity of *SPIB* (cluster 4, 9, and 10; Figure 11A). The activity of the TFs class E basic helix-loop-helix protein 40 and 41 (BHLHE40 and BHLHE41), and max-interacting protein 1 (MXI1) underlined the glycolytic/hypoxic state of the cells in the clusters 5, 6, and 9. Cluster 7, comprising the subpopulation C, was defined by DNA damage-inducible transcript 3 protein (DDIT3), CCAAT/enhancer-binding protein beta (CEBPB), cyclic AMP-dependent transcription factor ATF-3 (ATF3), and X-box-binding protein 1 (XBP1), reflecting the stress response in these cells.

Apart from subpopulation specific features, the SCENIC analysis revealed the suppressive effect of ibrutinib on NF-κB activity in REC-1 cells and the alterations in crucial transcriptional networks in the MCL cells.

10.3 Gene expression profile of REC-1 does not considerably change over 2- to 4-day treatment with ibrutinib

Given the heterogeneous appearance of REC-1 cells after 48 h of ibrutinib treatment in single-cell analysis, differential gene expression of surviving cells after prolonged treatment of more than 48 h was examined by bulk RNA-seq to characterize the surviving subpopulation (Figure 12A).

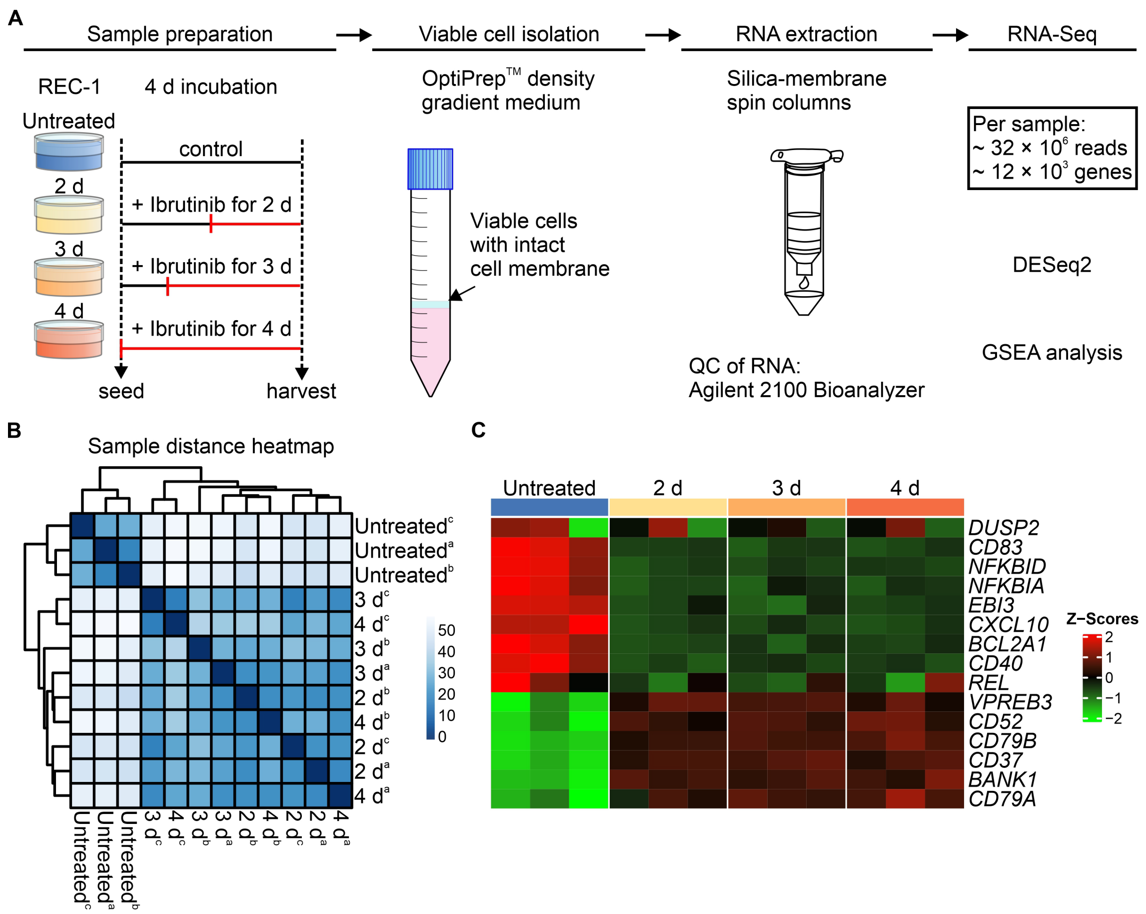

Figure 12: Bulk RNA sequencing of ibrutinib-treated REC-1. A) Sample preparation for bulk RNA sequencing (RNA-seq) with treatment of REC-1 with 400 nM ibrutinib (untreated as control) for up to 4 d, isolation of viable cells, RNA extraction, quality control (QC), sequencing and computational analysis with gene set enrichment analysis (GSEA; N = 3). B) Heatmap showing sample distances of three replicates (a, b, c) of each treatment based on the variance stabilizing transformed values. C) Heatmap with gene expression of bulk RNA-seq samples for top differentially expressed genes identified in the previous single-cell analysis. Modified from Fuhr et al. [158].

After treatment with 400 nM ibrutinib for up to 4 d, RNA of viable cells was isolated, underwent quality control, libraries were prepared and sequenced. Three replicates of every time point were included with around 32×10^6 reads and 12×10^3 detected genes per sample (Figure 12A). As illustrated by sample distances, the transcriptome of the ibrutinib-treated samples after 3 d and 4 d did not differ from that after 2 d of treatment (Figure 12B). This was reflected in the number of differentially regulated genes with 385 up- and 633 down-regulated genes for 2 d vs untreated and only 8 up- and 4 down-regulated genes for 2 d vs 4 d (|log2FC| ≥ 1, padj < 0.05). In line with the top DEGs from the single-cell analysis, the bulk RNA-seq approach revealed a similar expression pattern with downregulation of NF-κB associated genes, and upregulation of genes encoding for the BCR subunits and surface antigens CD37 and CD52 at 2 d, 3 d, and 4 d treatment with ibrutinib (Figure 12C). Despite the minor changes in DEGs upon prolonged ibrutinib treatment of more than 2 d, a GSEA for KEGG pathways was performed to assess altered features in 4 d treated cells compared to an untreated control. The analysis revealed 82 negatively enriched pathways and 16 gene sets with positive enrichment (|log2FC| ≥ 1, *q*-value < 0.05; Figure 13).

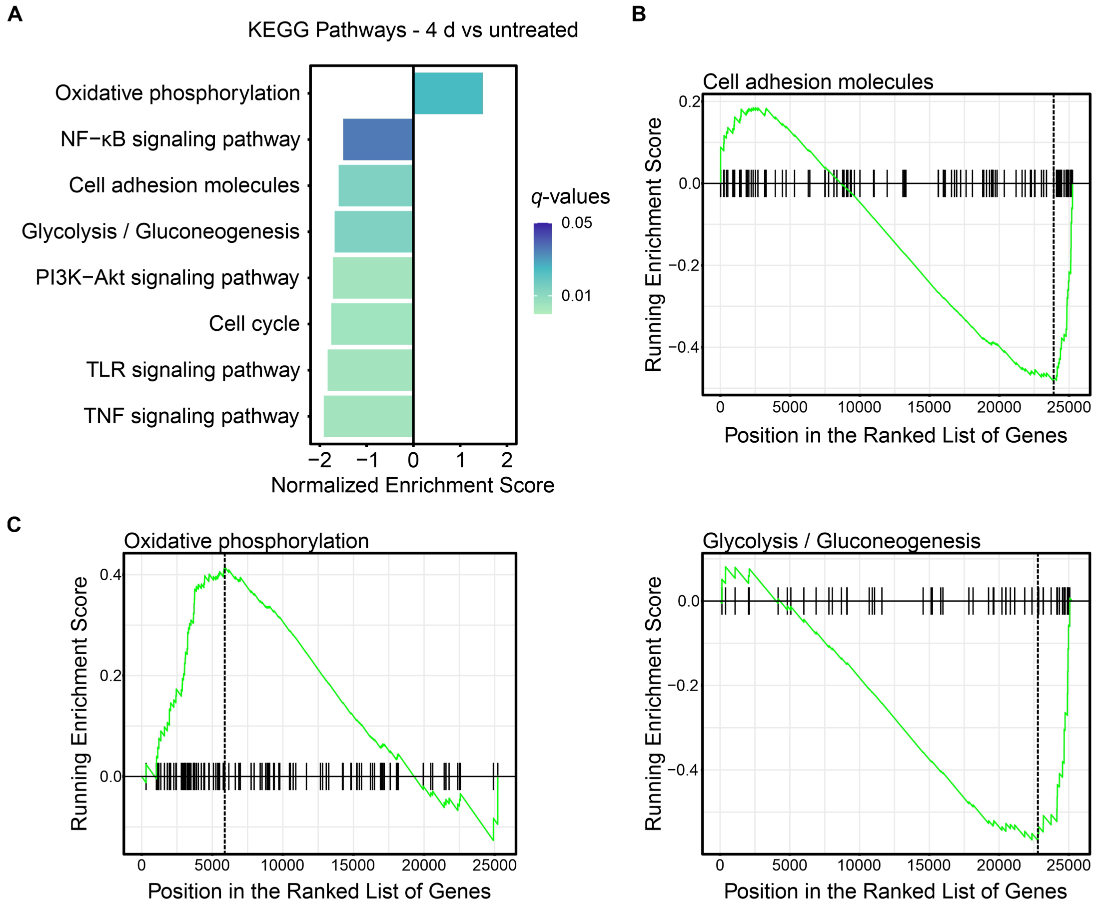

Figure 13: Gene set enrichment analysis of ibrutinib-treated REC-1. A) Gene set enrichment analysis (GSEA) for Kyoto Encyclopedia of Genes and Genomes (KEGG) pathways of 4 d ibrutinib-treated REC-1 vs untreated; selected significant pathways are shown (|log2FC| ≥ 1, *q*-value < 0.05). B) + C) Enrichment plots for KEGG pathways 'Cell adhesion molecules' (B) and metabolic pathways (C) as revealed by GSEA analysis shown in (A). Modified from Fuhr et al. [158].

As expected, NF-kB signaling, and cell cycle were suppressed after 4 d of treatment (Figure 13A). Furthermore, signaling pathways important for B-cell function were negatively enriched, namely PI3K-AKT, Toll-like receptor, and tumor necrosis factor (TNF) signaling.

REC-1 cells also exhibited reduced cell adhesion (Figure 13B). Alterations in metabolism were manifested by reduced glycolysis and increased OXPHOS (Figure 13C).

10.4 High sensitivity of REC-1 to concomitant treatment with IACS-010759 and ibrutinib

The effect of the OXPHOS inhibitor IACS-010759 (IACS) on the proliferation of MCL cell lines was tested. Titration of 1 to 100 nM IACS for 3 d resulted in moderate reduction of proliferation in all cell lines (Figure 14, left). The maximal effect of IACS was achieved at a minimal concentration of 25 nM, where the proliferation of all cell lines ranged from 55% to 75%. REC-1 showed higher sensitivity over incubation from 1 to 3 d compared to MAVER-1 (Figure 14, right). In contrast, proliferation of MAVER-1 decreased considerably from the 3rd to 4th day of treatment, while proliferation of REC-1 only slightly decreased.

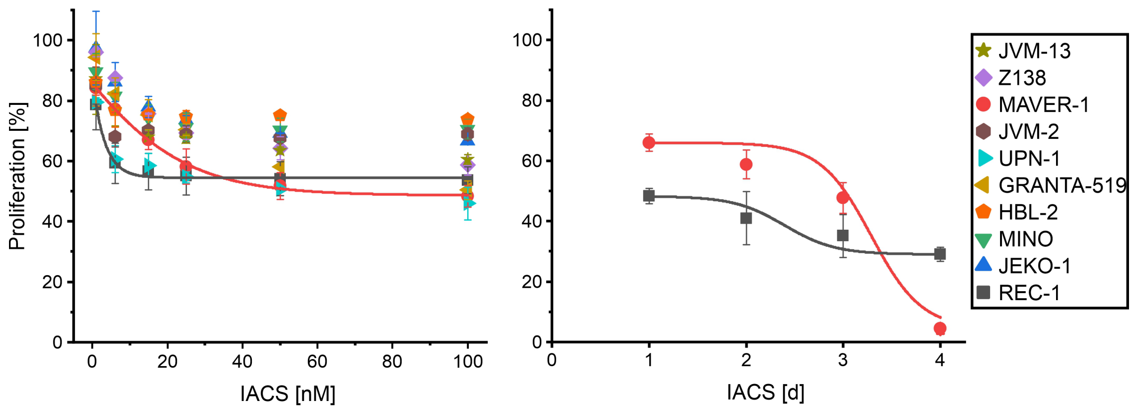

Figure 14: IACS-010759 titration and kinetics of mantle cell lymphoma cell lines. Proliferation of 10 MCL cell lines, with solid lines for REC-1 (gray) and MAVER-1 (red), after treatment with 1-100 nM IACS-010759 (IACS) for 3 d (N = 2, N = 3 for REC-1 and MAVER-1; left), and proliferation of REC-1 and MAVER-1 across 1 to 4 d treatment with 25 nM IACS (N = 3; right); as determined by 3-(4,5-dimethylthiazol-2-yl)-2,5-diphenyltetrazolium bromide (MTT) assay. Data shown as mean ± SEM. Modified from Fuhr et al. [158].

The combination of ibrutinib with IACS was first assessed by a consecutive approach. REC-1 cells were pretreated with 400 nM ibrutinib for 3 d to induce the metabolic switch to OXPHOS dependence, followed by separation of viable cells and incubation with 25 nM IACS for an additional 2 d.

IACS reduced proliferation to 29% and 74% in REC-1 and MAVER-1, respectively (Figure 15A). Ibrutinib caused a drop in proliferation of REC-1 to 37%. However, the addition of IACS to ibrutinib did not significantly increase toxicity compared to single-agent ibrutinib in REC-1. Because MAVER-1 cells were not affected by ibrutinib, proliferation was the same between IACS and ibrutinib plus IACS.

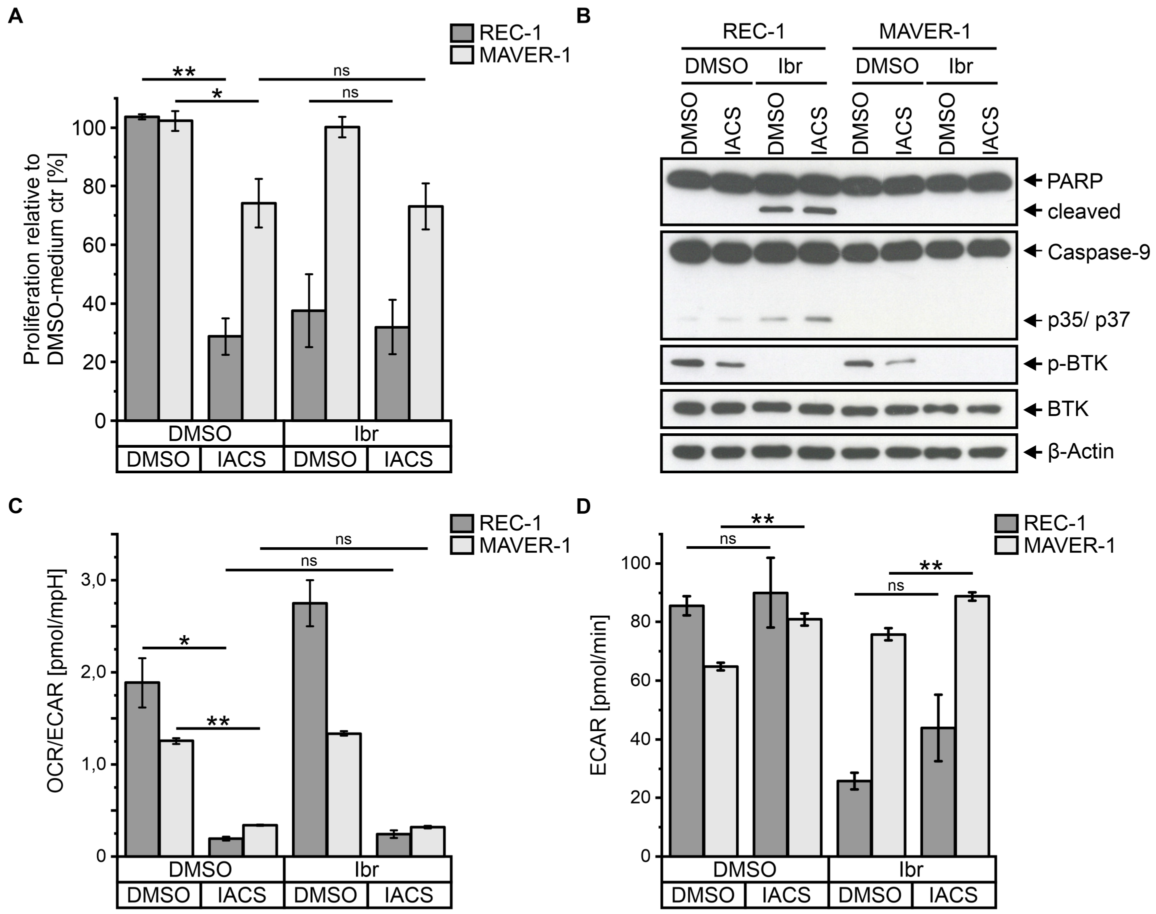

Figure 15: Consecutive treatment with ibrutinib and IACS-010759. A) Proliferation of REC-1 and MAVER-1 cells after 3 d pretreatment with 400 nM ibrutinib (Ibr; DMSO control) followed by viable cell isolation and 2 d treatment with 25 nM IACS-010759 (IACS; DMSO control) and the corresponding pretreatment (Ibr or DMSO); proliferation was assessed by 3-(4,5-dimethylthiazol-2-yl)-2,5-diphenyltetrazolium bromide (MTT) assay (N = 3). B) Western blot of protein lysates from cells treated as described in (A); β-Actin served as loading control (representative for N = 3). C) Extracellular flux analysis of cells treated as described in (A), but without isolation of viable cells after pretreatment; ratio of oxygen consumption rate (OCR) vs extracellular acidification rate (ECAR) is shown (N = 3). D) ECAR values from (C). Data shown as mean ± SEM. Significant alterations were assessed by two-sided t-test (* $P \leq 0.05$, ** $P \leq 0.01$, and ns = not significant). Modified from Fuhr et al. [158].

With respect to induction of apoptosis, western blot analysis revealed same level of PARP cleavage in cells treated with ibrutinib or the combination, and only slightly higher Caspase-9 cleavage for the combined treatment in REC-1 (Figure 15B). Neither ibrutinib nor IACS caused apoptosis in MAVER-1, as no cleavage products of PARP or Caspase-9 were detected. Phosphorylation of BTK was inhibited by ibrutinib and reduced after treatment with IACS alone in REC-1 and MAVER-1.

To study the metabolic effect of IACS on the cells, an extracellular flux analysis was performed. Treatment with IACS for 2 d strongly reduced the OCR/ECAR ratio in both cell lines without significant differences between IACS alone or in combination with ibrutinib (Figure 15C). IACS increased glycolytic activity in MAVER-1, as reflected by ECAR (Figure

15D). For REC-1, ibrutinib led to a reduction of ECAR, which increased again, although not significantly, when IACS was added.

Whether simultaneous OXPHOS inhibition plus ibrutinib treatment had a more potent effect was investigated using a concomitant approach. In REC-1, proliferation was weakened to 25% by ibrutinib and to 30% by IACS (Figure 16A).

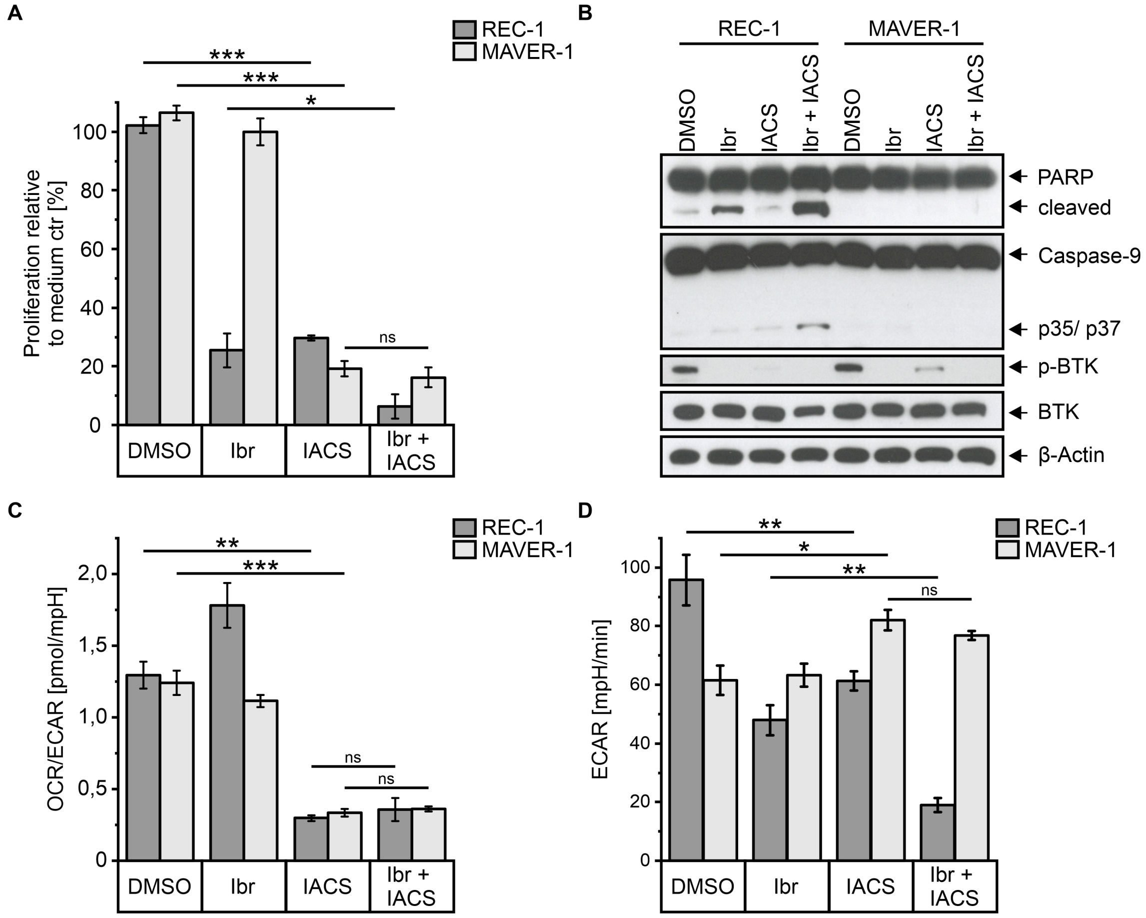

Figure 16: Concomitant treatment with ibrutinib and IACS-010759. A) Proliferation of REC-1 and MAVER-1 cells after 4 d treatment with 400 nM ibrutinib (Ibr; DMSO control) and 25 nM IACS-010759 (IACS; DMSO control); proliferation was assessed by 3-(4,5-dimethylthiazol-2-yl)-2,5-diphenyltetrazolium bromide (MTT) assay (N = 4). B) Western blot of protein lysates from cells treated for 3 d as described in (A); β-Actin served as loading control (representative for N = 3). C) Extracellular flux analysis of cells treated as described in (A) for 3 d; ratio of oxygen consumption rate (OCR) versus extracellular acidification rate (ECAR) is shown (N = 4). D) ECAR values from (C). Data shown as mean ± SEM. Significant alterations were assessed by two-sided t-test (* $P \leq 0.05$, ** $P \leq 0.01$, *** $P \leq 0.001$, and ns = not significant). Modified from Fuhr et al. [158].

The combination of both inhibitors significantly increased toxicity compared with ibrutinib as single agent. IACS reduced proliferation of MAVER-1 and led to lower proliferation than in REC-1 after 4 d. Ibrutinib had no effect on MAVER-1, so proliferation was equally reduced between IACS alone and ibrutinib plus IACS. In western blot analysis, increased PARP and Caspase-9 cleavage indicated higher apoptosis in REC-1 cells treated with the combination (Figure 16B). Similar to ibrutinib, IACS blocked phosphorylation of the BTK in REC-1 and reduced phosphorylation levels in MAVER-1.

Ibrutinib triggered an increased OCR/ECAR ratio in REC-1. When cells were treated with IACS, the ratio declined, with no difference between IACS as single or combined treatment (Figure 16C). The OCR/ECAR ratio of MAVER-1 was reduced to similarly low levels by IACS and the addition of ibrutinib had no effect. While MAVER-1 showed increased ECAR upon treatment with IACS, ECAR of REC-1 was reduced by ibrutinib and IACS as single agents (Figure 16D). The combination of the two inhibitors dramatically lowered ECAR of REC-1, which contrasted with the consecutive treatment described above, resulting in an increase, albeit not significant, of ECAR.

10.5 REC-1 cells are highly responsive to anti-CD52-mediated complement dependent cytotoxicity following ibrutinib pretreatment

Mantle cell lymphoma cell lines were treated with 400 nM ibrutinib for 3 d to assess whether CD52 expression increased. However, only the REC-1 cell line showed higher CD52 surface levels compared with DMSO control (Figure 17A).

Efficacy of combined treatment with ibrutinib and a monoclonal antibody targeting CD52 was investigated using a consecutive approach. REC-1 and MAVER-1 were pretreated with 400 nM ibrutinib for 3 d, before viable cells were isolated and treated with CD52 mAb and human serum as source of complement. Appropriate antibody concentration was tested with concentrations from 1 to 30 µg/ml in REC-1 (Figure 17B). Ibrutinib-pretreated REC-1 showed high sensitivity to treatment and a strong drop in viability upon increasing concentrations. The control group of DMSO-pretreated cells was less sensitive, resulting in 53% and 8% of viable cells after incubation with 30 µg/ml CD52 mAb for DMSO- and ibrutinib-pretreated cells, respectively. For subsequent experiments, 10 µg/ml CD52 mAb was set to achieve the maximal effect at the minimal dose.

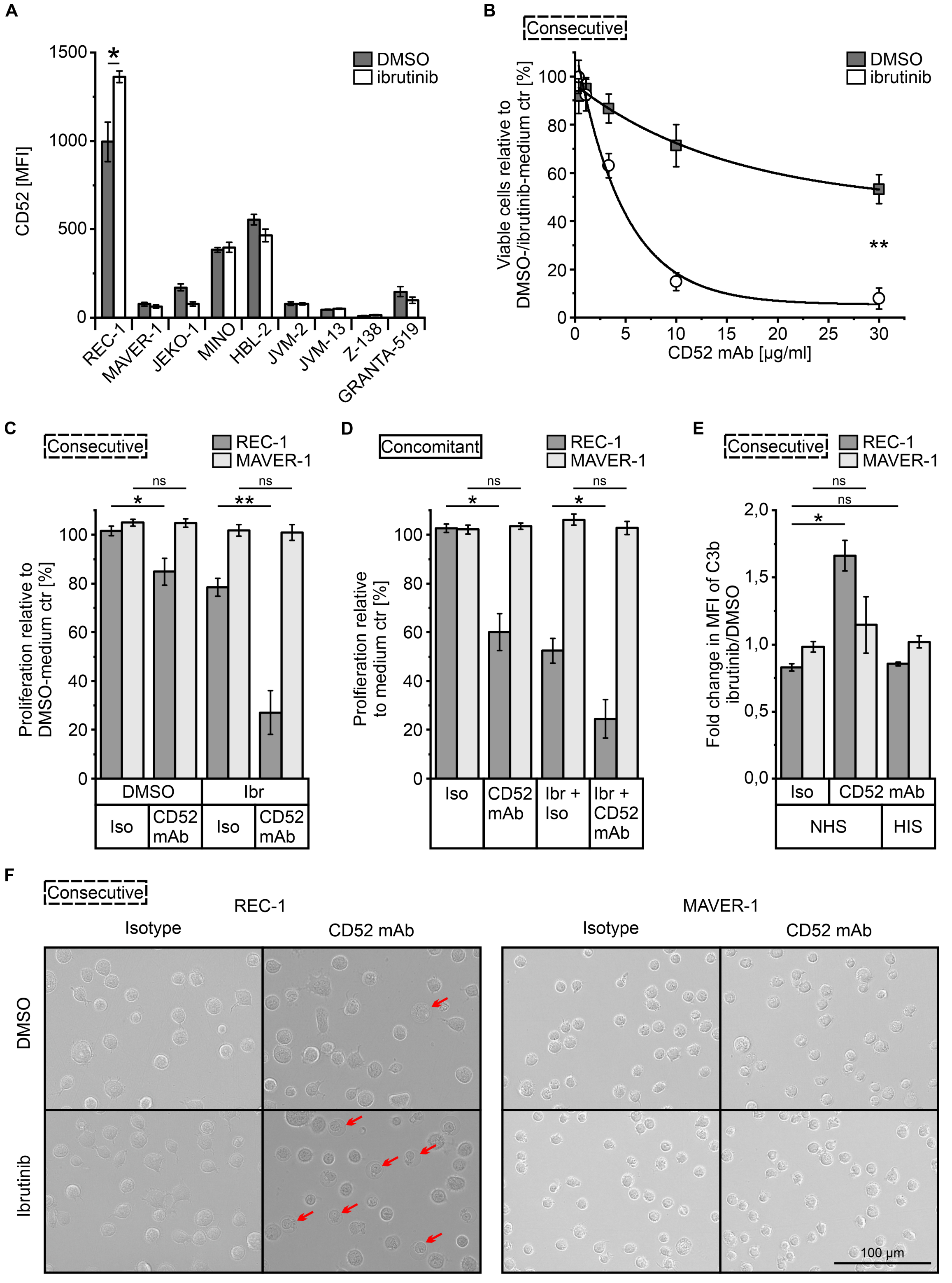

Figure 17: CD52 surface expression of mantle cell lymphoma cell lines following ibrutinib treatment and combination of ibrutinib with anti-CD52 treatment. A) Surface CD52 expression on 9 MCL cell lines treated with 400 nM ibrutinib (DMSO control) for 3 d (N = 3); mean fluorescence intensity (MFI, median) is plotted as analyzed by flow cytometry using CD52-PE staining. B) Percentage of viable REC-1 cells (propidium iodide negative, PI⁻) after pretreatment with 400 nM ibrutinib (DMSO control) followed by isolation of viable cells, addition of 1-30 µg/ml CD52 mAb and 10% normal human serum (NHS) for 15 min; cells were analyzed by flow cytometry (N = 3). C) Proliferation of REC-1 and MAVER-1 after consecutive treatment as described in (A) using 10 µg/ml CD52 mAb (N = 4), and D) after concomitant treatment with 400 nM ibrutinib plus 10 µg/ml CD52 mAb and NHS treatment for

48 h (N = 3); proliferation as assessed by 3-(4,5-dimethylthiazol-2-yl)-2,5-diphenyltetrazolium bromide (MTT) assay. E) Fold change of C3b deposition on cell surface between ibrutinib- and DMSO-pretreated cells after consecutive treatment described in (B) with NHS or heat-inactivated human serum (HIS) as control; C3b-FITC mean fluorescence intensity (MFI, geometric mean) was analyzed by flow cytometry. F) Microscopy after consecutive treatment as described in (B) showing bloated plasma membranes (red arrows); images were transferred to grayscale and are representative for N = 3. Data shown as mean ± SEM. Significant alterations were assessed by two-sided t-test (* $P \leq 0.05$, ** $P \leq 0.01$, and ns = not significant). Modified from Fuhr et al. [158].

In the consecutive approach, anti-CD52 treatment slightly reduced proliferation of DMSO-pretreated REC-1 cells (Figure 17C). Addition of CD52 mAb to ibrutinib-treated REC-1 cells led to a fast reduction in proliferation, with only 27% remaining proliferative activity compared to 78% in the isotype control. Neither ibrutinib nor anti-CD52 treatment altered proliferation of MAVER-1 cells.

Since the concomitant regimen with IACS yielded higher efficacy, the effect of simultaneous ibrutinib plus anti-CD52 treatment combined with human serum for 48 h was assessed. Anti-CD52 treatment for 48 h decreased proliferation of REC-1 to 60%, and to 24% when combined with ibrutinib (Figure 17D). Nevertheless, the add-on effect of anti-CD52 therapy relative to ibrutinib-isotype was lower with 28% decreased proliferation with the concomitant versus 51% with the consecutive approach. Again, MAVER-1 cells were not affected by ibrutinib and anti-CD52 treatment.

To retrace the CD52 mAb-induced mechanism of cell death in the consecutive setup, complement activation was assessed by detecting the complement component C3b on the cell surface. Treatment with anti-CD52 led to 1.7-fold higher C3b levels on ibrutinib-pretreated REC-1 compared with the DMSO-pretreated control (Figure 17E). Fold change of C3b deposition after anti-CD52 treatment was significantly higher than after treatment with the corresponding isotype control. Addition of HIS together with CD52 mAb did not result in complement activation or any difference between ibrutinib- and DMSO-pretreated REC-1. For MAVER-1 cells, no significant alterations in complement activation were observed upon anti-CD52 treatment.

CD52 mAb-mediated complement-dependent cytotoxicity (CDC) in ibrutinib-pretreated REC-1 cells was illustrated by microscopy (Figure 17F). Ibrutinib-pretreated REC-1 cells showed a high number of cells with bloated plasma membranes and lysed cells, whereas the morphology of MAVER-1 was not affected by anti-CD52 treatment.

For translation of the consecutive anti-CD52 treatment approach to primary cells, an improved B-cell cultivation protocol was needed to ascertain proper growth during the required 3-day incubation with ibrutinib.

10.6 Cultivation with IL-4 and CD40L alters response to ibrutinib and CD52 levels of primary mantle cell lymphoma cells

The use of cytokines can mimic microenvironmental signaling and trigger proliferation and activation of primary B cells. Besides standard cultivation with RPMI-1640 and 2 mM L-Glutamine (RPMI), StemMACS™ HSC Expansion Media XF from a B Cell Expansion Kit (Miltenyi Biotec) was tested. CD40 ligand (CD40L) and the cytokine IL-4 were added to MACS medium to trigger B-cell/MCL cell activation and proliferation. Instead of FBS, 10% HIS was used.

Frozen PBMC from an MCL patient were thawed and cultivated for 3 d with different media compositions and 400 nM ibrutinib or DMSO. Cultivation in RPMI and MACS without additives resulted in lowest proliferation (Figure 18A) and survival rate of viable MCL cells ($CD19^+PI^-$; Figure 18B).

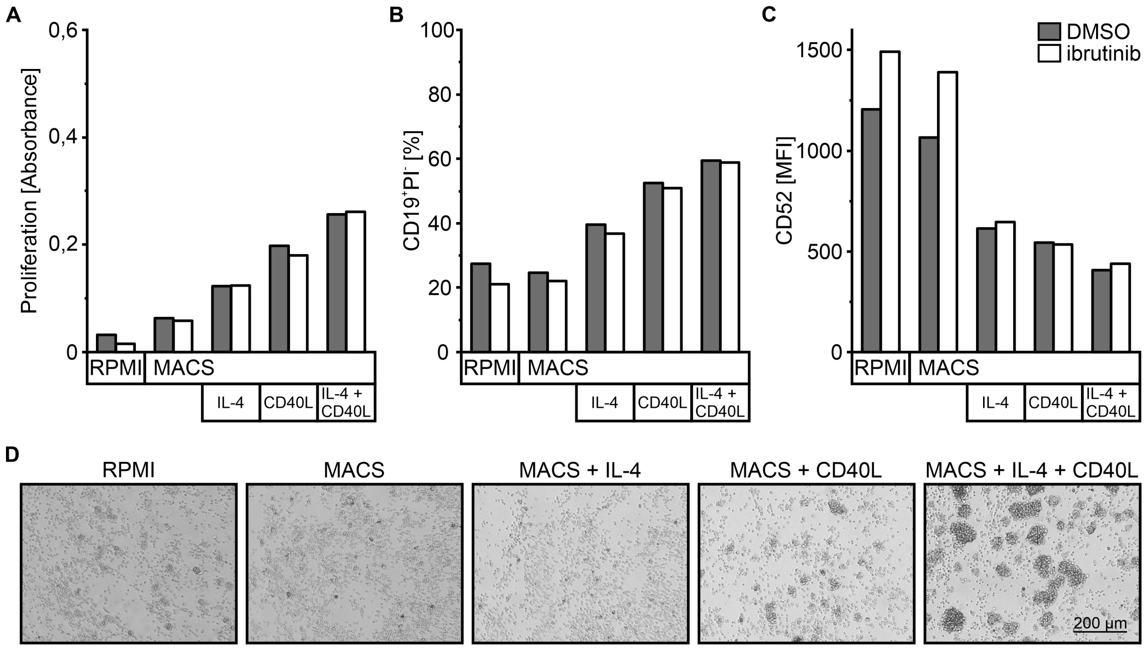

Figure 18: Cultivation of primary mantle cell lymphoma cells. Peripheral blood mononuclear cells (PBMC) from an MCL patient after cultivation with RPMI-1640 medium containing 2 mM L-Glutamine (RPMI), StemMACS™ HSC Expansion Media XF (MACS), the additives IL-4 (50 IU/ml) and CD40L (100 ng/ml) and 10% human serum and treatment with 400 nM ibrutinib (DMSO control) for 3 d. A) Proliferation of cells was determined by 3-(4,5-dimethylthiazol-2-yl)-2,5-diphenyltetrazolium bromide (MTT) assay, absorbance of respective media (RPMI or MACS) was subtracted. B) Percentage of viable MCL cells ($CD19^+PI^-$), and C) CD52 levels of viable MCL cells (MFI, geometric mean), analyzed by flow cytometry using CD19-FITC, CD52-APC, and propidium iodide (PI) staining with gating for doublets and debris. D) Microscopy of PBMCs treated with DMSO.

The addition of IL-4 to PBMCs growing in MACS medium increased proliferation and the percentage of surviving MCL cells (Figure 18A and 18B). The positive effect of CD40L was even higher, with the combination of both resulting in highest proliferative activity and survival. However, the toxic effect of ibrutinib on proliferation and MCL cell survival, which was visible in RPMI-cultivated cells, was diminished by using MACS medium and one or both additives. Measuring CD52 levels revealed that cells lost CD52 surface expression when cultured with one or both supplements (Figure 18C). In addition, cultivation with IL-4 and/or CD40L impeded the upregulation of CD52 surface levels triggered by ibrutinib that was observed when culturing in RPMI or MACS without additives. Lower CD52 expression was associated with a different morphology and behavior of the cells, which started to cluster upon addition of CD40L and formed large clusters when IL-4 and CD40L were present in MACS medium (Figure 18D).

10.7 Primary ibrutinib-sensitive mantle cell lymphoma cells are more prone to anti-CD52-mediated toxicity when pretreated with ibrutinib

Primary MCL cells from 10 patients were treated with ibrutinib to assess a potential increase of CD52 levels. PBMCs from 8 patients (P), lymph nodes from 2 patients (L), and 2 PBMC samples from healthy donors (H) were included (see Table 2 for patient characteristics).

Table 2: Characteristics of primary samples.

Sample	Type	Sex	Mantle cell lymphoma subtype	Therapy prior to sample collection	In vitro (treatment)
P1	PBMC	m	classic nodal	no	3 d
P2	PBMC	m	classic nodal	no	3 d
P3	PBMC	m	classic nodal	yes, Nordic protocol, ibrutinib	2 d
P4	PBMC	m	classic nodal	no	2 d
P5	PBMC	f	leukaemic non-nodal	no	3 d
P6	PBMC	m	classic nodal	no	3 d
P7	PBMC	m	classic nodal	no	3 d
P8	PBMC	m	classic nodal	no	3 d
L1	Lymph node	m	classic nodal	n.a., pre-ibrutinib era	2 d
L2	Lymph node	m	classic nodal	n.a., pre-ibrutinib era	2 d
H1	PBMC	f	healthy control	no	2 d
H2	PBMC	f	healthy control	no	3 d

PBMC = peripheral blood mononuclear cells, in vitro (treatment) = 2 or 3 d treatment with 400 nM ibrutinib, m = male, f = female, n.a. = not available; Nordic protocol = rituximab, augmented CHOP/cytarabine with high-dose consolidation and autoSCT [159]. Modified from Fuhr et al. [158].

After thawing of the frozen material, cells were seeded and incubated with 400 nM ibrutinib or DMSO for 2 to 3 d depending on cell fitness. The viability after ibrutinib treatment varied between patient samples and therefore P2, P6, P7, and P8 were considered as ibrutinib-sensitive (viability loss > 50%) and all other cases as ibrutinib-insensitive (viability loss ≤ 50%; Figure 19A). CD52 levels of primary MCL cells from peripheral blood and lymph nodes were higher than on healthy control B cells. MCL cells of PBMCs from 4 patients, including the ibrutinib-resistant patient sample (P3) and two ibrutinib-sensitive cases, showed a considerable upregulation of CD52 (> 25% compared to DMSO-treated control) following ibrutinib treatment.

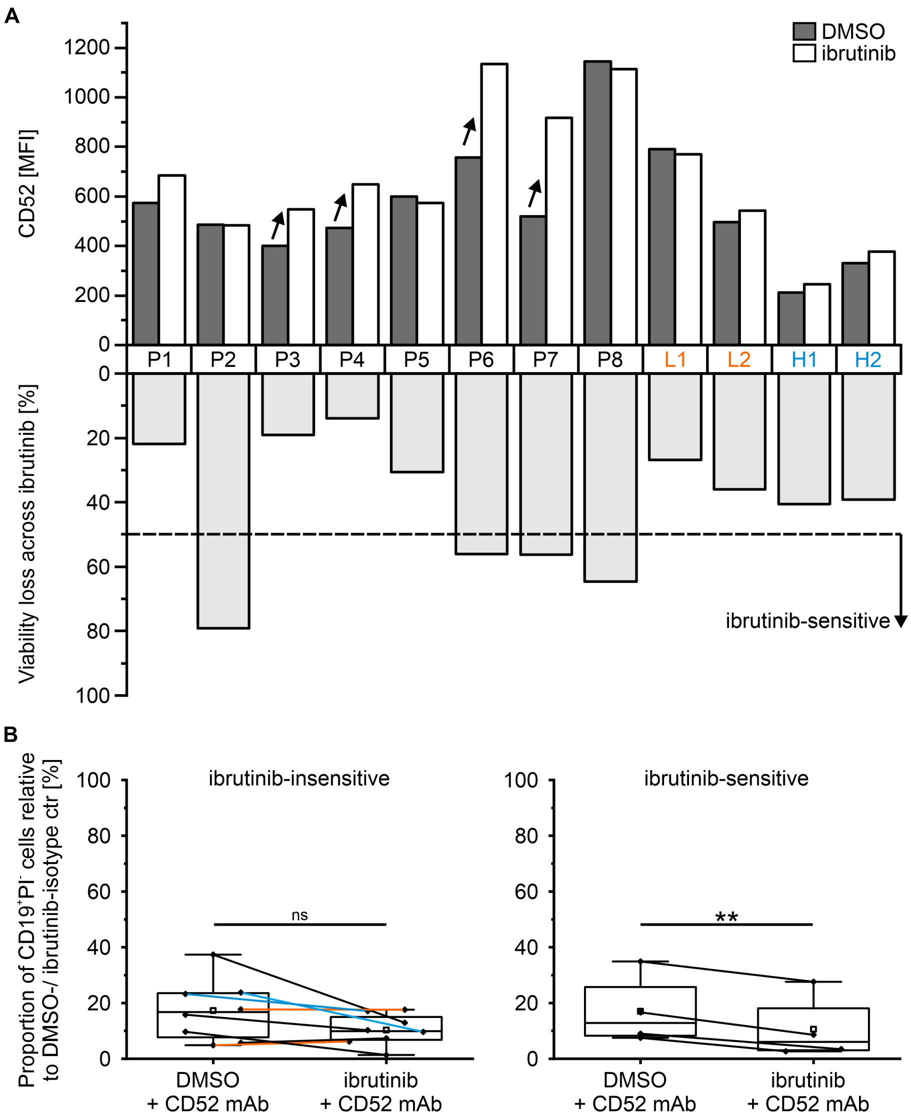

Figure 19: Ibrutinib and anti-CD52 treatment of primary mantle cell lymphoma cells. A) CD52 surface expression as mean fluorescence intensity (MFI, median) and viability loss (below) of primary mantle cell lymphoma (MCL) cells from 8 PBMC (P) and 2 lymph node (L, orange) samples from MCL patients, as well as 2 healthy controls (H, blue) after treatment with 400 nM ibrutinib (DMSO control) for 2 or 3 d (arrows indicate > 25% increase in CD52 levels compared with DMSO control); determined by flow cytometry using CD19-FITC, CD52-APC, and propidium iodide (PI) staining; debris and doublets were excluded and only viable MCL cells ($CD19^+PI^-$) were measured. B) Survival of primary MCL cells after consecutive approach with 2 or 3 d pretreatment with 400 nM ibrutinib (DMSO control) followed by addition of 10 µg/ml anti-CD52 and 10% normal human serum; boxplot depicts percentage of surviving MCL cells ($CD19^+PI^-$) of either ibrutinib-sensitive (viability loss > 50%) or ibrutinib-insensitive (viability loss ≤ 50%) cases after ibrutinib or DMSO pretreatment, with centerline and square indicating median and mean, respectively (ctr for control). Shapiro-Wilk test and Paired t-test were performed. Modified from Fuhr et al. [158].

After ibrutinib pretreatment, primary MCL cells were incubated with CD52 mAb and human serum. In ibrutinib-insensitive cases, ibrutinib pretreatment did not lead to higher toxicity of anti-CD52 treatment (Figure 19B). However, focusing on the ibrutinib-sensitive cases revealed that CD52 mAb-mediated loss in viability was higher when primary MCL cells were pretreated with ibrutinib.

11 Discussion

11.1 Addressing ibrutinib resistance in mantle cell lymphoma

Mantle cell lymphoma mostly follows an aggressive clinical course. Although treatment options have evolved in recent years, the disease remains incurable [57]. Ibrutinib serves as well-tolerated second-line treatment. Despite of improved progression-free survival with a median of over 2 years, ibrutinib is not curative, as patients relapse [160]. Along a multi-target approach, combination regimens are investigated to improve therapeutic efficacy, using drugs that are well studied in MCL and have a complementary mechanism of action to ibrutinib. To date, clinical trials assessed ibrutinib in combination with anti-CD20 treatment (rituximab or obinutuzumab) and lenalidomide, venetoclax or bendamustine [161-163].

This work is based on the hypothesis that the mechanisms leading to resistance in MCL cells that have previously responded to ibrutinib are potential therapeutic targets. Disabling these escape mechanisms along with ibrutinib treatment may have a synergistic effect, eliminating residual cells causing minimal residual disease (MRD) and preventing relapse. Since resistance mechanisms in MCL are only partially elucidated and are caused by diverse events, this work first elucidated potential resistance mechanisms following ibrutinib treatment in sensitive cells of a cell line. For studying MCL, several established MCL cell lines are available. MINO, JEKO-1, and REC-1 were described as ibrutinib-sensitive [53, 164]. However, only REC-1 showed a considerable decrease in proliferation with apoptosis under ibrutinib exposure [165]. Intriguingly, despite its sensitivity, a subgroup of cells persisted prolonged treatment suggesting that some cells adapted or harbored features providing higher resistance to ibrutinib. The observation of drug-tolerant cells has already been described for cell lines of other entities and these persistent cells are suspected to expand under further drug exposure due to acquired resistance mechanisms [138]. REC-1 was therefore selected as a suitable model to study the evolution of ibrutinib-surviving MCL cells across ibrutinib treatment.

11.2 Time-resolved single-cell RNA sequencing to identify targets in mantle cell lymphoma treated with ibrutinib

Sequencing at single-cell resolution is of interest, particularly with respect to detection of subpopulations resembling potential resistant clones [166] eventually causing MRD and relapse in MCL. Although data on MRD status after ibrutinib monotherapy is lacking, MRD assessment after other treatment regimens in MCL has highlighted its decisive role in prognosis [167], as detected MRD is usually followed by disease progression, as for instance after the combined use of ibrutinib with rituximab in patients with indolent MCL [168]. With help of scRNA-seq, the transcriptional evolution of surviving tumor cells was tracked, resolved on single-cell level and for the time period of treatment to identify alterations such as activation of compensatory signaling pathways or expansion of a subclonal resistant population under selective pressure of treatment.

A time point of 6 h was chosen to account for early transcriptomic alterations with ibrutinib treatment and 48 h as the end point. The heterogeneous appearance of REC-1 cells after 48 h of ibrutinib treatment indicated that the single-cell data did not already identify the cells that ultimately survived. However, evolution of REC-1 was dominated by common alterations in subpopulations. Therefore, a bulk RNA-seq analysis followed for an extended incubation of up to 4 d to allow characterization of the final persistent cells.

11.2.1 Identification of an ibrutinib susceptible and an aggressive subpopulation

In our single-cell data, we encountered considerable heterogeneity of the investigated ibrutinib-sensitive MCL cell line REC-1. Even though cell lines are often seen as a homogeneous population of tumor cells, the scRNA-seq study of Kinker et al. screened 198 cancer cell lines across 22 cancer entities and revealed heterogeneous constitution in 11% [169]. Besides common sources for heterogeneity caused by cell cycle and stress response, subpopulations seem to be characteristic and unique to cell lines. In particular, the differential regulation of genes in cycling cells can overshadow other sources of heterogeneity in single-cell data [170]. Therefore, the effect of cell cycle on the heterogeneity of the data was reduced in this work, still leaving 2 main and 2 smaller subpopulations for analysis. A biologically meaningful difference between the two main subpopulations was not evident. More interestingly, the two small subpopulations showed specific patterns. One subpopulation with lowest CD52 expression, highest number of resting cells and a linked stress response was the only one which disappeared after 48 h ibrutinib treatment. Therefore, low CD52 expression, quiescence, and stress might represent features rendering the cells more vulnerable to ibrutinib treatment. Another subpopulation, which was consistently present across treatment, was linked to aggressive behavior with higher risk for metastasis, promotion of angiogenesis, and immune escape due to higher expression of *CXCL10* [171], *SPP1* [172], and *LGALS1* [173]. Additionally, the GRN analysis detected dominant activity of HES4 regulated gene network pointing to active NOTCH1 signaling in this subgroup [174]. Previous studies revealed that REC-1 carries an activating NOTCH1 deletion [175, 174], suggesting an overall higher impact of NOTCH1 signaling on gene expression in this cell line. Interestingly, NOTCH1 signaling has been identified as an important mechanism of TME interaction in MCL cells [174]. As MCL cells also reside in the bone marrow, spleen, and GI tract, the crosstalk between tumor cells and surrounding stromal and immune cells, providing cytokines or chemokines as survival signals or for stimulation of proliferation and metastasis, may be involved in drug resistance [176]. Although research in this field is still scarce [114], the features identified in this aggressive subpopulation may be important drivers of MCL cells' intrinsic mechanisms to engage the TME.

11.2.2 Common response with high CD52 and oxidative phosphorylation characterize surviving mantle cell lymphoma cells after ibrutinib treatment

Despite their heterogeneity, all surviving MCL cells responded similarly to ibrutinib treatment. Early on, cells downregulated NF-κB associated genes due to blocking of BTK and downstream signaling by ibrutinib. In addition, we observed an overall shift to the G1 phase of the cell cycle, suggesting entry into a quiescent cell state. In response to decreased BCR signaling, cells may have attempted to compensate by increasing BCR gene expression. However, the upregulation of CD79B was only observed in the single-cell analysis but could not be validated on protein level. Such inconsistencies in the correlation of mRNA and protein abundance can result from post-transcriptional regulation and transcriptional-burst events that can be buffered at the protein level [177]. Focusing on alterations of gene regulatory networks highlighted a switch in activation of key transcription factors for proper B-cell function, with SPI1 dominating in ibrutinib-treated cells. This contrasts with a single-cell study of ibrutinib-treated CLL patients by Rendeiro et al. describing decreased activity of the transcription factor SPI1 [178]. On the other hand, the primary CLL cells showed gene signatures similar to our findings, with an attenuated NF-κB signature and a quiescent cell state triggered by ibrutinib.

Additional common responses of ibrutinib-treated cells included decreased surface expression of CD40, a mediator of alternative NF-κB signaling and an NF-κB target gene, which may be due to reduced NF-κB signaling [179]. In contrast, ibrutinib provoked elevated CD52 and CD37 levels. The study by Rendeiro et al. reported inverse results with decreased CD37 and CD52 levels in CLL patients following ibrutinib treatment [178]. This could indicate that inhibition of BCR signaling and the expression of these surface antigens are linked, although the differential regulation between the two entities remains to be elucidated. Considering their broad expression on healthy and malignant B cells [180, 181], both surface antigens serve as potential targets and were already evaluated, especially in CLL.

To target CD37, different therapeutic approaches, such as monoclonal antibodies (mAb) and CAR T-cell therapy, have been developed and investigated [182, 183]. A phase I trial in RR CLL recently suggested, that the combination of an anti-CD37 mAb in combination with ibrutinib is a safe treatment regimen with potentially improved efficacy, as the overall response rate was 83% [184]. As CD37 is highly expressed on MCL cells [185], and is presumably upregulated by ibrutinib therapy, the surface marker represents a potential beneficial target in ibrutinib-treated MCL.

CD52 is a cell surface glycoprotein expressed on B and T lymphocytes and most blood cells, except for erythrocytes, platelets, and hematopoietic progenitor cells, and is also found in the male reproductive tract on mature sperm cells [186, 187]. For T cells, its role in transducing signals for activation and proliferation or migration was reported [188-190]. Research on monocytes in systemic sclerosis by Rudnik et al. revealed an antiadhesive role of CD52 [191]. They reported, that CD52 may regulate the expression of integrins, thereby controlling cell adhesion properties of monocytes. In MCL, tumor cell adhesion to the TME mediated by integrin-β1-signaling is linked to BCR signaling and both are diminished by treatment with ibrutinib [115]. Accordingly, the ibrutinib triggered increase in CD52 surface expression along with the decreased cell adhesion signature in REC-1 suggests that CD52 may contribute *in vivo* to the loss of tumor cell adhesion in lymph nodes and lymphocytosis following ibrutinib treatment. Besides, a regulatory function of CD52 expression on BCR signaling was assumed for malignant B cells in systemic lupus erythematosus [192]. Thus, elevated CD52 levels could be directly related to inhibition of BCR and associated integrin signaling by ibrutinib.

In addition, time-resolved single-cell analysis revealed evolution of distinct metabolic states. Interestingly, every subpopulation (besides subpopulation C) at its untreated state contained a group of cells with a glycolytic/hypoxic gene expression pattern. Across treatment, ibrutinib triggered a greater differentiation between metabolic states resulting in split subpopulations with each containing a group of cells with high activity of OXPHOS and glycolysis. A prolonged treatment of 4 d revealed predominant OXPHOS in surviving cells. Extracellular flux analysis corroborated the metabolic switch and indicated ibrutinib's suppressive effect on glycolysis in sensitive cells.

Research on metabolism in cancer cells started a century ago, when Otto Warburg discovered the abnormal glucose uptake and lactate production in cancer cells despite of oxygen availability [193]. Mitochondrial defects and reliance on glycolysis for ATP production were assumed. This misconception has been revised, as the reason for metabolic reprogramming to aerobic glycolysis in cancer cells was traced back to the genomic alterations causing activation of oncogenes (*KRAS proto-oncogene*, *GTPase* [*KRAS*], *MYC*), loss of tumor suppressors (*TP53*), and high activity of the PI3K/AKT/mTOR network [194]. Rapidly proliferating tumor cells are thus enabled to meet the high demand for biomolecules whose intermediates are supplied by glycolysis. Nevertheless, mitochondrial respiration is the main source for ATP in many tumor cells [194].

MCL is described as an fluorodeoxyglucose (FDG)-positron emission tomography (PET)-avid lymphoma showing high FDG uptake [195], suggesting a high glycolytic activity of the tumor cells. However, there are intra- and interindividual differences that may be related to tumor aggressiveness [196]. Since *TP53* is frequently mutated, metabolic regulation may be abrogated in MCL cells [197, 198]. However, REC-1 are reported to harbor p53 wild-type [199]. The preference for glycolysis may be mediated by active PI3K/AKT pathway, especially in the more aggressive blastoid variant and in cell lines such as REC-1 that is also characterized by a blastoid morphology [200, 201]. Constitutive AKT and PI3K activation are suggested to result from loss of expression of a negative regulator of the PI3K/AKT axis, the phosphatase and tensin homolog (PTEN), and *PI3KCA* amplification, respectively [200, 202]. Downstream activation of mammalian target of rapamycin complex 1 (mTORC1) by AKT can cause induction of transcription factor hypoxia-inducible factor 1-alpha (HIF-1α) [203] with its regulated glycolytic enzymes like LDHA [204]. The reduced expression of LDHA upon ibrutinib treatment in REC-1 thus indicated the decreased glycolytic activity due to BCR inhibition with attenuated PI3K/AKT signaling.

A metabolomic and fluxomic study by Lee et al. described reduced glycolysis with reduced lactate levels in ibrutinib-sensitive MCL cells following treatment with ibrutinib [205]. Consistent with this, metabolic reprogramming to glutamine-fueled OXPHOS was observed by Zhang et al. in MCL patients with primary/acquired ibrutinib-resistance [206]. An increase in OXPHOS was reported as response to other tyrosine kinase inhibitors, by vemurafenib in melanoma [207] and imatinib in gastrointestinal stromal tumors [208]. Besides, an OXPHOS pattern was characteristic for therapy-resistance in CML stem cells [209], breast cancer stem cells [210], AML [211], NSCLC [212], and CLL [213], to name a few examples. The mechanisms and reasons still have to be elucidated [214].

The impact of ibrutinib on cell metabolism and surface antigen expression were considered favorable potential targets for further investigation (Figure 20).

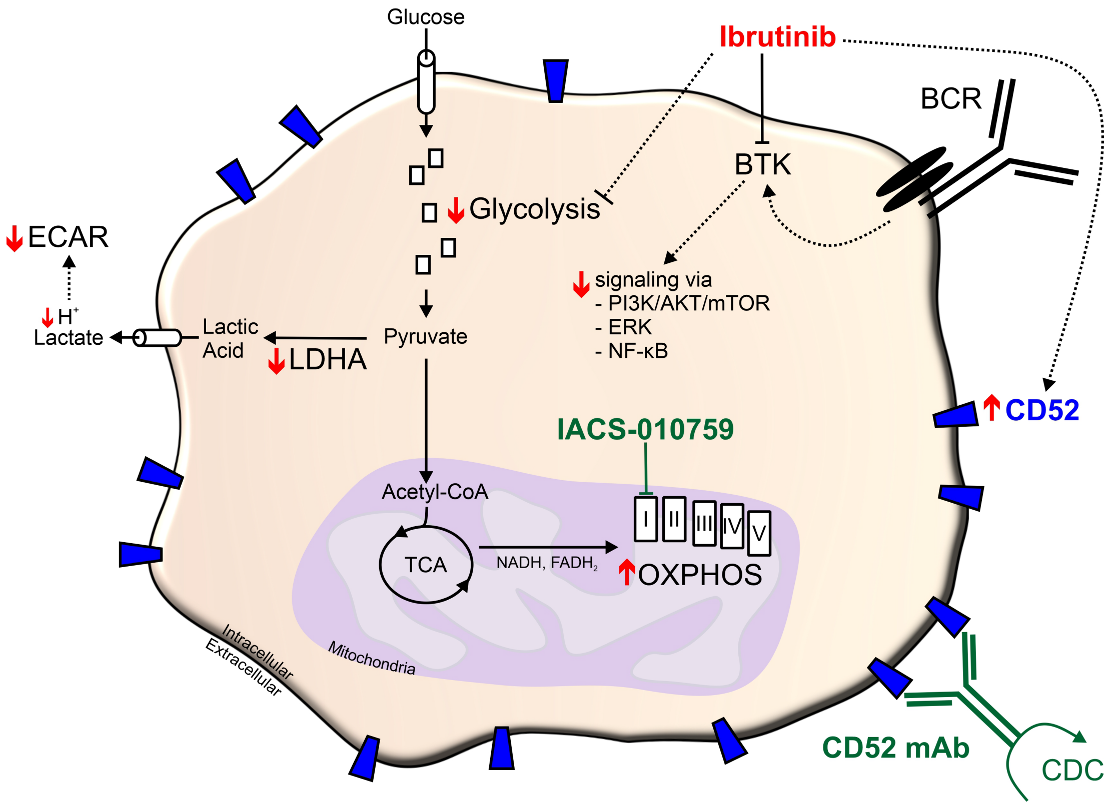

Figure 20: Effects of ibrutinib on the sensitive mantle cell lymphoma cell line REC-1 and resulting potential targets. Ibrutinib blocks B-cell receptor (BCR) signaling by inhibiting the BTK, resulting in decreased downstream signaling via PI3K/AKT/mTOR, ERK, and NF-κB. Treatment with the BTK inhibitor reduced glycolysis, as evidenced by lower ECAR and LDHA levels. Instead, ibrutinib triggered increased dependence on oxidative phosphorylation (OXPHOS), which was targeted by IACS-010759. Due to higher CD52 surface levels after ibrutinib treatment, anti-CD52 therapy with a CD52 monoclonal antibody (mAb) was used, which induced complement-dependent cytotoxicity (CDC).

11.3 Simultaneous inhibition of oxidative phosphorylation and ibrutinib treatment are highly toxic to ibrutinib-sensitive cells

Metabolic rewiring has been investigated as a target for cancer treatment [215]. Small molecules have been developed to intervene in aerobic glycolysis, glutamine metabolism, fatty acid synthesis, and mitochondrial respiration [216]. The agents IM156 and IACS-010759, that block OXPHOS by inhibition of the complex I of the mitochondrial electron transport chain (ETC), are investigated to assess their clinical benefits and feasibility [217, 218].

Zhang et al. studied the effect of IACS-010759 in MCL and reported higher growth inhibition in ibrutinib-resistant than in sensitive cells [206]. Contrarily, in this work, the inhibition of OXPHOS for 3 d resulted in similar reduced proliferation levels in all MCL cell lines, ibrutinib-sensitive and ibrutinib-resistant. These discrepancies might be due to distinct cell growth protocols. Especially distinct cell culture media composition and cell density during culturing with differing available nutrients may influence metabolic cell behavior and sensitivity to drug treatment [219, 220]. Moreover, prolonged incubation with IACS-010759 above 3-day treatment could reveal differential susceptibility among MCL cell lines, as ibrutinib-resistant MAVER-1 cells were more vulnerable to 4-day OXPHOS inhibition than ibrutinib-sensitive REC-1, which was in contrast to 3-day treatment. Given its anti-proliferative effect in ibrutinib-sensitive and resistant cell lines, IACS-010759 treatment alone could be a valuable approach for the treatment of MCL, regardless of susceptibility to ibrutinib.

Specifically, this study describes the coexistence of two metabolic subgroups, with OXPHOS enabled cells acquiring survival benefits through ibrutinib induced selection. On the other hand, it may be that REC-1 cells can switch between metabolic states during growth. Upon ibrutinib treatment, the equilibrium became imbalanced due to attenuated glycolytic activity and MCL cells increased their OXPHOS activity to meet energy demands. Interestingly, the co-occurrence of decreased BCR signaling with increased OXPHOS was identified in CLL cells with Richter Transformation supporting the hypothesis of a link between BCR and metabolism which is influenced by treatment induced evolution of malignant cells [221]. This emphasized the possible benefit of using a metabolic inhibitor together with ibrutinib to turn off crucial BCR signaling in MCL cells and target the resulting dependence on OXPHOS.

Based on this hypothesis, IACS-010759 was tested in combination with ibrutinib. As the consecutive approach was not successful in increasing toxicity, it is reasonable to assume that tumor cells can adapt to metabolic stressors by switching between glycolysis and OXPHOS. In contrast, counteracting simultaneous silencing of BCR signaling with reduced glycolysis and blocked OXPHOS appeared to be impossible for ibrutinib-sensitive cells and therefore may represent a beneficial approach for the treatment of MCL. As each individual small molecule inhibitor already had a considerable effect on cell viability, further *in vivo* studies must assess whether a combination of both is safe. Unfortunately, a recent preprint reported that the two phase I clinical trials of IACS-010759 (NCT02882321 for acute myeloid leukemia, NCT03291938 for advanced solid tumors) had to be discontinued due to severe toxicities such as elevated lactate levels and neurotoxicity [222]. Because clinically effective doses could not be achieved without severe toxicities, the authors were generally in doubt about using ETC complex I inhibitors in the clinical setting. However, with the successful completion of a phase I trial in advanced solid tumors (NCT03272256), IM156 may be a promising alternative candidate [217]. Therefore, future research is mandatory to determine whether mitochondrial OXPHOS can be efficiently and safely targeted.

11.4 Targeting CD52 following ibrutinib pretreatment has a synergistic effect on ibrutinib-sensitive mantle cell lymphoma cells

Immunotherapies targeting surface molecules on tumor cells are very effective strategies due to their recognition and depletion of specific target cells. Apart from CAR T-cell therapy, monoclonal antibodies are used and modified to increase their efficiency. The pool of approaches with radiolabeled antibody complexes, as well as bispecific T-cell engagers and antibody-drug-conjugates enables a broad use especially for hematologic malignancies [223]. Rituximab, an anti-CD20 monoclonal antibody was the first therapeutic antibody that was approved by the FDA in 1997 to treat B-cell NHLs [224]. Apart from its most common use in combination with chemotherapy, rituximab as a single agent also improved patient outcomes when used as maintenance therapy, in particular for MCL [79]. Besides, combinations with small molecule inhibitors were tested and seem to provide an efficient approach with fewer toxicities compared to chemoimmunotherapy [225, 107]. To date, the FDA has approved more than 30 therapeutic mAbs for hematological and solid cancers [226]. The mechanisms of action of these antibodies include direct cytotoxicity, e.g., by inhibiting the binding of growth factors or cytokines to receptors mediated by the Fab region, or induction of an immune response by antibody-dependent cellular cytotoxicity (ADCC), antibody-dependent cellular phagocytosis (ADCP), or CDC through the Fc region. When immune effector cells like natural killer cells bind to the Fc portion of the mAb with their Fcγ receptor, they get activated and release cytokines, lytic proteins, and enzymes, triggering an inflammatory response and apoptosis or lysis of the target cell [227]. In case of macrophages, target cells are phagocytosed [228]. Therapeutic antibodies can also activate the complement system and initiate the classical pathway [229]. Therein a cleavage cascade of 30 complement glycoproteins starts with binding of C1q to the Fc portion of the antibody and results in the formation of the membrane-attack complex (MAC), forming lytic pores and causing cell lysis [229]. However, the extent of these mechanisms in their *in vivo* performance is often not exactly understood [230].

To lower the immunogenicity of rodent-derived monoclonal antibodies, humanized antibodies were generated for therapeutic use. The first humanized mAb, alemtuzumab (CAMPATH-1H), was directed against CD52 [231]. Experiences of using the anti-CD52 mAb alemtuzumab in CLL are broad, whereas MCL patients were only marginally included in clinical trials [232-234]. Efficacy in MCL was not reported which may be due to low MCL patient numbers and the inclusion of heavily pretreated patients. The initial approval of alemtuzumab for treatment of CLL was withdrawn in 2012 [235]. Instead, the antibody gained a new approval for relapsing-remitting multiple sclerosis (MS) and is sold under the trade name Lemtrada® [236, 237]. Reasons for redesignation can be diverse and may include the intent to intervene against off-label use of alemtuzumab in MS, as well as economic benefits. Alemtuzumab's main mechanisms of lymphocyte depletion probably include ADCC and CDC [238, 239]. The most common adverse events are autoimmunity and infections apart from infusion-associated reactions, which require strict monitoring [240]. The most recent report of a phase I clinical trial testing ibrutinib in combination with alemtuzumab in CLL patients had to be stopped due to the occurrence of opportunistic infections, but clinical efficacy was observed rapidly [241].

Considering increased CD52 surface expression on ibrutinib-sensitive cells following treatment with the BTK inhibitor, CD52 was targeted in this work with a commercially available CD52 mAb of the IgG2 subclass in presence of human serum containing active complement. The fast depletion of REC-1 cells pretreated with ibrutinib underscored the high vulnerability of cells with upregulated CD52. The main mechanism of cell death could be linked to CD52 mAb-mediated CDC. To assess the benefit of a CD52 targeted approach in primary MCL, tumor cells from peripheral blood and lymph nodes from treatment-naïve patients and one ibrutinib-resistant patient were investigated. Distinct culture media were tested to optimize growth and to reflect *in vivo* conditions. However, standard B-cell culturing procedures with use of cytokines and stimulating ligands were not appropriate for this approach, as we observed considerable attenuating effects on toxicity of ibrutinib and CD52 expression levels. The use of CD40L, which induces alternative NF-κB signaling by activation of its target receptor CD40, probably served as bypass of the blocked classical NF-κB signaling by ibrutinib [242]. Along this line, IL-4 may have induced an alternate pathway for BCR signaling independent of ibrutinib inhibition [243]. Therefore, primary cells were cultured similarly to MCL cell lines with only the required nutrients for survival.

The effect of ibrutinib on viability of primary MCL cells varied. To account for the sensitivity of cells to ibrutinib treatment, samples were either defined as ibrutinib-sensitive (> 50% loss of viability) or ibrutinib-insensitive (≤ 50%) in our experimental approach. Clinical trials reported an ibrutinib-sensitivity in 68-69% of patients [94, 96], whereas we detected only 40%. This could be biased by the small patient numbers, the inclusion of primary cells from patients with leukemic course, and without prior treatment, which is in contrast to the patients with RR MCL studied in clinical trials. In addition, sensitivity to ibrutinib and upregulation of CD52 were detected only in MCL cells from peripheral blood. Because the two included lymph node samples were treated with ibrutinib for only 2 d due to poor cell fitness in *in vitro* culture, a considerable toxic effect of ibrutinib and its impact on CD52 surface levels may not have been demonstrated. MCL cells from lymph nodes may also show different susceptibility to treatment than MCL cells from peripheral blood. However, whether the microenvironment in lymph nodes can interfere with altered CD52 expression under ibrutinib was not assessed in this experimental setup.

Compared to healthy B cells, primary MCL cells had higher CD52 levels. The ibrutinib-triggered upregulation of CD52 expression was observed in 4 out of 10 patients. Because 2 patients belonged to the ibrutinib-sensitive and 2 to the insensitive group, no correlation between high ibrutinib-sensitivity and CD52 increase could be concluded.

Application of the anti-CD52 antibody was highly toxic to primary MCL cells, but also affected T lymphocytes due to their high expression of CD52. This was in line with the toxic profile of alemtuzumab in clinical trials and emphasized the need for its carefully monitored clinical use to benefit from its B-cell depleting efficacy. As we observed that the ibrutinib-sensitive group was significantly more affected by antibody-mediated cytotoxicity when pretreated with ibrutinib, this sensitive patient subpopulation may be a potential target group. In addition, screening of CD52 expression could identify patients who would benefit most from anti-CD52 therapy. The combination of ibrutinib, with its redistribution effect of tumor cells from lymph node into blood, and subsequent alemtuzumab consolidation, which is known for its higher efficacy in depletion of tumor cells in the blood [244], might clear all tumor cells and prevent survival of ibrutinib-resistant clones, thereby achieving MRD negativity and minimizing the risk for relapse.

11.5 Future perspectives

Time-resolved scRNA-seq enables tracking of heterogeneous tumor cells across drug treatment. Drug exposure causes a dynamic process in tumor cells and the interplay between altered signaling pathways, gene regulatory networks, and metabolic changes seem to be linked. This work focused on an MCL cell line model, benefiting from the possibility to intensively study the observed alterations of the transcriptome with additional molecular biological methods to corroborate and validate their impact on cell behavior and evaluate their potential for clinical use. Intriguingly, the here described features of increased anti-adhesion CD52 and metabolic dependence on OXPHOS in ibrutinib surviving cells might be correlated regarding ibrutinib's *in vivo* effect of forcing tumor cells to lose adhesion properties and leave the hypoxic niche in the lymph node to reenter oxygenated blood [245]. However, this hypothesized association needs to be corroborated by further studies focusing on how ibrutinib treatment induces higher CD52 levels in only some patients, how elevated CD52 levels affect MCL cell behavior, and whether the acquired features of high OXPHOS and CD52 represent a crucial resistance mechanism to ibrutinib therapy *in vivo*. Longitudinal single-cell analysis in primary MCL was applied by Zhang et al. to investigate samples from patients at different time points during ibrutinib plus venetoclax treatment [166]. They identified upregulation of an inhibitor of apoptosis that proved to be a promising target for tumor inhibition in a preclinical model, highlighting the approach as a powerful tool to identify efficient therapy options. As a follow-up to our study, longitudinal scRNA-seq combined with fluxomic studies and assessment of surface marker expression in ibrutinib-treated primary MCL cells will reveal whether the alterations observed in our cell line model are reflected in patients. Additionally, samples may include surrounding tumor tissue from different tumor sites to expand knowledge in effects of ibrutinib on the interaction of MCL cells and the TME. In this setup, subpopulations with a specific gene expression signature that allows crosstalk with the TME could be identified. In light of the resolution of intratumoral heterogeneity, scRNA-seq could thus detect and follow the development of resistant cells causing MRD [246]. This information would guide to appropriate therapies tailored to the evolution of MCL cells under ibrutinib treatment in each individual patient, as it was piloted in this work using a cell line model.

Owing to the synergistic effects of ibrutinib with subsequent anti-CD52 treatment, this work strongly encourages to further study the potential *in vivo* benefits for ibrutinib-sensitive patients showing CD52 increase. The combination might improve therapeutic efficacy, with eradication of otherwise residual tumor cells, and thereby minimize the risk for MRD and delay relapse. Given the side effect profile of alemtuzumab, other CD52 therapies may be a safer alternative. A bispecific antibody approach for instance, with a second B-cell-specific antibody added to alemtuzumab, could direct the cytotoxic effect to B cells and spare T cells, thereby reducing the severity of immunosuppression [247]. In view of the intertumoral heterogeneity in MCL, the effects seen in the cell line model might be only relevant for a subgroup of patients. However, this particular subgroup could greatly benefit from targeted CD52 treatment.

This urges the exploration of additional resistance mechanisms to ibrutinib treatment and the quest for adapted therapies. In general, the broader the available therapeutic approaches and the deeper the individual patient characterization, the better personalized medicine can be implemented in clinical practice.

12 References

1. World Health Organization. Global Health Estimates 2020: Deaths by Cause, Age, Sex, by Country and by Region, 2000-2019. https://www.who.int/data/gho/data/themes/mortality-and-global-health-estimates/ghe-leading-causes-of-death. Accessed April 4, 2022.

2. Hanahan D, Weinberg Robert A. Hallmarks of Cancer: The Next Generation. Cell. 2011;144(5):646-74. doi:10.1016/j.cell.2011.02.013

3. Hanahan D. Hallmarks of Cancer: New Dimensions. Cancer Discovery. 2022;12(1):31-46. doi:10.1158/2159-8290.Cd-21-1059

4. Feitelson MA, Arzumanyan A, Kulathinal RJ, Blain SW, Holcombe RF, Mahajna J, Marino M, Martinez-Chantar ML, Nawroth R, Sanchez-Garcia I, Sharma D, Saxena NK, Singh N, Vlachostergios PJ, Guo S, Honoki K, Fujii H, Georgakilas AG, Bilsland A, Amedei A, et al. Sustained proliferation in cancer: Mechanisms and novel therapeutic targets. Seminars in Cancer Biology. 2015;35:25-54. doi:10.1016/j.semcancer.2015.02.006

5. Gao J, Pickett HA. Targeting telomeres: advances in telomere maintenance mechanism-specific cancer therapies. Nat Rev Cancer. 2022;22(9):515-32. doi:10.1038/s41568-022-00490-1

6. Morris LGT, Chan TA. Therapeutic targeting of tumor suppressor genes. Cancer. 2015;121(9):1357-68. doi:10.1002/cncr.29140

7. Fernald K, Kurokawa M. Evading apoptosis in cancer. Trends Cell Biol. 2013;23(12):620-33. doi:10.1016/j.tcb.2013.07.006

8. Negrini S, Gorgoulis VG, Halazonetis TD. Genomic instability — an evolving hallmark of cancer. Nature Reviews Molecular Cell Biology. 2010;11(3):220-8. doi:10.1038/nrm2858

9. Stockmann C, Schadendorf D, Klose R, Helfrich I. The Impact of the Immune System on Tumor: Angiogenesis and Vascular Remodeling. Frontiers in Oncology. 2014;4. doi:10.3389/fonc.2014.00069

10. Quintero-Fabián S, Arreola R, Becerril-Villanueva E, Torres-Romero JC, Arana-Argáez V, Lara-Riegos J, Ramírez-Camacho MA, Alvarez-Sánchez ME. Role of Matrix Metalloproteinases in Angiogenesis and Cancer. Frontiers in Oncology. 2019;9. doi:10.3389/fonc.2019.01370

11. Fares J, Fares MY, Khachfe HH, Salhab HA, Fares Y. Molecular principles of metastasis: a hallmark of cancer revisited. Signal Transduction and Targeted Therapy. 2020;5(1):28. doi:10.1038/s41392-020-0134-x

12. Intlekofer AM, Finley LWS. Metabolic signatures of cancer cells and stem cells. Nature Metabolism. 2019;1(2):177-88. doi:10.1038/s42255-019-0032-0

13. Fritz A PC, Jack A, Shanmugaratnam K, Sobin L, Parkin DM, Whelan S. International classification of diseases for oncology (ICD-O), 3rd ed., 1st revision. Geneva: WHO Press; 2013.

14. Shankland KR, Armitage JO, Hancock BW. Non-Hodgkin lymphoma. The Lancet. 2012;380(9844):848-57. doi:10.1016/S0140-6736(12)60605-9

15. Swerdlow SH, Campo E, Pileri SA, Harris NL, Stein H, Siebert R, Advani R, Ghielmini M, Salles GA, Zelenetz AD, Jaffe ES. The 2016 revision of the World Health Organization classification of lymphoid neoplasms. Blood. 2016;127(20):2375-90. doi:10.1182/blood-2016-01-643569

16. de Leval L, Jaffe ES. Lymphoma Classification. The Cancer Journal. 2020;26(3):176-85. doi:10.1097/ppo.0000000000000451

17. Swerdlow SH CE, Harris NL, Jaffe ES, Pileri SA, Stein H, Thiele J, Vardiman JW. WHO Classification of Tumours of Haematopoietic and Lymphoid Tissues. Revised 4th Edition. Lyon, France: IARC; 2017.

18. Sung H, Ferlay J, Siegel RL, Laversanne M, Soerjomataram I, Jemal A, Bray F. Global Cancer Statistics 2020: GLOBOCAN Estimates of Incidence and Mortality Worldwide for 36 Cancers in 185 Countries. CA: A Cancer Journal for Clinicians. 2021;71(3):209-49. doi:10.3322/caac.21660

19. Armitage JO, Gascoyne RD, Lunning MA, Cavalli F. Non-Hodgkin lymphoma. The Lancet. 2017;390(10091):298-310. doi:10.1016/S0140-6736(16)32407-2

20. Blombery PA, Wall M, Seymour JF. The molecular pathogenesis of B-cell non-Hodgkin lymphoma. European Journal of Haematology. 2015;95(4):280-93. doi:10.1111/ejh.12589

21. Teras LR, DeSantis CE, Cerhan JR, Morton LM, Jemal A, Flowers CR. 2016 US lymphoid malignancy statistics by World Health Organization subtypes. CA Cancer J Clin. 2016;66(6):443-59. doi:10.3322/caac.21357

22. Smedby KE, Hjalgrim H. Epidemiology and etiology of mantle cell lymphoma and other non-Hodgkin lymphoma subtypes. Semin Cancer Biol. 2011;21(5):293-8. doi:10.1016/j.semcancer.2011.09.010

23. Silkenstedt E, Linton K, Dreyling M. Mantle cell lymphoma - advances in molecular biology, prognostication and treatment approaches. Br J Haematol. 2021;195(2):162-73. doi:10.1111/bjh.17419

24. Jain P, Wang M. Mantle cell lymphoma in 2022 - A comprehensive update on molecular pathogenesis, risk stratification, clinical approach, and current and novel treatments. Am J Hematol. 2022. doi:10.1002/ajh.26523

25. Eskelund CW, Kolstad A, Jerkeman M, Räty R, Laurell A, Eloranta S, Smedby KE, Husby S, Pedersen LB, Andersen NS, Eriksson M, Kimby E, Bentzen H, Kuittinen O, Lauritzsen GF, Nilsson-Ehle H, Ralfkiaer E, Ehinger M, Sundström C, Delabie J, et al. 15-year follow-up of the Second Nordic Mantle Cell Lymphoma trial (MCL2): prolonged remissions without survival plateau. Br J Haematol. 2016;175(3):410-8. doi:10.1111/bjh.14241

26. Dreyling M, Campo E, Hermine O, Jerkeman M, Le Gouill S, Rule S, Shpilberg O, Walewski J, Ladetto M. Newly diagnosed and relapsed mantle cell lymphoma: ESMO Clinical Practice Guidelines for diagnosis, treatment and follow-up. Ann Oncol. 2017;28(suppl_4):iv62-iv71. doi:10.1093/annonc/mdx223

27. Welzel N, Le T, Marculescu R, Mitterbauer G, Chott A, Pott C, Kneba M, Du MQ, Kusec R, Drach J, Raderer M, Mannhalter C, Lechner K, Nadel B, Jaeger U. Templated nucleotide addition and immunoglobulin JH-gene utilization in t(11;14) junctions: implications for the mechanism of translocation and the origin of mantle cell lymphoma. Cancer Res. 2001;61(4):1629-36.

28. Nadeu F, Martin-Garcia D, Clot G, Díaz-Navarro A, Duran-Ferrer M, Navarro A, Vilarrasa-Blasi R, Kulis M, Royo R, Gutiérrez-Abril J, Valdés-Mas R, López C, Chapaprieta V, Puiggros M, Castellano G, Costa D, Aymerich M, Jares P, Espinet B, Muntañola A, et al. Genomic and epigenomic insights into the origin, pathogenesis, and clinical behavior of mantle cell lymphoma subtypes. Blood. 2020;136(12):1419-32. doi:10.1182/blood.2020005289

29. Küppers R. Mechanisms of B-cell lymphoma pathogenesis. Nature Reviews Cancer. 2005;5(4):251-62. doi:10.1038/nrc1589

30. Jares P, Colomer D, Campo E. Genetic and molecular pathogenesis of mantle cell lymphoma: perspectives for new targeted therapeutics. Nat Rev Cancer. 2007;7(10):750-62. doi:10.1038/nrc2230

31. Mozos A, Royo C, Hartmann E, De Jong D, Baró C, Valera A, Fu K, Weisenburger DD, Delabie J, Chuang SS, Jaffe ES, Ruiz-Marcellan C, Dave S, Rimsza L, Braziel R, Gascoyne RD, Solé F, López-Guillermo A, Colomer D, Staudt LM, et al. SOX11 expression is highly specific for mantle cell lymphoma and identifies the cyclin D1-negative subtype. Haematologica. 2009;94(11):1555-62. doi:10.3324/haematol.2009.010264

32. Martín-Garcia D, Navarro A, Valdés-Mas R, Clot G, Gutiérrez-Abril J, Prieto M, Ribera-Cortada I, Woroniecka R, Rymkiewicz G, Bens S, de Leval L, Rosenwald A, Ferry JA, Hsi ED, Fu K, Delabie J, Weisenburger D, de Jong D, Climent F, O'Connor SJ, et al. CCND2 and CCND3 hijack immunoglobulin light-chain enhancers in cyclin D1− mantle cell lymphoma. Blood. 2019;133(9):940-51. doi:10.1182/blood-2018-07-862151

33. Navarro A, Beà S, Jares P, Campo E. Molecular Pathogenesis of Mantle Cell Lymphoma. Hematol Oncol Clin North Am. 2020;34(5):795-807. doi:10.1016/j.hoc.2020.05.002

34. Narurkar R, Alkayem M, Liu D. SOX11 is a biomarker for cyclin D1-negative mantle cell lymphoma. Biomarker Research. 2016;4(1):6. doi:10.1186/s40364-016-0060-9

35. Queirós Ana C, Beekman R, Vilarrasa-Blasi R, Duran-Ferrer M, Clot G, Merkel A, Raineri E, Russiñol N, Castellano G, Beà S, Navarro A, Kulis M, Verdaguer-Dot N, Jares P, Enjuanes A, Calasanz María J, Bergmann A, Vater I, Salaverría I, van de Werken Harmen JG, et al. Decoding the DNA Methylome of Mantle Cell Lymphoma in the Light of the Entire B Cell Lineage. Cancer Cell. 2016;30(5):806-21. doi:10.1016/j.ccell.2016.09.014

36. Navarro A, Clot G, Royo C, Jares P, Hadzidimitriou A, Agathangelidis A, Bikos V, Darzentas N, Papadaki T, Salaverria I, Pinyol M, Puig X, Palomero J, Vegliante MC, Amador V, Martinez-Trillos A, Stefancikova L, Wiestner A, Wilson W, Pott C, et al. Molecular subsets of mantle cell lymphoma defined by the IGHV mutational status and SOX11 expression have distinct biologic and clinical features. Cancer Res. 2012;72(20):5307-16. doi:10.1158/0008-5472.Can-12-1615

37. Ondrejka SL, Lai R, Smith SD, Hsi ED. Indolent mantle cell leukemia: a clinicopathological variant characterized by isolated lymphocytosis, interstitial bone marrow involvement, kappa light chain restriction, and good prognosis. Haematologica. 2011;96(8):1121-7. doi:10.3324/haematol.2010.036277

38. Navarro A, Clot G, Prieto M, Royo C, Vegliante MC, Amador V, Hartmann E, Salaverria I, Beà S, Martín-Subero JI, Rosenwald A, Ott G, Wiestner A, Wilson WH, Campo E, Hernández L. microRNA expression profiles identify subtypes of mantle cell lymphoma with different clinicobiological characteristics. Clin Cancer Res. 2013;19(12):3121-9. doi:10.1158/1078-0432.Ccr-12-3077

39. Hoster E, Rosenwald A, Berger F, Bernd H-W, Hartmann S, Loddenkemper C, Barth TFE, Brousse N, Pileri S, Rymkiewicz G, Kodet R, Stilgenbauer S, Forstpointner R, Thieblemont C, Hallek M, Coiffier B, Vehling-Kaiser U, Bouabdallah R, Kanz L, Pfreundschuh M, et al. Prognostic Value of Ki-67 Index, Cytology, and Growth Pattern in Mantle-Cell Lymphoma: Results From Randomized Trials of the European Mantle Cell Lymphoma Network. Journal of Clinical Oncology. 2016;34(12):1386-94. doi:10.1200/jco.2015.63.8387

40. Shrestha R, Bhatt VR, Guru Murthy GS, Armitage JO. Clinicopathologic features and management of blastoid variant of mantle cell lymphoma. Leuk Lymphoma. 2015;56(10):2759-67. doi:10.3109/10428194.2015.1026902

41. Carvajal-Cuenca A, Sua LF, Silva NM, Pittaluga S, Royo C, Song JY, Sargent RL, Espinet B, Climent F, Jacobs SA, Delabie J, Naresh KN, Bagg A, Brousset P, Warnke RA, Serrano S, Harris NL, Swerdlow SH, Jaffe ES, Campo E. In situ mantle cell lymphoma: clinical implications of an incidental finding with indolent clinical behavior. Haematologica. 2012;97(2):270-8. doi:10.3324/haematol.2011.052621

42. Zhang J, Jima D, Moffitt AB, Liu Q, Czader M, Hsi ED, Fedoriw Y, Dunphy CH, Richards KL, Gill JI, Sun Z, Love C, Scotland P, Lock E, Levy S, Hsu DS, Dunson D, Dave SS. The genomic landscape of mantle cell lymphoma is related to the epigenetically determined chromatin state of normal B cells. Blood. 2014;123(19):2988-96. doi:10.1182/blood-2013-07-517177

43. Beà S, Valdés-Mas R, Navarro A, Salaverria I, Martín-Garcia D, Jares P, Giné E, Pinyol M, Royo C, Nadeu F, Conde L, Juan M, Clot G, Vizán P, Croce LD, Puente DA, López-Guerra M, Moros A, Roue G, Aymerich M, et al. Landscape of somatic mutations and clonal evolution in mantle cell lymphoma. Proceedings of the National Academy of Sciences. 2013;110(45):18250-5. doi:doi:10.1073/pnas.1314608110

44. Hu Z, Medeiros LJ, Chen Z, Chen W, Li S, Konoplev SN, Lu X, Pham LV, Young KH, Wang W, Hu S. Mantle Cell Lymphoma With MYC Rearrangement: A Report of 17 Patients. Am J Surg Pathol. 2017;41(2):216-24. doi:10.1097/pas.0000000000000758

45. Hartmann EM, Campo E, Wright G, Lenz G, Salaverria I, Jares P, Xiao W, Braziel RM, Rimsza LM, Chan W-C, Weisenburger DD, Delabie J, Jaffe ES, Gascoyne RD, Dave SS, Mueller-Hermelink H-K, Staudt LM, Ott G, Beà S, Rosenwald A. Pathway discovery in mantle cell lymphoma by integrated analysis of high-resolution gene expression and copy number profiling. Blood. 2010;116(6):953-61. doi:10.1182/blood-2010-01-263806

46. Pinyol M, Bea S, Plà L, Ribrag V, Bosq J, Rosenwald A, Campo E, Jares P. Inactivation of RB1 in mantle-cell lymphoma detected by nonsense-mediated mRNA decay pathway inhibition and microarray analysis. Blood. 2007;109(12):5422-9. doi:10.1182/blood-2006-11-057208

47. Beà S, Tort F, Pinyol M, Puig X, Hernández L, Hernández S, Fernandez PL, van Lohuizen M, Colomer D, Campo E. BMI-1 gene amplification and overexpression in hematological malignancies occur mainly in mantle cell lymphomas. Cancer Res. 2001;61(6):2409-12.

48. Hernández L, Beà S, Pinyol M, Ott G, Katzenberger T, Rosenwald A, Bosch F, López-Guillermo A, Delabie J, Colomer D, Montserrat E, Campo E. CDK4 and MDM2 gene alterations mainly occur in highly proliferative and aggressive mantle cell lymphomas with wild-type INK4a/ARF locus. Cancer Res. 2005;65(6):2199-206. doi:10.1158/0008-5472.Can-04-1526

49. Camacho E, Hernández L, Hernández S, Tort F, Bellosillo B, Beà S, Bosch F, Montserrat E, Cardesa A, Fernández PL, Campo E. ATM gene inactivation in mantle cell lymphoma mainly occurs by truncating mutations and missense mutations involving the phosphatidylinositol-3 kinase domain and is associated with increasing numbers of chromosomal imbalances. Blood. 2002;99(1):238-44. doi:10.1182/blood.v99.1.238

50. Eskelund CW, Dahl C, Hansen JW, Westman M, Kolstad A, Pedersen LB, Montano-Almendras CP, Husby S, Freiburghaus C, Ek S, Pedersen A, Niemann C, Räty R, Brown P, Geisler CH, Andersen MK, Guldberg P, Jerkeman M, Grønbæk K. TP53 mutations identify younger mantle cell lymphoma patients who do not benefit from intensive chemoimmunotherapy. Blood. 2017;130(17):1903-10. doi:10.1182/blood-2017-04-779736

51. Puente XS, Jares P, Campo E. Chronic lymphocytic leukemia and mantle cell lymphoma: crossroads of genetic and microenvironment interactions. Blood. 2018;131(21):2283-96. doi:10.1182/blood-2017-10-764373

52. Kridel R, Meissner B, Rogic S, Boyle M, Telenius A, Woolcock B, Gunawardana J, Jenkins C, Cochrane C, Ben-Neriah S, Tan K, Morin RD, Opat S, Sehn LH, Connors JM, Marra MA, Weng AP, Steidl C, Gascoyne RD. Whole transcriptome sequencing reveals recurrent NOTCH1 mutations in mantle cell lymphoma. Blood. 2012;119(9):1963-71. doi:10.1182/blood-2011-11-391474

53. Rahal R, Frick M, Romero R, Korn JM, Kridel R, Chan FC, Meissner B, Bhang HE, Ruddy D, Kauffmann A, Farsidjani A, Derti A, Rakiec D, Naylor T, Pfister E, Kovats S, Kim S, Dietze K, Dörken B, Steidl C, et al. Pharmacological and genomic profiling identifies NF-κB-targeted treatment strategies for mantle cell lymphoma. Nat Med. 2014;20(1):87-92. doi:10.1038/nm.3435

54. Armitage JO, Longo DL. Mantle-Cell Lymphoma. N Engl J Med. 2022;386(26):2495-506. doi:10.1056/NEJMra2202672

55. Vose JM. Mantle cell lymphoma: 2017 update on diagnosis, risk-stratification, and clinical management. Am J Hematol. 2017;92(8):806-13. doi:10.1002/ajh.24797

56. Dreyling M, Klapper W, Rule S. Blastoid and pleomorphic mantle cell lymphoma: still a diagnostic and therapeutic challenge! Blood. 2018;132(26):2722-9. doi:10.1182/blood-2017-08-737502

57. Jain P, Wang ML. Mantle cell lymphoma in 2022-A comprehensive update on molecular pathogenesis, risk stratification, clinical approach, and current and novel treatments. Am J Hematol. 2022;97(5):638-56. doi:10.1002/ajh.26523

58. Dreyling M, Buske C, Cairoli A, Heß G, Mey UJM, Pott C, Raderer M. Onkopedia Leitlinien Mantelzell-Lymphom. DGHO Deutsche Gesellschaft für Hämatologie und Medizinische Onkologie e.V. https://www.onkopedia.com/de/onkopedia/guidelines/mantelzell-lymphom/. Published 2021. Updated May 2021. Accessed October 13, 2022.

59. Carbone PP, Kaplan HS, Musshoff K, Smithers DW, Tubiana M. Report of the Committee on Hodgkin's Disease Staging Classification. Cancer Res. 1971;31(11):1860-1.

60. Burger JA, Wiestner A. Targeting B cell receptor signalling in cancer: preclinical and clinical advances. Nature Reviews Cancer. 2018;18(3):148-67. doi:10.1038/nrc.2017.121

61. Tsukada S, Saffran DC, Rawlings DJ, Parolini O, Allen RC, Klisak I, Sparkes RS, Kubagawa H, Mohandas T, Quan S, Belmont JW, Cooper MD, Conley ME, Witte ON. Deficient expression of a B cell cytoplasmic tyrosine kinase in human X-linked agammaglobulinemia. Cell. 1993;72(2):279-90. doi:10.1016/0092-8674(93)90667-F

62. de Weers M, Brouns GS, Hinshelwood S, Kinnon C, Schuurman RK, Hendriks RW, Borst J. B-cell antigen receptor stimulation activates the human Bruton's tyrosine kinase, which is deficient in X-linked agammaglobulinemia. J Biol Chem. 1994;269(39):23857-60.

63. Hombach J, Tsubata T, Leclercq L, Stappert H, Reth M. Molecular components of the B-cell antigen receptor complex of the IgM class. Nature. 1990;343(6260):760-2. doi:10.1038/343760a0

64. Rolli V, Gallwitz M, Wossning T, Flemming A, Schamel WW, Zürn C, Reth M. Amplification of B cell antigen receptor signaling by a Syk/ITAM positive feedback loop. Mol Cell. 2002;10(5):1057-69. doi:10.1016/s1097-2765(02)00739-6

65. O'Rourke LM, Tooze R, Turner M, Sandoval DM, Carter RH, Tybulewicz VLJ, Fearon DT. CD19 as a Membrane-Anchored Adaptor Protein of B Lymphocytes: Costimulation of Lipid and Protein Kinases by Recruitment of Vav. Immunity. 1998;8(5):635-45. doi:10.1016/S1074-7613(00)80568-3

66. Manning BD, Toker A. AKT/PKB Signaling: Navigating the Network. Cell. 2017;169(3):381-405. doi:10.1016/j.cell.2017.04.001

67. Brunet A, Bonni A, Zigmond MJ, Lin MZ, Juo P, Hu LS, Anderson MJ, Arden KC, Blenis J, Greenberg ME. Akt Promotes Cell Survival by Phosphorylating and Inhibiting a Forkhead Transcription Factor. Cell. 1999;96(6):857-68. doi:10.1016/S0092-8674(00)80595-4

68. Saxton RA, Sabatini DM. mTOR Signaling in Growth, Metabolism, and Disease. Cell. 2017;168(6):960-76. doi:10.1016/j.cell.2017.02.004

69. Saito K, Scharenberg AM, Kinet J-P. Interaction between the Btk PH Domain and Phosphatidylinositol-3,4,5-trisphosphate Directly Regulates Btk *. Journal of Biological Chemistry. 2001;276(19):16201-6. doi:10.1074/jbc.M100873200

70. Rawlings DJ, Scharenberg AM, Park H, Wahl MI, Lin S, Kato RM, Fluckiger AC, Witte ON, Kinet JP. Activation of BTK by a phosphorylation mechanism initiated by SRC family kinases. Science. 1996;271(5250):822-5. doi:10.1126/science.271.5250.822

71. Kim YJ, Sekiya F, Poulin B, Bae YS, Rhee SG. Mechanism of B-cell receptor-induced phosphorylation and activation of phospholipase C-gamma2. Mol Cell Biol. 2004;24(22):9986-99. doi:10.1128/mcb.24.22.9986-9999.2004

72. Petro JB, Rahman SM, Ballard DW, Khan WN. Bruton's tyrosine kinase is required for activation of IkappaB kinase and nuclear factor kappaB in response to B cell receptor engagement. J Exp Med. 2000;191(10):1745-54. doi:10.1084/jem.191.10.1745

73. Saba NS, Liu D, Herman SEM, Underbayev C, Tian X, Behrend D, Weniger MA, Skarzynski M, Gyamfi J, Fontan L, Melnick A, Grant C, Roschewski M, Navarro A, Beà S, Pittaluga S, Dunleavy K, Wilson WH, Wiestner A. Pathogenic role of B-cell receptor signaling and canonical NF-κB activation in mantle cell lymphoma. Blood. 2016;128(1):82-92. doi:10.1182/blood-2015-11-681460

74. Rule S. The modern approach to mantle cell lymphoma. Hematol Oncol. 2019;37 Suppl 1:66-9. doi:10.1002/hon.2596

75. Martin P, Ruan J, Leonard JP. The potential for chemotherapy-free strategies in mantle cell lymphoma. Blood. 2017;130(17):1881-8. doi:10.1182/blood-2017-05-737510

76. Delarue R, Haioun C, Ribrag V, Brice P, Delmer A, Tilly H, Salles G, Van Hoof A, Casasnovas O, Brousse N, Lefrere F, Hermine O. CHOP and DHAP plus rituximab followed by autologous stem cell transplantation in mantle cell lymphoma: a phase 2 study from the Groupe d'Etude des Lymphomes de l'Adulte. Blood. 2013;121(1):48-53. doi:10.1182/blood-2011-09-370320

77. Hermine O, Hoster E, Walewski J, Bosly A, Stilgenbauer S, Thieblemont C, Szymczyk M, Bouabdallah R, Kneba M, Hallek M, Salles G, Feugier P, Ribrag V, Birkmann J, Forstpointner R, Haioun C, Hänel M, Casasnovas RO, Finke J, Peter N, et al. Addition of high-dose cytarabine to immunochemotherapy before autologous stem-cell transplantation in patients aged 65 years or younger with mantle cell lymphoma (MCL Younger): a randomised, open-label, phase 3 trial of the European Mantle Cell Lymphoma Network. The Lancet. 2016;388(10044):565-75. doi:10.1016/S0140-6736(16)00739-X

78. Hoster E, Geisler CH, Doorduijn J, van der Holt B, Walewski J, Bloehdorn J, Ribrag V, Salles G, Hallek M, Pott C, Szymczyk M, Kolstad A, Laurell A, Räty R, Jerkeman M, Van't Veer M, Kluin-Nelemans JC, Klapper W, Unterhalt M, Dreyling M, et al. Total body irradiation after high-dose cytarabine in mantle cell lymphoma: a comparison of Nordic MCL2, HOVON-45, and European MCL Younger trials. Leukemia. 2016;30(6):1428-30. doi:10.1038/leu.2015.322

79. Le Gouill S, Thieblemont C, Oberic L, Moreau A, Bouabdallah K, Dartigeas C, Damaj G, Gastinne T, Ribrag V, Feugier P, Casasnovas O, Zerazhi H, Haioun C, Maisonneuve H, Houot R, Jardin F, Van Den Neste E, Tournilhac O, Le Dû K, Morschhauser F, et al. Rituximab after Autologous Stem-Cell Transplantation in Mantle-Cell Lymphoma. New England Journal of Medicine. 2017;377(13):1250-60. doi:10.1056/NEJMoa1701769

80. Kluin-Nelemans HC, Hoster E, Hermine O, Walewski J, Geisler CH, Trneny M, Stilgenbauer S, Kaiser F, Doorduijn JK, Salles G, Szymczyk M, Tilly H, Kanz L, Schmidt C, Feugier P, Thieblemont C, Zijlstra JM, Ribrag V, Klapper W, Pott C, et al. Treatment of Older Patients With Mantle Cell Lymphoma (MCL): Long-Term Follow-Up of the Randomized European MCL Elderly Trial. Journal of Clinical Oncology. 2020;38(3):248-56. doi:10.1200/jco.19.01294

81. Robak T, Jin J, Pylypenko H, Verhoef G, Siritanaratkul N, Drach J, Raderer M, Mayer J, Pereira J, Tumyan G, Okamoto R, Nakahara S, Hu P, Appiani C, Nemat S, Cavalli F, Van Hoof A, Sheliga A, Teixeira A, Tomita A, et al. Frontline bortezomib, rituximab, cyclophosphamide, doxorubicin, and prednisone (VR-CAP) versus rituximab, cyclophosphamide, doxorubicin, vincristine, and prednisone (R-CHOP) in transplantation-ineligible patients with newly diagnosed mantle cell lymphoma: final overall survival results of a randomised, open-label, phase 3 study. The Lancet Oncology. 2018;19(11):1449-58. doi:10.1016/S1470-2045(18)30685-5

82. Visco C, Finotto S, Zambello R, Paolini R, Menin A, Zanotti R, Zaja F, Semenzato G, Pizzolo G, D'Amore ES, Rodeghiero F. Combination of rituximab, bendamustine, and cytarabine for patients with mantle-cell non-Hodgkin lymphoma ineligible for intensive regimens or autologous transplantation. J Clin Oncol. 2013;31(11):1442-9. doi:10.1200/jco.2012.45.9842

83. Kumar A, Sha F, Toure A, Dogan A, Ni A, Batlevi CL, Palomba MLM, Portlock C, Straus DJ, Noy A, Horwitz SM, Moskowitz A, Hamlin P, Moskowitz CH, Matasar MJ, Zelenetz AD, Younes A. Patterns of survival in patients with recurrent mantle cell lymphoma in the modern era: progressive shortening in response duration and survival after each relapse. Blood Cancer J. 2019;9(6):50. doi:10.1038/s41408-019-0209-5

84. Marangon M, Visco C, Barbui AM, Chiappella A, Fabbri A, Ferrero S, Galimberti S, Luminari S, Musuraca G, Re A, Zilioli VR, Ladetto M. Allogeneic Stem Cell Transplantation in Mantle Cell Lymphoma in the Era of New Drugs and CAR-T Cell Therapy. Cancers (Basel). 2021;13(2). doi:10.3390/cancers13020291

85. Zhong L, Li Y, Xiong L, Wang W, Wu M, Yuan T, Yang W, Tian C, Miao Z, Wang T, Yang S. Small molecules in targeted cancer therapy: advances, challenges, and future perspectives. Signal Transduction and Targeted Therapy. 2021;6(1):201. doi:10.1038/s41392-021-00572-w

86. Trněný M, Lamy T, Walewski J, Belada D, Mayer J, Radford J, Jurczak W, Morschhauser F, Alexeeva J, Rule S, Afanasyev B, Kaplanov K, Thyss A, Kuzmin A, Voloshin S, Kuliczkowski K, Giza A, Milpied N, Stelitano C, Marks R, et al. Lenalidomide versus investigator's choice in relapsed or refractory mantle cell lymphoma (MCL-002; SPRINT): a phase 2, randomised, multicentre trial. The Lancet Oncology. 2016;17(3):319-31. doi:10.1016/S1470-2045(15)00559-8

87. Ruan J, Martin P, Christos P, Cerchietti L, Tam W, Shah B, Schuster SJ, Rodriguez A, Hyman D, Calvo-Vidal MN, Smith SM, Svoboda J, Furman RR, Coleman M, Leonard JP. Five-year follow-up of lenalidomide plus rituximab as initial treatment of mantle cell lymphoma. Blood. 2018;132(19):2016-25. doi:10.1182/blood-2018-07-859769

88. Goy A, Bernstein SH, Kahl BS, Djulbegovic B, Robertson MJ, de Vos S, Epner E, Krishnan A, Leonard JP, Lonial S, Nasta S, O'Connor OA, Shi H, Boral AL, Fisher RI. Bortezomib in patients with relapsed or refractory mantle cell lymphoma: updated time-to-event analyses of the multicenter phase 2 PINNACLE study. Annals of Oncology. 2009;20(3):520-5. doi:10.1093/annonc/mdn656

89. Weigert O, Weidmann E, Mueck R, Bentz M, von Schilling C, Rohrberg R, Jentsch-Ullrich K, Hiddemann W, Dreyling M. A novel regimen combining high dose cytarabine and bortezomib has activity in multiply relapsed and refractory mantle cell lymphoma – long-term results of a multicenter observation study. Leukemia & Lymphoma. 2009;50(5):716-22. doi:10.1080/10428190902856790

90. Furtado M, Johnson R, Kruger A, Turner D, Rule S. Addition of bortezomib to standard dose chop chemotherapy improves response and survival in relapsed mantle cell lymphoma. Br J Haematol. 2015;168(1):55-62. doi:10.1111/bjh.13101

91. Hess G, Herbrecht R, Romaguera J, Verhoef G, Crump M, Gisselbrecht C, Laurell A, Offner F, Strahs A, Berkenblit A, Hanushevsky O, Clancy J, Hewes B, Moore L, Coiffier B. Phase III study to evaluate temsirolimus compared with investigator's choice therapy for the treatment of relapsed or refractory mantle cell lymphoma. J Clin Oncol. 2009;27(23):3822-9. doi:10.1200/jco.2008.20.7977

92. Hess G, Wagner K, Keller U, La Rosee P, Atta J, Hübel K, Lerchenmueller C, Schoendube D, Witzens-Harig M, Ruckes C, Medler C, van Oordt C, Klapper W, Theobald M, Dreyling M. Final Results of a Phase I/II Trial of the Combination Bendamustine and Rituximab With Temsirolimus (BeRT) in Relapsed Mantle Cell Lymphoma and Follicular Lymphoma. Hemasphere. 2020;4(3):e398. doi:10.1097/hs9.0000000000000398

93. Davids MS, Roberts AW, Seymour JF, Pagel JM, Kahl BS, Wierda WG, Puvvada S, Kipps TJ, Anderson MA, Salem AH, Dunbar M, Zhu M, Peale F, Ross JA, Gressick L, Desai M, Kim SY, Verdugo M, Humerickhouse RA, Gordon GB, et al. Phase I First-in-Human Study of Venetoclax in Patients With Relapsed or Refractory Non-Hodgkin Lymphoma. Journal of Clinical Oncology. 2017;35(8):826-33. doi:10.1200/jco.2016.70.4320

94. Wang ML, Rule S, Martin P, Goy A, Auer R, Kahl BS, Jurczak W, Advani RH, Romaguera JE, Williams ME, Barrientos JC, Chmielowska E, Radford J, Stilgenbauer S, Dreyling M, Jedrzejczak WW, Johnson P, Spurgeon SE, Li L, Zhang L, et al. Targeting BTK with ibrutinib in relapsed or refractory mantle-cell lymphoma. N Engl J Med. 2013;369(6):507-16. doi:10.1056/NEJMoa1306220

95. Visco C, Di Rocco A, Evangelista A, Quaglia FM, Tisi MC, Morello L, Zilioli VR, Rusconi C, Hohaus S, Sciarra R, Re A, Tecchio C, Chiappella A, Marin-Niebla A, McCulloch R, Gini G, Perrone T, Nassi L, Pennese E, Stefani PM, et al. Outcomes in first relapsed-refractory younger patients with mantle cell lymphoma: results from the MANTLE-FIRST study. Leukemia. 2021;35(3):787-95. doi:10.1038/s41375-020-01013-3

96. McCulloch R, Lewis D, Crosbie N, Eyre TA, Bolam S, Arasaretnam A, Creasey T, Goradia H, McMillan A, Dawi S, Harrison S, Miles O, Robinson A, Dutton D, Wilson MR, McKay P, Follows G, Phillips N, Patmore R, Lambert J, et al. Ibrutinib for mantle cell lymphoma at first relapse: a United Kingdom real-world analysis of outcomes in 211 patients. Br J Haematol. 2021;193(2):290-8. doi:10.1111/bjh.17363

97. Tam CS, Anderson MA, Pott C, Agarwal R, Handunnetti S, Hicks RJ, Burbury K, Turner G, Di Iulio J, Bressel M, Westerman D, Lade S, Dreyling M, Dawson S-J, Dawson MA, Seymour JF, Roberts AW. Ibrutinib plus Venetoclax for the Treatment of Mantle-Cell Lymphoma. New England Journal of Medicine. 2018;378(13):1211-23. doi:10.1056/NEJMoa1715519

98. Cohen P, Cross D, Jänne PA. Kinase drug discovery 20 years after imatinib: progress and future directions. Nature Reviews Drug Discovery. 2021;20(7):551-69. doi:10.1038/s41573-021-00195-4

99. Mahajan S, Ghosh S, Sudbeck EA, Zheng Y, Downs S, Hupke M, Uckun FM. Rational Design and Synthesis of a Novel Anti-leukemic Agent Targeting Bruton′s Tyrosine Kinase (BTK), LFM-A13 [α-Cyano-β-Hydroxy-β-Methyl-N-(2,5-Dibromophenyl)Propenamide]*. Journal of Biological Chemistry. 1999;274(14):9587-99. doi:10.1074/jbc.274.14.9587

100. Honigberg LA, Smith AM, Sirisawad M, Verner E, Loury D, Chang B, Li S, Pan Z, Thamm DH, Miller RA, Buggy JJ. The Bruton tyrosine kinase inhibitor PCI-32765 blocks B-cell activation and is efficacious in models of autoimmune disease and B-cell malignancy. Proc Natl Acad Sci U S A. 2010;107(29):13075-80. doi:10.1073/pnas.1004594107

101. Pan Z, Scheerens H, Li S-J, Schultz BE, Sprengeler PA, Burrill LC, Mendonca RV, Sweeney MD, Scott KCK, Grothaus PG, Jeffery DA, Spoerke JM, Honigberg LA, Young PR, Dalrymple SA, Palmer JT. Discovery of Selective Irreversible Inhibitors for Bruton’s Tyrosine Kinase. ChemMedChem. 2007;2(1):58-61. doi:doi.org/10.1002/cmdc.200600221

102. Cinar M, Hamedani F, Mo Z, Cinar B, Amin HM, Alkan S. Bruton tyrosine kinase is commonly overexpressed in mantle cell lymphoma and its attenuation by Ibrutinib induces apoptosis. Leuk Res. 2013;37(10):1271-7. doi:10.1016/j.leukres.2013.07.028

103. Ma J, Lu P, Guo A, Cheng S, Zong H, Martin P, Coleman M, Wang YL. Characterization of ibrutinib-sensitive and -resistant mantle lymphoma cells. Br J Haematol. 2014;166(6):849-61. doi:10.1111/bjh.12974

104. Chang BY, Francesco M, De Rooij MF, Magadala P, Steggerda SM, Huang MM, Kuil A, Herman SE, Chang S, Pals ST, Wilson W, Wiestner A, Spaargaren M, Buggy JJ, Elias L. Egress of CD19(+)CD5(+) cells into peripheral blood following treatment with the Bruton tyrosine kinase inhibitor ibrutinib in mantle cell lymphoma patients. Blood. 2013;122(14):2412-24. doi:10.1182/blood-2013-02-482125

105. Advani RH, Buggy JJ, Sharman JP, Smith SM, Boyd TE, Grant B, Kolibaba KS, Furman RR, Rodriguez S, Chang BY, Sukbuntherng J, Izumi R, Hamdy A, Hedrick E, Fowler NH. Bruton tyrosine kinase inhibitor ibrutinib (PCI-32765) has significant activity in patients with relapsed/refractory B-cell malignancies. J Clin Oncol. 2013;31(1):88-94. doi:10.1200/jco.2012.42.7906

106. O'Brien S, Hillmen P, Coutre S, Barr PM, Fraser G, Tedeschi A, Burger JA, Dilhuydy MS, Hess G, Moreno C, Cramer P, Liu E, Chang S, Vermeulen J, Styles L, Howes A, James DF, Patel K, Graef T, Valentino R. Safety Analysis of Four Randomized Controlled Studies of Ibrutinib in Patients With Chronic Lymphocytic Leukemia/Small Lymphocytic Lymphoma or Mantle Cell Lymphoma. Clin Lymphoma Myeloma Leuk. 2018;18(10):648-57.e15. doi:10.1016/j.clml.2018.06.016

107. Jain P, Zhao S, Lee HJ, Hill HA, Ok CY, Kanagal-Shamanna R, Hagemeister FB, Fowler N, Fayad L, Yao Y, Liu Y, Moghrabi OB, Navsaria L, Feng L, Nogueras Gonzalez GM, Xu G, Thirumurthi S, Santos D, Iliescu C, Tang G, et al. Ibrutinib With Rituximab in First-Line Treatment of Older Patients With Mantle Cell Lymphoma. J Clin Oncol. 2022;40(2):202-12. doi:10.1200/jco.21.01797

108. Hershkovitz-Rokah O, Pulver D, Lenz G, Shpilberg O. Ibrutinib resistance in mantle cell lymphoma: clinical, molecular and treatment aspects. Br J Haematol. 2018;181(3):306-19. doi:10.1111/bjh.15108

109. Chiron D, Di Liberto M, Martin P, Huang X, Sharman J, Blecua P, Mathew S, Vijay P, Eng K, Ali S, Johnson A, Chang B, Ely S, Elemento O, Mason CE, Leonard JP, Chen-Kiang S. Cell-cycle reprogramming for PI3K inhibition overrides a relapse-specific C481S BTK mutation revealed by longitudinal functional genomics in mantle cell lymphoma. Cancer Discov. 2014;4(9):1022-35. doi:10.1158/2159-8290.Cd-14-0098

110. Colomer D, Campo E. Unlocking new therapeutic targets and resistance mechanisms in mantle cell lymphoma. Cancer Cell. 2014;25(1):7-9. doi:10.1016/j.ccr.2013.12.011

111. Wang L, Yang P, Zhang W, Wang J, Jing H. Clinical and Molecular Biology Analysis of Patients with Mantle Cell Lymphoma Resistant to BTK Inhibitor. Blood. 2021;138(Supplement 1):4527-. doi:10.1182/blood-2021-149114

112. Jain P, Kanagal-Shamanna R, Zhang S, Ahmed M, Ghorab A, Zhang L, Ok CY, Li S, Hagemeister F, Zeng D, Gong T, Chen W, Badillo M, Nomie K, Fayad L, Medeiros LJ, Neelapu S, Fowler N, Romaguera J, Champlin R, et al. Long-term outcomes and mutation profiling of patients with mantle cell lymphoma (MCL) who discontinued ibrutinib. Br J Haematol. 2018;183(4):578-87. doi:10.1111/bjh.15567

113. Wu C, de Miranda NF, Chen L, Wasik AM, Mansouri L, Jurczak W, Galazka K, Dlugosz-Danecka M, Machaczka M, Zhang H, Peng R, Morin RD, Rosenquist R, Sander B, Pan-Hammarström Q. Genetic heterogeneity in primary and relapsed mantle cell lymphomas: Impact of recurrent CARD11 mutations. Oncotarget. 2016;7(25):38180-90. doi:10.18632/oncotarget.9500

114. Chiron D, Bellanger C, Papin A, Tessoulin B, Dousset C, Maiga S, Moreau A, Esbelin J, Trichet V, Chen-Kiang S, Moreau P, Touzeau C, Le Gouill S, Amiot M, Pellat-Deceunynck C. Rational targeted therapies to overcome microenvironment-dependent expansion of mantle cell lymphoma. Blood. 2016;128(24):2808-18. doi:10.1182/blood-2016-06-720490

115. Zhao X, Lwin T, Silva A, Shah B, Tao J, Fang B, Zhang L, Fu K, Bi C, Li J, Jiang H, Meads MB, Jacobson T, Silva M, Distler A, Darville L, Zhang L, Han Y, Rebatchouk D, Di Liberto M, et al. Unification of de novo and acquired ibrutinib resistance in mantle cell lymphoma. Nat Commun. 2017;8:14920. doi:10.1038/ncomms14920

116. Kaptein A, de Bruin G, Emmelot-van Hoek M, van de Kar B, de Jong A, Gulrajani M, Demont D, Covey T, Mittag D, Barf T. Potency and Selectivity of BTK Inhibitors in Clinical Development for B-Cell Malignancies. Blood. 2018;132(Supplement 1):1871. doi:10.1182/blood-2018-99-109973

117. Flinsenberg TWH, Tromedjo CC, Hu N, Liu Y, Guo Y, Thia KYT, Noori T, Song X, Aw Yeang HX, Tantalo DG, Handunnetti S, Seymour JF, Roberts AW, Ritchie D, Koldej R, Neeson PJ, Wang L, Trapani JA, Tam CS, Voskoboinik I. Differential effects of BTK inhibitors ibrutinib and zanubrutinib on NK-cell effector

function in patients with mantle cell lymphoma. Haematologica. 2020;105(2):e76-e9. doi:10.3324/haematol.2019.220590

118. Levade M, David E, Garcia C, Laurent PA, Cadot S, Michallet AS, Bordet JC, Tam C, Sié P, Ysebaert L, Payrastre B. Ibrutinib treatment affects collagen and von Willebrand factor-dependent platelet functions. Blood. 2014;124(26):3991-5. doi:10.1182/blood-2014-06-583294

119. Borge M, Belén Almejún M, Podaza E, Colado A, Fernández Grecco H, Cabrejo M, Bezares RF, Giordano M, Gamberale R. Ibrutinib impairs the phagocytosis of rituximab-coated leukemic cells from chronic lymphocytic leukemia patients by human macrophages. Haematologica. 2015;100(4):e140-2. doi:10.3324/haematol.2014.119669

120. Dubovsky JA, Beckwith KA, Natarajan G, Woyach JA, Jaglowski S, Zhong Y, Hessler JD, Liu TM, Chang BY, Larkin KM, Stefanovski MR, Chappell DL, Frissora FW, Smith LL, Smucker KA, Flynn JM, Jones JA, Andritsos LA, Maddocks K, Lehman AM, et al. Ibrutinib is an irreversible molecular inhibitor of ITK driving a Th1-selective pressure in T lymphocytes. Blood. 2013;122(15):2539-49. doi:10.1182/blood-2013-06-507947

121. Burger JA. Bruton Tyrosine Kinase Inhibitors: Present and Future. Cancer J. 2019;25(6):386-93. doi:10.1097/ppo.0000000000000412

122. Xiao L, Salem JE, Clauss S, Hanley A, Bapat A, Hulsmans M, Iwamoto Y, Wojtkiewicz G, Cetinbas M, Schloss MJ, Tedeschi J, Lebrun-Vignes B, Lundby A, Sadreyev RI, Moslehi J, Nahrendorf M, Ellinor PT, Milan DJ. Ibrutinib-Mediated Atrial Fibrillation Attributable to Inhibition of C-Terminal Src Kinase. Circulation. 2020;142(25):2443-55. doi:10.1161/circulationaha.120.049210

123. Byrd JC, Hillmen P, Ghia P, Kater AP, Chanan-Khan AAA, Furman RR, O'Brien SM, Yenerel MN, Illés Á, Kay NE, Marco JAG, Mato AR, Seymour JF, Leprêtre S, Stilgenbauer S, Robak T, Patel P, Higgins K, Sohoni S, Jurczak W. First results of a head-to-head trial of acalabrutinib versus ibrutinib in previously treated chronic lymphocytic leukemia. Journal of Clinical Oncology. 2021;39(15_suppl):7500-. doi:10.1200/JCO.2021.39.15_suppl.7500

124. Wang M, Shah NN, Alencar AJ, Gerson JN, Patel MR, Fakhri B, Jurczak W, Tan XN, Lewis K, Fenske TS, Coombs CC, Flinn IW, Lewis DJ, Le Gouill S, Palomba ML, Woyach JA, Pagel JM, Lamanna N, Cohen JB, Barve MA, et al. Pirtobrutinib, A Next Generation, Highly Selective, Non-Covalent BTK Inhibitor in Previously Treated Mantle Cell Lymphoma: Updated Results from the Phase 1/2 BRUIN Study. Blood. 2021;138:381. doi:10.1182/blood-2021-149138

125. Cohen JB, Shah NN, Alencar AJ, Gerson JN, Patel MR, Fakhri B, Jurczak W, Tan XN, Lewis KL, Fenske T, Coombs CC, Flinn IW, Lewis DJ, Gouill SL, Palomba ML, Woyach JA, Pagel JM, Lamanna N, Barve MA, Ghia P, et al. MCL-133 Pirtobrutinib, a Highly Selective, Non-Covalent (Reversible) BTK Inhibitor in Previously Treated Mantle Cell Lymphoma: Updated Results From the Phase 1/2 BRUIN Study. Clin Lymphoma Myeloma Leuk. 2022;22 Suppl 2:S394-s5. doi:10.1016/s2152-2650(22)01569-5

126. Martin P, Maddocks K, Leonard JP, Ruan J, Goy A, Wagner-Johnston N, Rule S, Advani R, Iberri D, Phillips T, Spurgeon S, Kozin E, Noto K, Chen Z, Jurczak W, Auer R, Chmielowska E, Stilgenbauer S, Bloehdorn J, Portell C, et al. Postibrutinib outcomes in patients with mantle cell lymphoma. Blood. 2016;127(12):1559-63. doi:10.1182/blood-2015-10-673145

127. Cheah CY, Chihara D, Romaguera JE, Fowler NH, Seymour JF, Hagemeister FB, Champlin RE, Wang ML. Patients with mantle cell lymphoma failing ibrutinib are unlikely to respond to salvage chemotherapy and have poor outcomes. Ann Oncol. 2015;26(6):1175-9. doi:10.1093/annonc/mdv111

128. McCulloch R, Visco C, Eyre TA, Frewin R, Phillips N, Tucker DL, Quaglia FM, McMillan A, Lambert J, Crosbie N, Rule S. Efficacy of R-BAC in relapsed, refractory mantle cell lymphoma post BTK inhibitor therapy. Br J Haematol. 2020;189(4):684-8. doi:10.1111/bjh.16416

129. Eyre TA, Walter HS, Iyengar S, Follows G, Cross M, Fox CP, Hodson A, Coats J, Narat S, Morley N, Dyer MJS, Collins GP. Efficacy of venetoclax monotherapy in patients with relapsed, refractory mantle cell lymphoma after Bruton tyrosine kinase inhibitor therapy. Haematologica. 2019;104(2):e68-e71. doi:10.3324/haematol.2018.198812

130. Wang M, Schuster SJ, Phillips T, Lossos IS, Goy A, Rule S, Hamadani M, Ghosh N, Reeder CB, Barnett E, Bravo MC, Martin P. Observational study of lenalidomide in patients with mantle cell lymphoma who

relapsed/progressed after or were refractory/intolerant to ibrutinib (MCL-004). J Hematol Oncol. 2017;10(1):171. doi:10.1186/s13045-017-0537-5

131. Newcomb R, Jacobson C. Chimeric Antigen Receptor T Cells for B-Cell Lymphoma. The Cancer Journal. 2021;27(2). doi:10.1097/PPO.0000000000000509

132. Wang M, Munoz J, Goy A, Locke FL, Jacobson CA, Hill BT, Timmerman JM, Holmes H, Jaglowski S, Flinn IW, McSweeney PA, Miklos DB, Pagel JM, Kersten MJ, Bouabdallah K, Khanal R, Topp MS, Houot R, Beitinjaneh A, Peng W, et al. Three-Year Follow-Up of KTE-X19 in Patients With Relapsed/Refractory Mantle Cell Lymphoma, Including High-Risk Subgroups, in the ZUMA-2 Study. Journal of Clinical Oncology.0(0):JCO.21.02370. doi:10.1200/jco.21.02370

133. Wang M, Munoz J, Goy A, Locke FL, Jacobson CA, Hill BT, Timmerman JM, Holmes H, Jaglowski S, Flinn IW, McSweeney PA, Miklos DB, Pagel JM, Kersten MJ, Bouabdallah K, Khanal R, Topp MS, Houot R, Beitinjaneh A, Peng W, et al. Three-Year Follow-Up of KTE-X19 in Patients With Relapsed/Refractory Mantle Cell Lymphoma, Including High-Risk Subgroups, in the ZUMA-2 Study. J Clin Oncol. 2022:Jco2102370. doi:10.1200/jco.21.02370

134. Gauthier J, Turtle CJ. Insights into cytokine release syndrome and neurotoxicity after CD19-specific CAR-T cell therapy. Curr Res Transl Med. 2018;66(2):50-2. doi:10.1016/j.retram.2018.03.003

135. Hyman DM, Taylor BS, Baselga J. Implementing Genome-Driven Oncology. Cell. 2017;168(4):584-99. doi:10.1016/j.cell.2016.12.015

136. Kharchenko PV. The triumphs and limitations of computational methods for scRNA-seq. Nat Methods. 2021;18(7):723-32. doi:10.1038/s41592-021-01171-x

137. Gerlinger M, Rowan AJ, Horswell S, Math M, Larkin J, Endesfelder D, Gronroos E, Martinez P, Matthews N, Stewart A, Tarpey P, Varela I, Phillimore B, Begum S, McDonald NQ, Butler A, Jones D, Raine K, Latimer C, Santos CR, et al. Intratumor heterogeneity and branched evolution revealed by multiregion sequencing. N Engl J Med. 2012;366(10):883-92. doi:10.1056/NEJMoa1113205

138. Ramirez M, Rajaram S, Steininger RJ, Osipchuk D, Roth MA, Morinishi LS, Evans L, Ji W, Hsu CH, Thurley K, Wei S, Zhou A, Koduru PR, Posner BA, Wu LF, Altschuler SJ. Diverse drug-resistance mechanisms can emerge from drug-tolerant cancer persister cells. Nat Commun. 2016;7:10690. doi:10.1038/ncomms10690

139. Kalisky T, Blainey P, Quake SR. Genomic analysis at the single-cell level. Annu Rev Genet. 2011;45:431-45. doi:10.1146/annurev-genet-102209-163607

140. Saliba AE, Westermann AJ, Gorski SA, Vogel J. Single-cell RNA-seq: advances and future challenges. Nucleic Acids Res. 2014;42(14):8845-60. doi:10.1093/nar/gku555

141. Aissa AF, Islam A, Ariss MM, Go CC, Rader AE, Conrardy RD, Gajda AM, Rubio-Perez C, Valyi-Nagy K, Pasquinelli M, Feldman LE, Green SJ, Lopez-Bigas N, Frolov MV, Benevolenskaya EV. Single-cell transcriptional changes associated with drug tolerance and response to combination therapies in cancer. Nat Commun. 2021;12(1):1628. doi:10.1038/s41467-021-21884-z

142. Zheng GX, Terry JM, Belgrader P, Ryvkin P, Bent ZW, Wilson R, Ziraldo SB, Wheeler TD, McDermott GP, Zhu J, Gregory MT, Shuga J, Montesclaros L, Underwood JG, Masquelier DA, Nishimura SY, Schnall-Levin M, Wyatt PW, Hindson CM, Bharadwaj R, et al. Massively parallel digital transcriptional profiling of single cells. Nat Commun. 2017;8:14049. doi:10.1038/ncomms14049

143. Eisenstein M. Startups use short-read data to expand long-read sequencing market. Nat Biotechnol. 2015;33(5):433-5. doi:10.1038/nbt0515-433

144. Picelli S, Faridani OR, Björklund AK, Winberg G, Sagasser S, Sandberg R. Full-length RNA-seq from single cells using Smart-seq2. Nat Protoc. 2014;9(1):171-81. doi:10.1038/nprot.2014.006

145. Martin M. Cutadapt removes adapter sequences from high-throughput sequencing reads. 2011. 2011;17(1):3. doi:10.14806/ej.17.1.200

146. Schneider CA, Rasband WS, Eliceiri KW. NIH Image to ImageJ: 25 years of image analysis. Nature Methods. 2012;9(7):671-5. doi:10.1038/nmeth.2089

147. R Development Core Team. R: A language and environment for statistical computing. Vienna, Austria: R Foundation for Statistical Computing; 2019. Retrieved from: https://www.R-project.org/.

148. RStudio Team. RStudio: Integrated Development for R. Boston, MA: RStudio, Inc.; 2016. Retrieved from: http://www.rstudio.com/.

149. Yu G, Wang LG, Han Y, He QY. clusterProfiler: an R package for comparing biological themes among gene clusters. Omics. 2012;16(5):284-7. doi:10.1089/omi.2011.0118

150. Love MI, Huber W, Anders S. Moderated estimation of fold change and dispersion for RNA-seq data with DESeq2. Genome Biol. 2014;15(12):550. doi:10.1186/s13059-014-0550-8

151. Liao Y, Smyth GK, Shi W. featureCounts: an efficient general purpose program for assigning sequence reads to genomic features. Bioinformatics. 2014;30(7):923-30. doi:10.1093/bioinformatics/btt656

152. Aibar S, González-Blas CB, Moerman T, Huynh-Thu VA, Imrichova H, Hulselmans G, Rambow F, Marine J-C, Geurts P, Aerts J, van den Oord J, Atak ZK, Wouters J, Aerts S. SCENIC: single-cell regulatory network inference and clustering. Nature Methods. 2017;14(11):1083-6. doi:10.1038/nmeth.4463

153. Butler A, Hoffman P, Smibert P, Papalexi E, Satija R. Integrating single-cell transcriptomic data across different conditions, technologies, and species. Nat Biotechnol. 2018;36(5):411-20. doi:10.1038/nbt.4096

154. Dobin A, Davis CA, Schlesinger F, Drenkow J, Zaleski C, Jha S, Batut P, Chaisson M, Gingeras TR. STAR: ultrafast universal RNA-seq aligner. Bioinformatics. 2013;29(1):15-21. doi:10.1093/bioinformatics/bts635

155. Stuart T, Butler A, Hoffman P, Hafemeister C, Papalexi E, Mauck WM, 3rd, Hao Y, Stoeckius M, Smibert P, Satija R. Comprehensive Integration of Single-Cell Data. Cell. 2019;177(7):1888-902.e21. doi:10.1016/j.cell.2019.05.031

156. Fuhr V, Vafadarnejad E, Dietrich O, Arampatzi P, Riedel A, Saliba AE, Rosenwald A, Rauert-Wunderlich H. Time-Resolved scRNA-Seq Tracks the Adaptation of a Sensitive MCL Cell Line to Ibrutinib Treatment. Int J Mol Sci. 2021;22(5). doi:10.3390/ijms22052276

157. Fuhr V, Vafadarnejad E, Dietrich O, Arampatzi P, Riedel A, Saliba A-E, Rosenwald A, Rauert-Wunderlich H. Eine Einzelzell-RNA-Sequenzierung identifiziert Metabolismus und CD52 als neue Angriffspunkte in Ibrutinib-persistenten Mantelzelllymphomzellen. Die Pathologie. 2022. doi:10.1007/s00292-022-01136-7

158. Fuhr V, Heidenreich S, Srivastava M, Riedel A, Düll J, Gerhard-Hartmann E, Rosenwald A, Rauert-Wunderlich H. CD52 and OXPHOS – potential targets in ibrutinib-treated mantle cell lymphoma. *Accepted for publication in Cell Death Discovery on 16 December 2022*.

159. Geisler CH, Kolstad A, Laurell A, Jerkeman M, Räty R, Andersen NS, Pedersen LB, Eriksson M, Nordström M, Kimby E, Bentzen H, Kuittinen O, Lauritzsen GF, Nilsson-Ehle H, Ralfkiaer E, Ehinger M, Sundström C, Delabie J, Karjalainen-Lindsberg ML, Brown P, et al. Nordic MCL2 trial update: six-year follow-up after intensive immunochemotherapy for untreated mantle cell lymphoma followed by BEAM or BEAC + autologous stem-cell support: still very long survival but late relapses do occur. Br J Haematol. 2012;158(3):355-62. doi:10.1111/j.1365-2141.2012.09174.x

160. Dreyling M, Goy A, Hess G, Kahl BS, Hernández-Rivas J, Schuier N, Qi K, Deshpande S, Zhu A, Parisi L, Wang ML. Long-term Outcomes With Ibrutinib Treatment for Patients With Relapsed/Refractory Mantle Cell Lymphoma: A Pooled Analysis of 3 Clinical Trials With Nearly 10 Years of Follow-up. Hemasphere. 2022;6(5):e712. doi:10.1097/hs9.0000000000000712

161. Wang ML, Jurczak W, Jerkeman M, Trotman J, Zinzani PL, Belada D, Boccomini C, Flinn IW, Giri P, Goy A, Hamlin PA, Hermine O, Hernández-Rivas J, Hong X, Kim SJ, Lewis D, Mishima Y, Özcan M, Perini GF, Pocock C, et al. Ibrutinib plus Bendamustine and Rituximab in Untreated Mantle-Cell Lymphoma. N Engl J Med. 2022;386(26):2482-94. doi:10.1056/NEJMoa2201817

162. Tam CS, Anderson MA, Pott C, Agarwal R, Handunnetti S, Hicks RJ, Burbury K, Turner G, Di Iulio J, Bressel M, Westerman D, Lade S, Dreyling M, Dawson SJ, Dawson MA, Seymour JF, Roberts AW. Ibrutinib plus Venetoclax for the Treatment of Mantle-Cell Lymphoma. N Engl J Med. 2018;378(13):1211-23. doi:10.1056/NEJMoa1715519

163. Le Gouill S, Morschhauser F, Chiron D, Bouabdallah K, Cartron G, Casasnovas O, Bodet-Milin C, Ragot S, Bossard C, Nadal N, Herbaux C, Tessoulin B, Tchernonog E, Rossi C, McCulloch R, Gastinne T, Callanan MB, Rule S. Ibrutinib, obinutuzumab, and venetoclax in relapsed and untreated patients with mantle cell lymphoma: a phase 1/2 trial. Blood. 2021;137(7):877-87. doi:10.1182/blood.2020008727

164. Wu W, Wang W, Franzen CA, Guo H, Lee J, Li Y, Sukhanova M, Sheng D, Venkataraman G, Ming M, Lu P, Gao A, Xia C, Li J, Zhang LL, Jiang VC, Wang ML, Andrade J, Zhou X, Wang YL. Inhibition of B-cell receptor signaling disrupts cell adhesion in mantle cell lymphoma via RAC2. Blood Adv. 2021;5(1):185-97. doi:10.1182/bloodadvances.2020001665

165. Rauert-Wunderlich H, Rudelius M, Ott G, Rosenwald A. Targeting protein kinase C in mantle cell lymphoma. Br J Haematol. 2016;173(3):394-403. doi:10.1111/bjh.13973

166. Zhang S, Jiang VC, Han G, Hao D, Lian J, Liu Y, Zhang R, McIntosh J, Wang R, Dang M, Dai E, Wang Y, Santos D, Badillo M, Leeming A, Chen Z, Hartig K, Bigcal J, Zhou J, Kanagal-Shamanna R, et al. Longitudinal single-cell profiling reveals molecular heterogeneity and tumor-immune evolution in refractory mantle cell lymphoma. Nat Commun. 2021;12(1):2877. doi:10.1038/s41467-021-22872-z

167. Ferrero S, Grimaldi D, Genuardi E, Drandi D, Zaccaria GM, Alessandria B, Ghislieri M, Ferrante M, Evangelista A, Mantoan B, De Luca G, Stefani PM, Benedetti F, Casaroli I, Zanni M, Castellino C, Pavone V, Petrini M, Re F, Hohaus S, et al. Punctual and kinetic MRD analysis from the Fondazione Italiana Linfomi MCL0208 phase 3 trial in mantle cell lymphoma. Blood. 2022;140(12):1378-89. doi:10.1182/blood.2021014270

168. Giné E, de la Cruz F, Jiménez Ubieto A, López Jimenez J, Martín García-Sancho A, Terol MJ, González Barca E, Casanova M, de la Fuente A, Marín-Niebla A, Muntañola A, González-López TJ, Aymerich M, Setoain X, Cortés-Romera M, Rotger A, Rodríguez S, Medina Herrera A, García Sanz R, Nadeu F, et al. Ibrutinib in Combination With Rituximab for Indolent Clinical Forms of Mantle Cell Lymphoma (IMCL-2015): A Multicenter, Open-Label, Single-Arm, Phase II Trial. J Clin Oncol. 2022;40(11):1196-205. doi:10.1200/jco.21.02321

169. Kinker GS, Greenwald AC, Tal R, Orlova Z, Cuoco MS, McFarland JM, Warren A, Rodman C, Roth JA, Bender SA, Kumar B, Rocco JW, Fernandes P, Mader CC, Keren-Shaul H, Plotnikov A, Barr H, Tsherniak A, Rozenblatt-Rosen O, Krizhanovsky V, et al. Pan-cancer single-cell RNA-seq identifies recurring programs of cellular heterogeneity. Nat Genet. 2020;52(11):1208-18. doi:10.1038/s41588-020-00726-6

170. Nestorowa S, Hamey FK, Pijuan Sala B, Diamanti E, Shepherd M, Laurenti E, Wilson NK, Kent DG, Göttgens B. A single-cell resolution map of mouse hematopoietic stem and progenitor cell differentiation. Blood. 2016;128(8):e20-31. doi:10.1182/blood-2016-05-716480

171. Wightman SC, Uppal A, Pitroda SP, Ganai S, Burnette B, Stack M, Oshima G, Khan S, Huang X, Posner MC, Weichselbaum RR, Khodarev NN. Oncogenic CXCL10 signalling drives metastasis development and poor clinical outcome. Br J Cancer. 2015;113(2):327-35. doi:10.1038/bjc.2015.193

172. Shevde LA, Samant RS. Role of osteopontin in the pathophysiology of cancer. Matrix Biol. 2014;37:131-41. doi:10.1016/j.matbio.2014.03.001

173. Storti P, Marchica V, Giuliani N. Role of Galectins in Multiple Myeloma. Int J Mol Sci. 2017;18(12). doi:10.3390/ijms18122740

174. Silkenstedt E, Arenas F, Colom-Sanmartí B, Xargay-Torrent S, Higashi M, Giró A, Rodriguez V, Fuentes P, Aulitzky WE, van der Kuip H, Beà S, Toribio ML, Campo E, López-Guerra M, Colomer D. Notch1 signaling in NOTCH1-mutated mantle cell lymphoma depends on Delta-Like ligand 4 and is a potential target for specific antibody therapy. J Exp Clin Cancer Res. 2019;38(1):446. doi:10.1186/s13046-019-1458-7

175. Kridel R, Meissner B, Rogic S, Boyle M, Telenius A, Woolcock B, Gunawardana J, Jenkins C, Cochrane C, Ben-Neriah S, Tan K, Morin RD, Opat S, Sehn LH, Connors JM, Marra MA, Weng AP, Steidl C, Gascoyne RD. Whole transcriptome sequencing reveals recurrent NOTCH1 mutations in mantle cell lymphoma. Blood. 2012;119(9):1963-71. doi:10.1182/blood-2011-11-391474

176. Kurtova AV, Tamayo AT, Ford RJ, Burger JA. Mantle cell lymphoma cells express high levels of CXCR4, CXCR5, and VLA-4 (CD49d): importance for interactions with the stromal microenvironment and specific targeting. Blood. 2009;113(19):4604-13. doi:10.1182/blood-2008-10-185827

177. Buccitelli C, Selbach M. mRNAs, proteins and the emerging principles of gene expression control. Nat Rev Genet. 2020;21(10):630-44. doi:10.1038/s41576-020-0258-4

178. Rendeiro AF, Krausgruber T, Fortelny N, Zhao F, Penz T, Farlik M, Schuster LC, Nemc A, Tasnády S, Réti M, Mátrai Z, Alpár D, Bödör C, Schmidl C, Bock C. Chromatin mapping and single-cell immune profiling define the temporal dynamics of ibrutinib response in CLL. Nat Commun. 2020;11(1):577. doi:10.1038/s41467-019-14081-6

179. Hinz M, Löser P, Mathas S, Krappmann D, Dörken B, Scheidereit C. Constitutive NF-kappaB maintains high expression of a characteristic gene network, including CD40, CD86, and a set of antiapoptotic genes in Hodgkin/Reed-Sternberg cells. Blood. 2001;97(9):2798-807. doi:10.1182/blood.v97.9.2798

180. Barrena S, Almeida J, Yunta M, López A, Fernández-Mosteirín N, Giralt M, Romero M, Perdiguer L, Delgado M, Orfao A, Lazo PA. Aberrant expression of tetraspanin molecules in B-cell chronic lymphoproliferative disorders and its correlation with normal B-cell maturation. Leukemia. 2005;19(8):1376-83. doi:10.1038/sj.leu.2403822

181. Rodig SJ, Abramson JS, Pinkus GS, Treon SP, Dorfman DM, Dong HY, Shipp MA, Kutok JL. Heterogeneous CD52 expression among hematologic neoplasms: implications for the use of alemtuzumab (CAMPATH-1H). Clin Cancer Res. 2006;12(23):7174-9. doi:10.1158/1078-0432.Ccr-06-1275

182. Frigault MJ, Chen Y-B, Gallagher KME, Horick NK, El-Jawahri A, Scarfò I, Wehrli M, Huang L, Casey K, Cook D, Spitzer T, McAfee S, Preffer FI, Armant M, Shaw KL, Daley H, Nikiforow S, Ritz J, Maus MV. Phase 1 Study of CD37-Directed CAR T Cells in Patients with Relapsed or Refractory CD37+ Hematologic Malignancies. Blood. 2021;138(Supplement 1):653-. doi:10.1182/blood-2021-146236

183. Stilgenbauer S, Aurran Schleinitz T, Eichhorst B, Lang F, Offner F, Rossi JF, Schroyens W, Van Den Neste E, Ysebaert L, von Wangenheim U, Ursula Kress U, Blum P, Zenz T. Phase 1 first-in-human trial of the anti-CD37 antibody BI 836826 in relapsed/refractory chronic lymphocytic leukemia. Leukemia. 2019;33(10):2531-5. doi:10.1038/s41375-019-0475-z

184. Danilov AV, Spurgeon SE, Siddiqi T, Quinson AM, Maier D, Smith D, Brown JR. A phase Ib, open label, dose escalation trial of the anti-CD37 monoclonal antibody, BI 836826, in combination with ibrutinib in patients with relapsed/refractory chronic lymphocytic leukemia. Invest New Drugs. 2021;39(4):1099-105. doi:10.1007/s10637-020-01056-4

185. Vaisitti T, Vitale N, Micillo M, Brandimarte L, Iannello A, Papotti MG, Jaksic O, Lopez G, Di Napoli A, Cutrin JC, Orlik C, Kulke M, Pahl A, Deaglio S. Anti-CD37 α-amanitin-conjugated antibodies as potential therapeutic weapons for Richter syndrome. Blood. 2022;140(13):1565-9. doi:10.1182/blood.2022016211

186. Rao SP, Sancho J, Campos-Rivera J, Boutin PM, Severy PB, Weeden T, Shankara S, Roberts BL, Kaplan JM. Human peripheral blood mononuclear cells exhibit heterogeneous CD52 expression levels and show differential sensitivity to alemtuzumab mediated cytolysis. PLoS One. 2012;7(6):e39416. doi:10.1371/journal.pone.0039416

187. Kirchhoff C, Schröter S. New insights into the origin, structure and role of CD52: a major component of the mammalian sperm glycocalyx. Cells Tissues Organs. 2001;168(1-2):93-104. doi:10.1159/000016810

188. Rowan WC, Hale G, Tite JP, Brett SJ. Cross-linking of the CAMPATH-1 antigen (CD52) triggers activation of normal human T lymphocytes. International Immunology. 1995;7(1):69-77. doi:10.1093/intimm/7.1.69

189. Watanabe T, Masuyama J-i, Sohma Y, Inazawa H, Horie K, Kojima K, Uemura Y, Aoki Y, Kaga S, Minota S, Tanaka T, Yamaguchi Y, Kobayashi T, Serizawa I. CD52 is a novel costimulatory molecule for induction of CD4+ regulatory T cells. Clinical Immunology. 2006;120(3):247-59. doi:10.1016/j.clim.2006.05.006

190. Masuyama J-i, Yoshio T, Suzuki K, Kitagawa S, Iwamoto M, Kamimura T, Hirata D, Takeda A, Kano S, Minota S. Characterization of the 4C8 Antigen Involved in Transendothelial Migration of CD26hi T Cells after Tight Adhesion to Human Umbilical Vein Endothelial Cell Monolayers. Journal of Experimental Medicine. 1999;189(6):979-90. doi:10.1084/jem.189.6.979

191. Rudnik M, Rolski F, Jordan S, Mertelj T, Stellato M, Distler O, Blyszczuk P, Kania G. Regulation of Monocyte Adhesion and Type I Interferon Signaling by CD52 in Patients With Systemic Sclerosis. Arthritis Rheumatol. 2021;73(9):1720-30. doi:10.1002/art.41737

192. Bhamidipati K, Silberstein JL, Chaichian Y, Baker MC, Lanz TV, Zia A, Rasheed YS, Cochran JR, Robinson WH. CD52 Is Elevated on B cells of SLE Patients and Regulates B Cell Function. Front Immunol. 2020;11:626820. doi:10.3389/fimmu.2020.626820

193. Warburg O, Wind F, Negelein E. THE METABOLISM OF TUMORS IN THE BODY. J Gen Physiol. 1927;8(6):519-30. doi:10.1085/jgp.8.6.519

194. DeBerardinis RJ, Chandel NS. Fundamentals of cancer metabolism. Sci Adv. 2016;2(5):e1600200. doi:10.1126/sciadv.1600200

195. Albano D, Treglia G, Gazzilli M, Cerudelli E, Giubbini R, Bertagna F. (18)F-FDG PET or PET/CT in Mantle Cell Lymphoma. Clin Lymphoma Myeloma Leuk. 2020;20(7):422-30. doi:10.1016/j.clml.2020.01.018

196. Bailly C, Carlier T, Touzeau C, Arlicot N, Kraeber-Bodéré F, Le Gouill S, Bodet-Milin C. Interest of FDG-PET in the Management of Mantle Cell Lymphoma. Front Med (Lausanne). 2019;6:70. doi:10.3389/fmed.2019.00070

197. Kruiswijk F, Labuschagne CF, Vousden KH. p53 in survival, death and metabolic health: a lifeguard with a licence to kill. Nat Rev Mol Cell Biol. 2015;16(7):393-405. doi:10.1038/nrm4007

198. Kliebhan J, Besse A, Kampa-Schittenhelm K, Schittenhelm M, Driessen C. Mutant TP53 driving the Warburg Effect in Mantle Cell lymphoma. Clin Case Rep. 2022;10(10):e6296. doi:10.1002/ccr3.6296

199. Camps J, Salaverria I, Garcia MJ, Prat E, Beà S, Pole JC, Hernández L, Del Rey J, Cigudosa JC, Bernués M, Caldas C, Colomer D, Miró R, Campo E. Genomic imbalances and patterns of karyotypic variability in mantle-cell lymphoma cell lines. Leuk Res. 2006;30(8):923-34. doi:10.1016/j.leukres.2005.11.013

200. Rudelius M, Pittaluga S, Nishizuka S, Pham TH, Fend F, Jaffe ES, Quintanilla-Martinez L, Raffeld M. Constitutive activation of Akt contributes to the pathogenesis and survival of mantle cell lymphoma. Blood. 2006;108(5):1668-76. doi:10.1182/blood-2006-04-015586

201. Szepetowski P, Simon MP, Grosgeorge J, Huebner K, Bastard C, Evans GA, Tsujimoto Y, Birnbaum D, Theillet C, Gaudray P. Localization of 11q13 loci with respect to regional chromosomal breakpoints. Genomics. 1992;12(4):738-44. doi:10.1016/0888-7543(92)90303-a

202. Psyrri A, Papageorgiou S, Liakata E, Scorilas A, Rontogianni D, Kontos CK, Argyriou P, Pectasides D, Harhalakis N, Pappa V, Kolialexi A, Economopoulou C, Kontsioti F, Maratou E, Dimitriadis G, Economopoulou P, Economopoulos T. Phosphatidylinositol 3'-kinase catalytic subunit alpha gene amplification contributes to the pathogenesis of mantle cell lymphoma. Clin Cancer Res. 2009;15(18):5724-32. doi:10.1158/1078-0432.Ccr-08-3215

203. Düvel K, Yecies JL, Menon S, Raman P, Lipovsky AI, Souza AL, Triantafellow E, Ma Q, Gorski R, Cleaver S, Vander Heiden MG, MacKeigan JP, Finan PM, Clish CB, Murphy LO, Manning BD. Activation of a metabolic gene regulatory network downstream of mTOR complex 1. Mol Cell. 2010;39(2):171-83. doi:10.1016/j.molcel.2010.06.022

204. Hu CJ, Wang LY, Chodosh LA, Keith B, Simon MC. Differential roles of hypoxia-inducible factor 1alpha (HIF-1alpha) and HIF-2alpha in hypoxic gene regulation. Mol Cell Biol. 2003;23(24):9361-74. doi:10.1128/mcb.23.24.9361-9374.2003

205. Lee SC, Shestov AA, Guo L, Zhang Q, Roman JC, Liu X, Wang HY, Pickup S, Nath K, Lu P, Hofbauer S, Mesaros C, Wang YL, Nelson DS, Schuster SJ, Blair IA, Glickson JD, Wasik MA. Metabolic Detection of Bruton's Tyrosine Kinase Inhibition in Mantle Cell Lymphoma Cells. Mol Cancer Res. 2019;17(6):1365-77. doi:10.1158/1541-7786.Mcr-18-0256

206. Zhang L, Yao Y, Zhang S, Liu Y, Guo H, Ahmed M, Bell T, Zhang H, Han G, Lorence E, Badillo M, Zhou S, Sun Y, Di Francesco ME, Feng N, Haun R, Lan R, Mackintosh SG, Mao X, Song X, et al. Metabolic reprogramming toward oxidative phosphorylation identifies a therapeutic target for mantle cell lymphoma. Sci Transl Med. 2019;11(491). doi:10.1126/scitranslmed.aau1167

207. Haq R, Shoag J, Andreu-Perez P, Yokoyama S, Edelman H, Rowe GC, Frederick DT, Hurley AD, Nellore A, Kung AL, Wargo JA, Song JS, Fisher DE, Arany Z, Widlund HR. Oncogenic BRAF regulates oxidative metabolism via PGC1α and MITF. Cancer Cell. 2013;23(3):302-15. doi:10.1016/j.ccr.2013.02.003

208. Vitiello GA, Medina BD, Zeng S, Bowler TG, Zhang JQ, Loo JK, Param NJ, Liu M, Moral AJ, Zhao JN, Rossi F, Antonescu CR, Balachandran VP, Cross JR, DeMatteo RP. Mitochondrial Inhibition Augments the Efficacy of Imatinib by Resetting the Metabolic Phenotype of Gastrointestinal Stromal Tumor. Clin Cancer Res. 2018;24(4):972-84. doi:10.1158/1078-0432.Ccr-17-2697

209. Kuntz EM, Baquero P, Michie AM, Dunn K, Tardito S, Holyoake TL, Helgason GV, Gottlieb E. Targeting mitochondrial oxidative phosphorylation eradicates therapy-resistant chronic myeloid leukemia stem cells. Nat Med. 2017;23(10):1234-40. doi:10.1038/nm.4399

210. Lee KM, Giltnane JM, Balko JM, Schwarz LJ, Guerrero-Zotano AL, Hutchinson KE, Nixon MJ, Estrada MV, Sánchez V, Sanders ME, Lee T, Gómez H, Lluch A, Pérez-Fidalgo JA, Wolf MM, Andrejeva G, Rathmell JC, Fesik SW, Arteaga CL. MYC and MCL1 Cooperatively Promote Chemotherapy-Resistant Breast Cancer Stem Cells via Regulation of Mitochondrial Oxidative Phosphorylation. Cell Metab. 2017;26(4):633-47.e7. doi:10.1016/j.cmet.2017.09.009

211. Farge T, Saland E, de Toni F, Aroua N, Hosseini M, Perry R, Bosc C, Sugita M, Stuani L, Fraisse M, Scotland S, Larrue C, Boutzen H, Féliu V, Nicolau-Travers ML, Cassant-Sourdy S, Broin N, David M, Serhan N, Sarry A, et al. Chemotherapy-Resistant Human Acute Myeloid Leukemia Cells Are Not Enriched for Leukemic Stem Cells but Require Oxidative Metabolism. Cancer Discov. 2017;7(7):716-35. doi:10.1158/2159-8290.Cd-16-0441

212. Lee S, Lee JS, Seo J, Lee SH, Kang JH, Song J, Kim SY. Targeting Mitochondrial Oxidative Phosphorylation Abrogated Irinotecan Resistance in NSCLC. Sci Rep. 2018;8(1):15707. doi:10.1038/s41598-018-33667-6

213. Guièze R, Liu VM, Rosebrock D, Jourdain AA, Hernández-Sánchez M, Martinez Zurita A, Sun J, Ten Hacken E, Baranowski K, Thompson PA, Heo JM, Cartun Z, Aygün O, Iorgulescu JB, Zhang W, Notarangelo G, Livitz D, Li S, Davids MS, Biran A, et al. Mitochondrial Reprogramming Underlies Resistance to BCL-2 Inhibition in Lymphoid Malignancies. Cancer Cell. 2019;36(4):369-84.e13. doi:10.1016/j.ccell.2019.08.005

214. Faubert B, Solmonson A, DeBerardinis RJ. Metabolic reprogramming and cancer progression. Science. 2020;368(6487). doi:10.1126/science.aaw5473

215. Luengo A, Gui DY, Vander Heiden MG. Targeting Metabolism for Cancer Therapy. Cell Chem Biol. 2017;24(9):1161-80. doi:10.1016/j.chembiol.2017.08.028

216. Stine ZE, Schug ZT, Salvino JM, Dang CV. Targeting cancer metabolism in the era of precision oncology. Nat Rev Drug Discov. 2022;21(2):141-62. doi:10.1038/s41573-021-00339-6

217. Janku F, Beom SH, Moon YW, Kim TW, Shin YG, Yim DS, Kim GM, Kim HS, Kim SY, Cheong JH, Lee YW, Geiger B, Yoo S, Thurston A, Welsch D, Rudoltz MS, Rha SY. First-in-human study of IM156, a novel potent biguanide oxidative phosphorylation (OXPHOS) inhibitor, in patients with advanced solid tumors. Invest New Drugs. 2022;40(5):1001-10. doi:10.1007/s10637-022-01277-9

218. Molina JR, Sun Y, Protopopova M, Gera S, Bandi M, Bristow C, McAfoos T, Morlacchi P, Ackroyd J, Agip AA, Al-Atrash G, Asara J, Bardenhagen J, Carrillo CC, Carroll C, Chang E, Ciurea S, Cross JB, Czako B, Deem A, et al. An inhibitor of oxidative phosphorylation exploits cancer vulnerability. Nat Med. 2018;24(7):1036-46. doi:10.1038/s41591-018-0052-4

219. Ackermann T, Tardito S. Cell Culture Medium Formulation and Its Implications in Cancer Metabolism. Trends Cancer. 2019;5(6):329-32. doi:10.1016/j.trecan.2019.05.004

220. Muir A, Vander Heiden MG. The nutrient environment affects therapy. Science. 2018;360(6392):962-3. doi:10.1126/science.aar5986

221. Nadeu F, Royo R, Massoni-Badosa R, Playa-Albinyana H, Garcia-Torre B, Duran-Ferrer M, Dawson KJ, Kulis M, Diaz-Navarro A, Villamor N, Melero JL, Chapaprieta V, Dueso-Barroso A, Delgado J, Moia R, Ruiz-Gil S, Marchese D, Giró A, Verdaguer-Dot N, Romo M, et al. Detection of early seeding of Richter transformation in chronic lymphocytic leukemia. Nat Med. 2022;28(8):1662-71. doi:10.1038/s41591-022-01927-8

222. Konopleva M, Yap T, Daver N, Mahendra M, Zhang J, Kamiya-Matsuoka C, Meric-Bernstam F, Kantarjian H, Ravandi F, Collins M, Francesco MD, Dumbrava E, Fu S, Gao S, Gay J, Gera S, Han J, Hong D, Jabbour E, Ju Z, et al. Targeting Oxidative Phosphorylation with a Mitochondrial Complex I Inhibitor is limited by Mechanism-based Toxicity. Research Square; 2022.

223. Scott AM, Wolchok JD, Old LJ. Antibody therapy of cancer. Nat Rev Cancer. 2012;12(4):278-87. doi:10.1038/nrc3236

224. Maloney DG, Grillo-López AJ, Bodkin DJ, White CA, Liles TM, Royston I, Varns C, Rosenberg J, Levy R. IDEC-C2B8: results of a phase I multiple-dose trial in patients with relapsed non-Hodgkin's lymphoma. J Clin Oncol. 1997;15(10):3266-74. doi:10.1200/jco.1997.15.10.3266

225. Shanafelt TD, Wang XV, Kay NE, Hanson CA, O'Brien S, Barrientos J, Jelinek DF, Braggio E, Leis JF, Zhang CC, Coutre SE, Barr PM, Cashen AF, Mato AR, Singh AK, Mullane MP, Little RF, Erba H, Stone RM, Litzow M, et al. Ibrutinib-Rituximab or Chemoimmunotherapy for Chronic Lymphocytic Leukemia. N Engl J Med. 2019;381(5):432-43. doi:10.1056/NEJMoa1817073

226. Tsao LC, Force J, Hartman ZC. Mechanisms of Therapeutic Antitumor Monoclonal Antibodies. Cancer Res. 2021;81(18):4641-51. doi:10.1158/0008-5472.Can-21-1109

227. Wang W, Erbe AK, Hank JA, Morris ZS, Sondel PM. NK Cell-Mediated Antibody-Dependent Cellular Cytotoxicity in Cancer Immunotherapy. Front Immunol. 2015;6:368. doi:10.3389/fimmu.2015.00368

228. Weiskopf K, Weissman IL. Macrophages are critical effectors of antibody therapies for cancer. MAbs. 2015;7(2):303-10. doi:10.1080/19420862.2015.1011450

229. Meyer S, Leusen JH, Boross P. Regulation of complement and modulation of its activity in monoclonal antibody therapy of cancer. MAbs. 2014;6(5):1133-44. doi:10.4161/mabs.29670

230. Pierpont TM, Limper CB, Richards KL. Past, Present, and Future of Rituximab-The World's First Oncology Monoclonal Antibody Therapy. Front Oncol. 2018;8:163. doi:10.3389/fonc.2018.00163

231. Riechmann L, Clark M, Waldmann H, Winter G. Reshaping human antibodies for therapy. Nature. 1988;332(6162):323-7. doi:10.1038/332323a0

232. Faderl S, Thomas DA, O'Brien S, Garcia-Manero G, Kantarjian HM, Giles FJ, Koller C, Ferrajoli A, Verstovsek S, Pro B, Andreeff M, Beran M, Cortes J, Wierda W, Tran N, Keating MJ. Experience with alemtuzumab plus rituximab in patients with relapsed and refractory lymphoid malignancies. Blood. 2003;101(9):3413-5. doi:10.1182/blood-2002-07-1952

233. Yi JH, Kim SJ, Ko YH, Kim WS. Treatment of patients with refractory diffuse large B-cell lymphoma or mantle cell lymphoma with alemtuzumab, alone or in combination with cytotoxic chemotherapy. Leuk Lymphoma. 2011;52(2):317-20. doi:10.3109/10428194.2010.529203

234. Rieger K, Von Grünhagen U, Fietz T, Thiel E, Knauf W. Efficacy and tolerability of alemtuzumab (CAMPATH-1H) in the salvage treatment of B-cell chronic lymphocytic leukemia--change of regimen needed? Leuk Lymphoma. 2004;45(2):345-9. doi:10.1080/10428190310001598017

235. Keating MJ, Flinn I, Jain V, Binet J-L, Hillmen P, Byrd J, Albitar M, Brettman L, Santabarbara P, Wacker B, Rai KR. Therapeutic role of alemtuzumab (Campath-1H) in patients who have failed fludarabine: results of a large international study. Blood. 2002;99(10):3554-61. doi:10.1182/blood.V99.10.3554

236. Cohen JA, Coles AJ, Arnold DL, Confavreux C, Fox EJ, Hartung H-P, Havrdova E, Selmaj KW, Weiner HL, Fisher E, Brinar VV, Giovannoni G, Stojanovic M, Ertik BI, Lake SL, Margolin DH, Panzara MA, Compston DAS. Alemtuzumab versus interferon beta 1a as first-line treatment for patients with relapsing-remitting multiple sclerosis: a randomised controlled phase 3 trial. The Lancet. 2012;380(9856):1819-28. doi:10.1016/S0140-6736(12)61769-3

237. Coles AJ, Twyman CL, Arnold DL, Cohen JA, Confavreux C, Fox EJ, Hartung H-P, Havrdova E, Selmaj KW, Weiner HL, Miller T, Fisher E, Sandbrink R, Lake SL, Margolin DH, Oyuela P, Panzara MA, Compston DAS. Alemtuzumab for patients with relapsing multiple sclerosis after disease-modifying therapy: a randomised controlled phase 3 trial. The Lancet. 2012;380(9856):1829-39. doi:10.1016/S0140-6736(12)61768-1

238. Nückel H, Frey UH, Röth A, Dührsen U, Siffert W. Alemtuzumab induces enhanced apoptosis in vitro in B-cells from patients with chronic lymphocytic leukemia by antibody-dependent cellular cytotoxicity. Eur J Pharmacol. 2005;514(2-3):217-24. doi:10.1016/j.ejphar.2005.03.024

239. Zent CS, Secreto CR, LaPlant BR, Bone ND, Call TG, Shanafelt TD, Jelinek DF, Tschumper RC, Kay NE. Direct and complement dependent cytotoxicity in CLL cells from patients with high-risk early-intermediate stage chronic lymphocytic leukemia (CLL) treated with alemtuzumab and rituximab. Leuk Res. 2008;32(12):1849-56. doi:10.1016/j.leukres.2008.05.014

240. Syed YY. Alemtuzumab: A Review in Relapsing Remitting Multiple Sclerosis. Drugs. 2021;81(1):157-68. doi:10.1007/s40265-020-01437-2

241. Winqvist M, Palma M, Heimersson K, Mellstedt H, Österborg A, Lundin J. Dual targeting of Bruton tyrosine kinase and CD52 induces minimal residual disease-negativity in the bone marrow of poor-prognosis chronic lymphocytic leukaemia patients but is associated with opportunistic infections - Results from a phase I study. Br J Haematol. 2018;182(4):590-4. doi:10.1111/bjh.14836

242. Rauert-Wunderlich H, Rudelius M, Berberich I, Rosenwald A. CD40L mediated alternative NFκB-signaling induces resistance to BCR-inhibitors in patients with mantle cell lymphoma. Cell Death & Disease. 2018;9(2):86. doi:10.1038/s41419-017-0157-6

243. Khan N, Rothstein TL. The Alternate Pathway for BCR Signaling Induced by IL-4 Requires Lyn Tyrosine Kinase. J Mol Biol. 2021;433(1):166667. doi:10.1016/j.jmb.2020.10.002

244. Osterborg A, Mellstedt H, Keating M. Clinical effects of alemtuzumab (Campath-1H) in B-cell chronic lymphocytic leukemia. Med Oncol. 2002;19 Suppl:S21-6. doi:10.1385/mo:19:2s:s21

245. Gdynia G, Robak T, Kopitz J, Heller A, Grekova S, Duglova K, Laukemper G, Heinzel-Gutenbrunner M, Gutenbrunner C, Roth W, Ho AD, Schirmacher P, Schmitt M, Dreger P, Sellner L. Distinct Activities of Glycolytic Enzymes Identify Chronic Lymphocytic Leukemia Patients with a more Aggressive Course and Resistance to Chemo-Immunotherapy. EBioMedicine. 2018;32:125-33. doi:10.1016/j.ebiom.2018.05.030

246. Anderson KC, Auclair D, Adam SJ, Agarwal A, Anderson M, Avet-Loiseau H, Bustoros M, Chapman J, Connors DE, Dash A, Di Bacco A, Du L, Facon T, Flores-Montero J, Gay F, Ghobrial IM, Gormley NJ, Gupta I, Higley H, Hillengass J, et al. Minimal Residual Disease in Myeloma: Application for Clinical Care and New Drug Registration. Clin Cancer Res. 2021;27(19):5195-212. doi:10.1158/1078-0432.Ccr-21-1059

247. Qi J, Chen SS, Chiorazzi N, Rader C. An IgG1-like bispecific antibody targeting CD52 and CD20 for the treatment of B-cell malignancies. Methods. 2019;154:70-6. doi:10.1016/j.ymeth.2018.08.008

13 Acknowledgements

This work would not have been possible without the support and motivation of many people.

First, I would like to thank Prof. Dr. Andreas Rosenwald for giving me the opportunity to work in his research group, participate in congresses to think outside the box, and for the fruitful discussions. I am very grateful to have had a motivated mentor in Dr. Hilka Rauert-Wunderlich, who taught me scientific thinking and working, guided me through challenging times, and was always there to answer my questions and support me. Thank you so much for the effort you put in me and this work!

Many thanks to Dr. Antoine-Emmanuel Saliba for welcoming me into his group and introducing me to the world of single-cell genomics. I would also like to thank Dr. Ehsan Vafadarnejad and Dr. Panagiota Arampatzi for their support and answering all my questions about single-cell analysis.

PD Dr. Robert Hock provided me with objective advice and I thank him for his commitment to this work.

The lab work and breaks would not have been the same without my colleagues from AG Leich and AG Rosenwald. Thank you for sharing your knowledge with me and for the great time. Special thanks to Tina Grieb and Shanice Heidenreich, who contributed with excellent experimental work, and Marietheres Evers, who took the time to proofread this work.

During my research project, the Core Unit Systems Medicine, especially Dr. Panagiota Arampatzi and Dr. Mugdha Srivastava, Dr. Angela Riedel, Dr. Johannes Düll, and Dr. Elena Gerhard-Hartmann provided me with valuable expertise in conducting the experimental work and analysis and I thank them for the successful collaboration.

As a student in the Graduate School of Life Sciences, I have benefited from many interesting workshops and activities and thank the entire team for their support and organization of the structured doctoral research training.

I would like to thank my parents Andrea and Michael, my brothers Valentin and Benedikt, as well as all my family and friends for their guidance during my career, their motivation, their unwavering belief in my abilities and their love. Most of all, I thank Simon for putting up with my bad moods, cheering me up with his encouragement and love, and standing by my side during these four years.

14 Affidavit

I hereby confirm that my thesis entitled “Target Identification and Validation in Ibrutinib-treated Mantle Cell Lymphoma” is the result of my own work. I did not receive any help or support from commercial consultants. All sources and/or materials applied are listed and specified in the thesis.

Furthermore, I confirm that this thesis has not yet been submitted as part of another examination process neither in identical nor in similar form.

Würzburg,

Eidesstattliche Erklärung

Hiermit erkläre ich an Eides statt, die Dissertation „Target-Identifizierung und Validierung im Ibrutinib-behandelten Mantelzell-Lymphom“ eigenständig, d.h. insbesondere selbständig und ohne Hilfe eines kommerziellen Promotionsberaters, angefertigt und keine anderen als die von mir angegebenen Quellen und Hilfsmittel verwendet zu haben.

Ich erkläre außerdem, dass die Dissertation weder in gleicher noch in ähnlicher Form bereits in einem anderen Prüfungsverfahren vorgelegt wurde.

Würzburg,

15 List of Publications

Viktoria Fuhr, Ehsan Vafadarnejad, Oliver Dietrich, Panagiota Arampatzi, Angela Riedel, Antoine-Emmanuel Saliba, Andreas Rosenwald, and Hilka Rauert-Wunderlich. Time-Resolved scRNA-Seq Tracks the Adaptation of a Sensitive MCL Cell Line to Ibrutinib Treatment. International Journal of Molecular Sciences. 2021;22(5):2276.

Viktoria Fuhr, Ehsan Vafadarnejad, Oliver Dietrich, Panagiota Arampatzi, Angela Riedel, Antoine-Emmanuel Saliba, Andreas Rosenwald, and Hilka Rauert-Wunderlich. Eine Einzelzell-RNA-Sequenzierung identifiziert Metabolismus und CD52 als neue Angriffspunkte in Ibrutinib-persistenten Mantelzelllymphomzellen. Pathologie (2022). [Presentations: Award Winners - Doctoral Award]

Viktoria Fuhr, Shanice Heidenreich, Mugdha Srivastava, Angela Riedel, Johannes Düll, Elena Gerhard-Hartmann, Andreas Rosenwald, and Hilka Rauert-Wunderlich. CD52 and OXPHOS – potential targets in ibrutinib-treated mantle cell lymphoma. *Accepted for publication in Cell Death Discovery on 16 December 2022.*

Matteo C. Da Vià, Oliver Dietrich, Marietta Truger, Panagiota Arampatzi, Johannes Duell, Anke Heidemeier, Xiang Zhou, Sophia Danhof, Sabrina Kraus, Manik Chatterjee, Manja Meggendorfer, Sven Twardziok, Maria-Elisabeth Goebeler, Max S. Topp, Michael Hudecek, Sabrina Prommersberger, Kristen Hege, Shari Kaiser, **Viktoria Fuhr**, Niels Weinhold, Andreas Rosenwald, Florian Erhard, Claudia Haferlach, Hermann Einsele, K. Martin Kortüm, Antoine-Emmanuel Saliba & Leo Rasche. Homozygous BCMA gene deletion in response to anti-BCMA CAR T cells in a patient with multiple myeloma. Nature Medicine. 2021;27(4):616-9.

16 Curriculum Vitae